THE MICROSTRUCTURE AND SOME PHASE TRANSFORMATION CHARACTERISTICS OF THE DUAL PHASE STEEL 3CR12

by

EUGENIE PROTOPAPPAS

A thesis submitted to the Faculty of Engineering, University of Cape Town, in fulfilment of the degree of Master of Science in Applied Science.

Department of Metallurgy and Materials Science
University of Cape Town

The copyright of this thesis vests in the author. No quotation from it or information derived from it is to be published without full acknowledgement of the source. The thesis is to be used for private study or non-commercial research purposes only.

Published by the University of Cape Town (UCT) in terms of the non-exclusive license granted to UCT by the author.

University of Cape Town

TO MY PARENTS

DIMITRI AND DINA

ACKNOWLEDGEMENTS

I wish to express my sincere thanks and appreciation to the following people:

Firstly, Professor A Ball, for his supervision, and guidance and unlimited help throughout the research project.

Professor O Heckroodt for his willing help with the dilatometric technique.

Monsieur Nicholas Dreze and Mr Andrew Rapley are thanked for their technical assistance.

Bernard Greeves for the photographic work.

Nicky and Gillian for their assistance with the preparation of the manuscript.

My friends and colleagues in the Metallurgy Department for their stimulating companionship.

Middelburg Steel and Alloys (Pty) Ltd are gratefully acknowledged for their financial support.

ABSTRACT

Dilatometry and metallography have been used to establish the phase transformation diagram of a steel containing 12% chromium and 0,03% carbon. A dual phase material with attractive mechanical properties and adequate corrosion resistance can be achieved by careful control of alloy content and heat treatment. The work has demonstrated the influence of the addition of alloying elements (in particular nickel), and thermal history. The dual phase (ferrite plus martensite) nature of the steel has been identified and characterised by both optical and transmission electron microscopy. The islands of lath martensite and the attendant high dislocation densities present good mechanical behaviour. In particular, the continuous yielding, work hardening, formability and toughness can be attributed to this microstructure. The thesis provides a base for the discussion of methods of "designing" the steel for particular applications.

LIST OF ABBREVIATIONS

AC	air cool
AHR	as-hot-rolled
$\sim$	approximately
α	ferrite or alpha iron
α'	martensite
BCC	body centred cubic structure
CCT	continuous cooling transformation
γ	austenite or gamma iron
DBTT	ductile to brittle transition temperature
δ	delta ferrite or delta iron
FC	furnace cool
FCC	face centred cubic structure
HT	heat treatment
Mf	the temperature at which complete transformation to martensite occurs upon cooling an austenitic structure
Ms	the temperature at which transformation to martensite begins upon cooling an austenitic structure
OQ	oil quench
Q	quench
RT	room temperature
T	transformation temperature
($T<1000^{o}C$)	low temperature experiment
($T>1000^{o}C$)	high temperature experiment
TEM	transmission electron microscopy
TTT	time temperature transformation
WQ	water quench

CONTENTS

		Page
TITLE PAGE		(i)
ACKNOWLEDGEMENTS		(iii)
ABSTRACT		(iv)
LIST OF ABBREVIATIONS		(v)
CHAPTER 1 :	GENERAL INTRODUCTION	1
CHAPTER 2 :	STRUCTURE-PROPERTY RELATIONSHIPS	4
2.1	Introduction	4
2.2	Mechanical Properties	8
2.3	Deformation Characteristics	22
CHAPTER 3 :	THE EFFECTS OF ALLOYING ELEMENTS	24
CHAPTER 4 :	EXPERIMENTAL TECHNIQUES	34
4.1	Alloy Compositions	34
4.2	Dilatometry	39
4.3	Metallography	51
4.4	TEM	52
4.5	Hardness Measurements	53
4.6	Tempering Characteristics	54
CHAPTER 5 :	RESULTS	55
5.1	The 11,5%Cr-Ni Alloys	55
5.1.1	Dilatometry	55
5.1.1.1	Low Temperature Experiment (T<1000°C)	55
5.1.1.2	High Temperature Experiment (T>1000°C)	55
5.1.2	The Phase Transformation Diagram	57
5.1.3	Metallography	71
5.1.4	TEM	80
5.1.5	Hardness Measurements	85
5.1.6	Tempering Characteristics	89
5.2	The 14,3%Cr-Ni Alloys	92
5.2.1	Dilatometry	92
5.2.1.1	Low Temperature Experiment (T<1000°C)	92
5.2.1.2	High Temperature Experiment (T>1000°C)	92
5.2.2	The Phase Transformation Diagram	94
5.2.3	Metallography	105
5.2.4	TEM	115
5.2.5	Hardness Measurements	120

Continued/...

CONTENTS (cont'd)

		Page
CHAPTER 6 :	DISCUSSION	125
CHAPTER 7 :	SUMMARY	147
REFERENCES		150
APPENDIX :	A	164
	B	173
	C	175
	D	177
	E	179
	F	184

CHAPTER 1 : GENERAL INTRODUCTION

The compositional and microstructural design of a steel depends greatly upon its intended end use. The desired properties can include strength, formability, toughness, weldability and corrosion resistance, but it is often the case that improvements in one property may degrade a second desired property. For instance, increasing the strength of a steel generally decreases its ductility. Thus, in most cases it is necessary to produce the required combination of properties for the application by means of optimisation programmes. Economic factors play an ever increasing role in alloy design. The constituent of many of today's sophisticated alloys contain expensive elemental additions such as nickel and chromium, and care needs to be exercised not to overdesign and thus jeopardise the alloy's competitiveness.

The successful design process consists of the following:

(a) The identification of a useful class of alloys which may have a unique combination of properties for a particular application.

(b) A complete survey of the properties of this class of alloys, including the deformation

characteristics and the way in which alloying additions affect these properties.

(c) The development stage - achieving a product which encompasses the desired properties.

(d) The experimental deduction of the phase transformation diagram for the alloy. This phase transformation diagram may indicate which phase or phases are likely to exist at a particular temperature (taking into consideration the conditions specified). Information concerning the effect which different alloy additions and temperature have on the resultant microstructure is also required. Since the microstructure is the primary factor influencing the strength properties, the importance of this aspect of the development program cannot be overlooked.

(e) Using the phase transformation diagram as a guide, the metallurgist can now optimise heat treatments and alloy composition to obtain the desired microstructure and combination of properties. This process requires in addition a TTT (Time, Temperature, Transformation) diagram, as well as information concerning continuous cooling transformation characteristics (CCT). The TTT and CCT diagrams are the process metallurgist's guide for the alloy.

In this thesis a study has been made of the corrosion resistant alloy 3CR12. This alloy is a dual phase (ferritic - martensitic) 12% Cr steel having potential as a replacement for coated mild steel. An attempt has been made to identify the anticipated properties of such an alloy (Chapter 2) and to ascertain the role that alloying additions may have on strength and the structure - property relationships (Chapter 3). The major part of the program was to obtain the phase transformation diagram for two series of alloys (11,5% and 14,3% Cr) as a function of nickel content (Chapters 4 and 5). Information that may be obtained from these phase transformation diagrams for the experimental alloys is discussed in Chapter 6. A summary and some recommendations for future work is included in Chapter 7.

The scope of the work embraces the first four points of the design process. The experimental 'phase transformation diagram' may now be used to optimise heat treatments for commercial exploitation of the alloy.

CHAPTER 2 : STRUCTURE - PROPERTY RELATIONSHIPS

2.1 INTRODUCTION

There is little doubt that a steel that can combine the strength properties of plain carbon steel with a high degree of corrosion resistance will be economically attractive. Maintenance costs are now a major factor in the economic assessment of a structure, and the reduction of corrosion and wear through alloy design is a major goal of materials engineering disciplines.

One significant breakthrough in recent years has been the devlopment of tough, weldable steels containing approximately 12% Cr, which are derivatives of AISI 409 and AISI 410 stainless steels. These steels exploit the existence of the so-called gamma-loop in the Fe-Cr phase diagram (Fig. 2.1a). It can be seen from Fig. 2.1b that the γ-loop forms a dual phase austenitic - ferritic region at temperatures between 840^{o}C and 1400^{o}C. Upon quenching to room temperature, the austenite transforms to martensite, resulting in a martensitic - ferritic structure which is similar to that of the new family of alloys known as "dual phase" or microduplex steels.

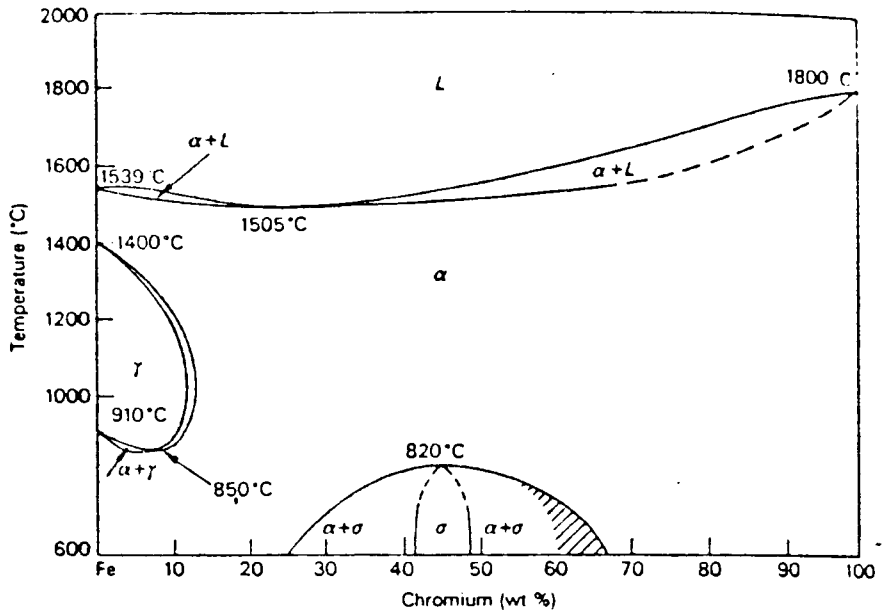

FIG. 2.1(a) The Fe-Cr 'equilibrium' diagram. (0,01%C).

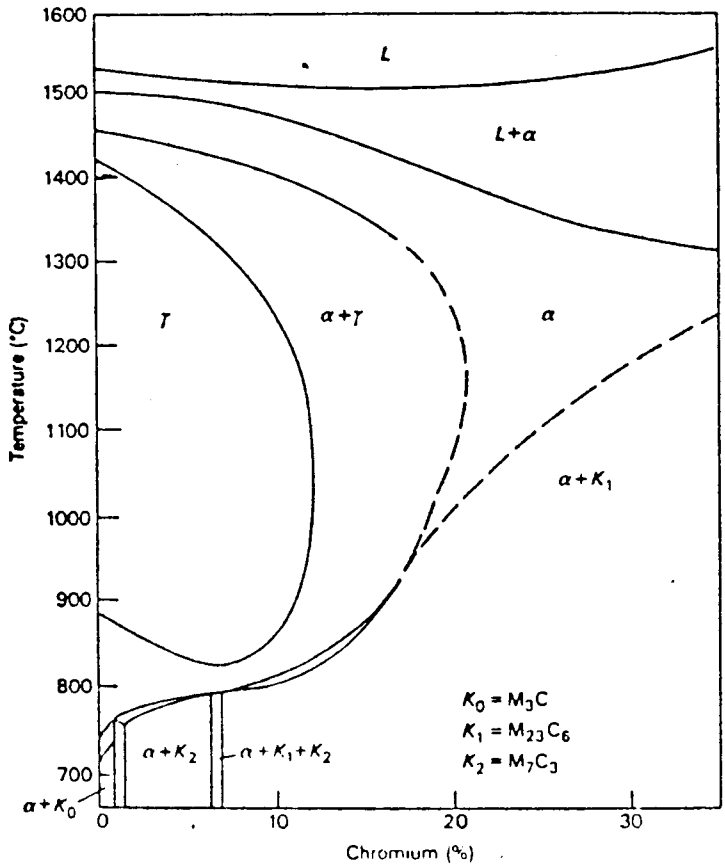

FIG. 2.1(b) Portion of the Fe-Cr diagram with (0,05%C) showing dual phase ($\alpha + \gamma$) region. (Taken from Colombier and Hochmann, 1967)

Type 410 W (Nippon Steel Corporation) has been developed from AISI 410 and has a low carbon and nitrogen interstitial content. Increased strength results from the addition of higher manganese and nickel contents than type 410 (Melvill et al, 1980). Type E4 (Colt Crucible, USA) has 0,85% nickel added to reduce the grain size and increase the toughness.

In South Africa, Middelburg Steel and Alloys (Pty) Ltd has developed the Type 3CR12* from AISI 409. A typical composition (in weight percent) for both steels is shown below in Table 2.1.

TABLE 2.1

Typical Composition of 3CR12

C	S	P	Mn	Si	Cr	Ni	Ti	N
0,025	0,014	0,020	0,80	0,45	11,5	0,6	0,21	0,01

Typical Composition of Type AISI 409

C	S	P	Mn	Si	Cr	Ni	Ti	N
0,08	0,045	0,045	1,06	1,0	11,5	0,5	0,75	-

* *patent application SA 78/4764*

In 3CR12 , the nickel content is approximately 0,6% and interstitial carbon and nitrogen are each kept characteristically low (0,03%). This results in much improved proerties as compared with those for AISI 409 (Ball and Hoffman, 1981). Typical values of Charpy V-notch impact tests are shown below in Table 2.2.

TABLE 2.2

	3CR12	AISI 409
RT 20°C	85J	20J
0°C	65J	10J
DBTT	-20°C	40 - 100°C

An important point to note is the greatly reduced impact transition temperature (-20°C) of alloy 3CR12. In addition to the good toughness characteristics, 3CR12 has a moderate degree of corrosion resistance making it superior to the performance of coated mild steel in some aggressive environments. Furthermore it should prove possible to exploit the dual phase nature of these 12% chromium steels and hence provide fabricators with a product which combines adequate strength with good formability and corrosion

resistance. However, the beneficial effects of such alloys relies critically upon a cost effective product, in which the expensive chromium and nickel fractions are optimised, and corrosion control made competitive with traditional maintenance schedules. A strategic consideration for South Africa is the exploitation of the vast chromium reserves of this country (85% of the free world's known resources) (Melvill et al, 1980) which may result from the major use of 3CR12 as a competitive replacement for mild steel.

2.2 MECHANICAL PROPERTIES

Table 2.3 compares the mechanical properties of dual phase 3CR12 with a range of structural steels. Included is a conventional micro-alloyed high-strength low-alloy (HSLA) steel (ferrite-pearlite microstructure); stainless steel (types 304 and 409) and mild steel. A plain carbon dual- phase steel, type GM 980X is also included. It is to be noted that the strength of 3CR12 is significantly higher than that of mild steel and compares favourably with the limits for the HSLA steel (type SAE 950X). The degree of formability, as reflected in the elongation, shows similar values (25 - 30%) for 3CR12, the plain carbon dual phase steel and the duplex stainless IN 744. The improved elongation of this class of alloys over the conventional HSLA steel is to be noted. Type 304 shows superior elongation

(60%), but the high Cr(18%) and Ni(8%) contents of this alloy make it expensive and uneconomic in non-specialist applications. The ferritic-martensitic microduplex stainless steel IN-744 (Japan) containing approximately 26% chromium and 5% nickel combines high strength and ductility with excellent corrosion resistance.

PROPERTY UNIT	1 3CR12	1 409	1 304	Duplex stainless steel 2 IN 744	Plain 3 Carbon Steel (0,05%C)	Plain Carbon 3 dual phase Steel GM 980X	3 HSLA SAE 950X	SAE 980X
U.T.S. MPa	455	450	600	650	284	650	462	682
Proof Stress (0,2%) offset MPa	360	250	310	497	232	350	380	548
Total Elongation (in 50mm) %	28	28	60	25	38	30	27	22
Yield Point Elongation or Lüders Band	no	yes	yes	no	yes	no	yes	yes
YS/UTS	0,79	0,5	0,5	0,76	0,82	0,53	0,82	0,80

1 taken from Comparative Data Sheet [Middelburg Steel and Alloys (Pty) Ltd]
2 taken from Gibson, 1977
3 taken from Rashid, 1979

TABLE 2.3 Mechanical properties of 3CR12 as compared with a plain carbon steel; a duplex stainless steel (IN 744); HSLA; type 409 and 304; and also a plain carbon dual phase steel.

The stress-strain diagrams (Fig. 2.2) for these steels highlight the fundamental differences between the HSLA; plain carbon steel and a typical dual phase steel. Both the plain carbon steel and HSLA steel exhibit a pronounced yield point, discontinuous yielding behaviour, and a high ratio of yield strength to ultimate tensile strength. (Coldren and Eldis, 1980). On the other hand, the dual phase steel shows continuous yielding; no sharply defined yield point and a low YS/UTS ratio. A high work hardening rate, particularly at low strains is also typical of this steel.

An important consequence of the continuous yielding behaviour is that the strain is more evenly distributed during deformation resulting in much improved formability characteristics. The difference in mechanical behaviour can be related to the microstructure of these alloys and the relative proportions of the constituent phases.

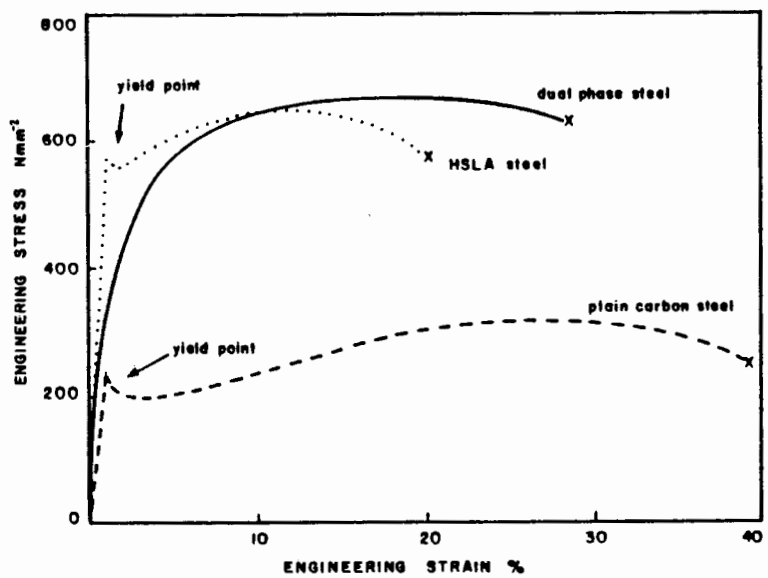

FIG. 2.2 Comparison of stress-strain curves for a dual phase steel, conventional microalloyed HSLA steel and a plain carbon steel. (Taken from Coldren & Eldis, 1980).

To understand the origin of the dual phase microstructure (in the plain carbon steels) reference is made to the Fe-C diagram (Fig. 2.3). A eutectoid is present at 0,8%C, and slow cooling a steel of this composition usually results in the formation of a fully pearlitic microstructure. For a carbon content less than 0,8% slow cooling results in a ferrite plus pearlite microstructure typical of the HSLA steels and plain carbon steel. To achieve the desirable dual-phase ferritic-martensitic structure an "intercritical" anneal is carried out in the ($\alpha + \gamma$) region between the Ac_1 and Ac_3 temperatures. This is followed by a controlled quench at the critical cooling rate to transform the austenite to martensite. Too slow a cooling rate may result in the ferrite plus pearlite microstructure, (Tanaka et al, 1979). A similar heat treatment is used to obtain the dual-phase structure in the 12% Cr steels.

Since the Fe-Cr phase diagram (Fig. 2.1) has a ($\alpha + \gamma$) region, a similar intercritical anneal followed by a controlled quench should result in the ferrite plus martensite structure.

The relation between cooling rate, alloy content and physical properties is schematically shown in Fig. 2.4 (taken from Tanaka et al, 1979). The diagram can be divided into three regions: The ferrite-pearlite region, the non-tempering, dual-phase region and the tempering dual-phase region. The boundary line

between the ferrite-pearlite and the dual-phase regions is decided by the critical cooling rate required to accomplish the martensite transformation. In order to accomplish the austenite to martensite tranformation during cooling, an alloy content greater than some critical value is required, where the critical value depends on cooling rate. The faster the cooling rate the less alloy content is required. Tempering is required to decrease excessively dissolved carbon, and thereby to improve ductility and the strength-elongation relationship. In the non-tempering region, equi-yield stress curves are drawn (Fig. 2.4) which are dependant on alloy content. With an increase in alloy content, the yield stress decreases.

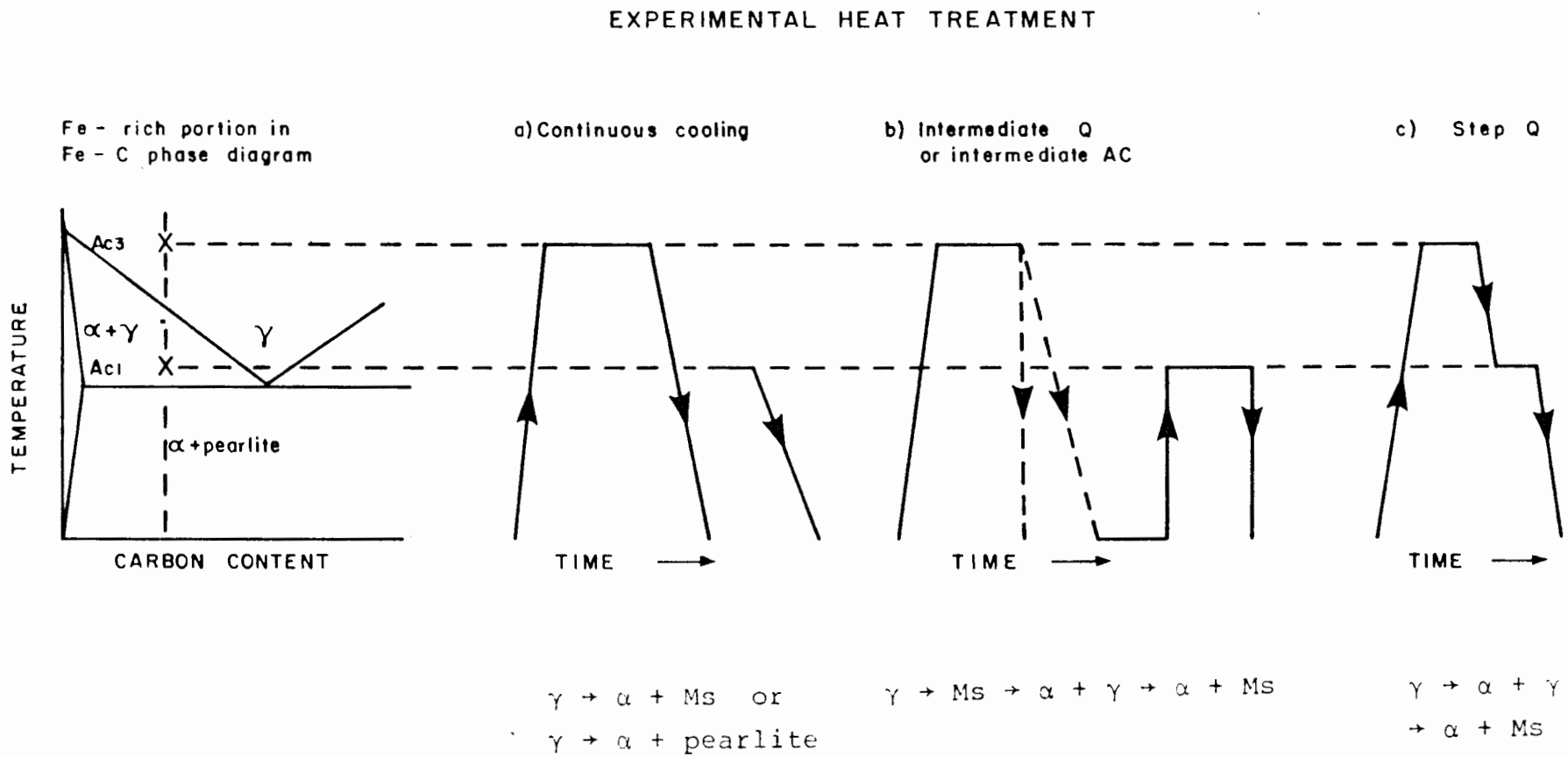

FIG. 2.3 Schematic diagram utilizing the Fe-C system to show heat treatments used to obtain duplex ferrite-martensite microstructures in plain carbon steels (taken from Thomas and Koo, 1979).

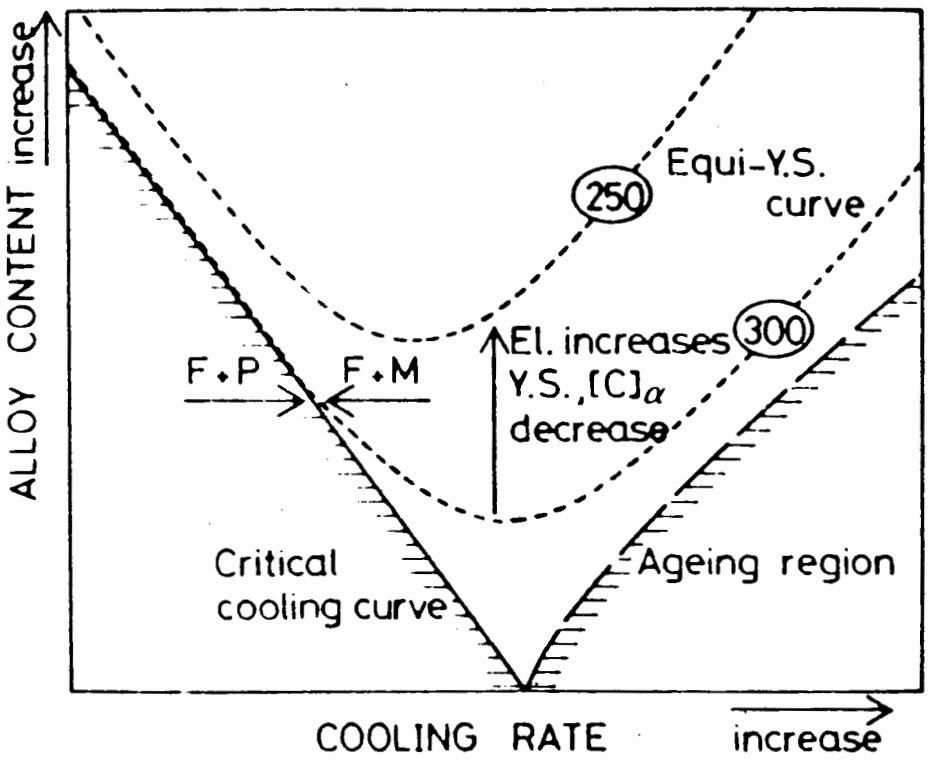

FIG. 2.4 Schematic illustration of cooling rate - alloy content - physical property diagram. Diagram is divided into ferrite-pearlite, non-tempering dual-phase and tempering dual-phase regions.
(Taken from Tanaka et al, 1979)

The strengthening character of the dual-phase steel (carbon or stainless) results from the mechanical behaviour of the hard martensite and the considerably softer ferrite matrix.

The exact micromechanical response is complex but involves the following principles:

(1) An increase in the volume fraction of martensite increases the strength of the steel (Davies, 1978; Marder, 1981; and Eldis, 1979) with a corresponding decrease in ductility (Fig. 2.5). The maximum strength is reached for a fully martensitic structure.

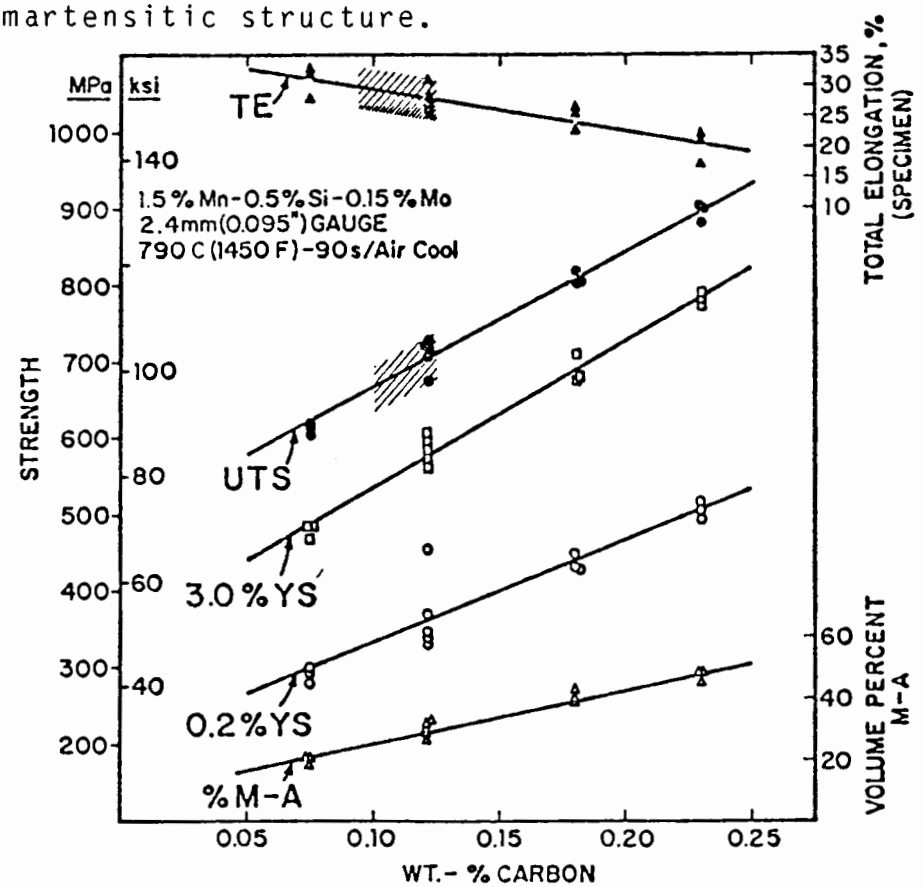

FIG. 2.5 Effect of carbon content and volume fraction of M-A (martensite-austenite) constituent on Mechanical Properties. (Taken from Eldis, 1979)

(2) Ferrite lowers the impact strength of the alloy since this phase is inherently susceptible to fracture due to its body centred cubic structure and the yield phenomenon.

(3) The exact value of toughness of the martensitic phase also controls the impact properties (Koo and Thomas, 1979 {a}).

(4) Martensite toughness can be increased by lowering the carbon content.

The volume fraction of martensite in plain carbon dual phase steel is controlled by the intercritical anneal temperature, time at temperature and cooling rate (Tanaka et al, 1979; Lanzillotto and Pickering, 1982; and Matlock et al, 1979) as follows:

(a) The higher the annealing temperature the greater the volume fraction of austenite formed at that particular temperature (as dictated by the lever rule). This in turn will result in a greater volume fraction of martensite upon quenching to room temperature.

(b) A sufficient time period at temperature must be allowed to equilibrate the structure as far as possible (i.e. too short a time at temperature will not allow the 'equilibrium' amount of austenite to form and this subsequently will

result in less martensite upon quenching). It would be interesting to note that in practice the holding (or soaking) time at a particular temperature during an intercritical anneal of a plain carbon dual phase steel is usually within the range of a few seconds to a few minutes, (Rashid, 1981). It is doubtful that 'equilibrium' conditions are attained during such short time periods.

(c) A fast cooling rate ensures a greater martensite fraction. For instance, Marder and Bramfitt, 1979, have shown that the percentage of second phase (martensite) increases with an increase in cooling rate.

In steels heated to just above the Ac_1 temperature the proportion of austenite formed is at a minimum. This austenite has a high carbon content since the carbon is more soluble in austenite (FCC) than ferrite (BCC). As the intercritical anneal temperature is raised, the proportion of austenite increases and the overall carbon content in the austenite is reduced. This diminished carbon content reduces the hardenability of the alloy. This in turn will influence the critical cooling rate required to form martensite upon quenching. An optimum alloy design could take advantage of the enhanced strength through high volume fraction of martensite, and increased toughness through a reduced carbon content. This

suggests that high intercritical anneal temperatures are desired, and emphasises the necessity of obtaining the accurate phase diagram of the alloy.

However, it should be noted that in practice, 3CR12 is not normally intercritically annealed. Subcritical annealing or tempering may be used in order to inprove the ductility and toughness of the steel. 3CR12 is processed during hot rolling, which may be be referred to as dual-phase rolling or 'DPR Process'.

A continuous cooling transformation diagram of an as-rolled dual-phase steel is shown below in Fig. 2.6. In the as-rolled process, for dual phase plain carbon steels, composition of the steel must be chosen such that 80 - 90% of the steel transforms to ferrite after the final roll pass in normal conventional hot rolling and before entering the coiler. The remaining 10 - 20% does not transform until later, during slow cooling in the coil, (Rashid, 1980). This is possible with steel compositions that exhibit certain special characteristics in their continuous cooling transformation (CCT) diagram:

(i) an elongated ferrite C-curve, ie the ability to form very large amounts of ferrite over a wide range of cooling rates on the run-out table;
(ii) a suppressed or delayed pearlite nose and a

high pearlite finish temperature in order to avoid the formation of pearlite during cooling to the coiling temperature; and

(iii) a gap between pearlite and bainite regions to provide a temperature range within which no transformation occurs, and allowing sufficient time for the steel to be coiled, (Rashid, 1980).

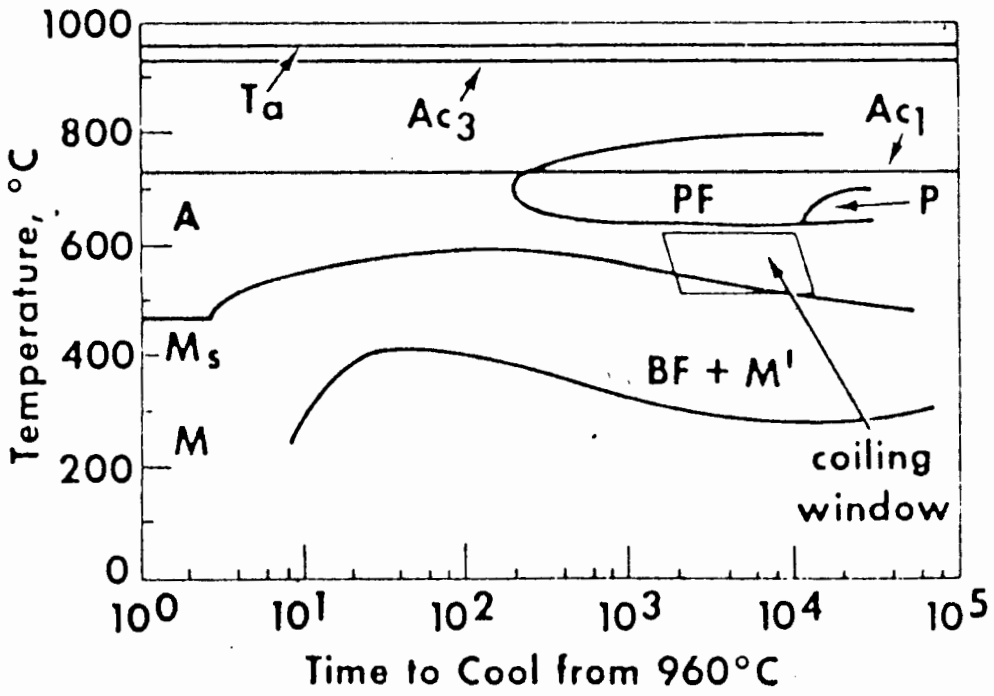

FIG. 2.6 Schematic Continuous Cooling Transformation diagram of an as-rolled dual-phase steel.
(A = austenite, PF = polygonal ferrite, P = pearlite, BF = bainitic ferrite, M = martensite of average C content, M' = martensite from carbon-enriched austenite, Ta = austenitisation temperature.)
Taken from Rashid, 1981.

Coldren and Eldis (1980) used continuous cooling transformation diagrams (CCT) in order to optimise the composition of a plain carbon as-rolled dual-phase (ARDP) steel. It was possible to determine the individual effects of various elements such as chromium and molybdenum on the allowable cooling rates. In dual-phase rolling, important parameters may include the finish rolling temperature; the coiling temperature; the amount of reduction and the cooling rate, (Gréday et al, 1979; Furukawa et at, 1979 and Coldren and Cornford et al, 1979).

2.3 DEFORMATION CHARACTERISTICS

The deformation characteristics of these dual phase steels is quite complex (Rashid, 1981). It could be considered that on straining, dislocation slip occurs first in the constituent with the lowest yield strength (ie. the ferrite phase). When this constituent work hardens to the yield strength of the second constituent (ie. the martensite) this second phase yields. This subsequently results in the total strain being distributed more uniformly amongst both phases and delays or prevents localised necking.

The enhanced formability of these alloys is due to this so-called 'multi-stage' deformation behaviour. This process could also explain the absence of the pronounced yield point. Another possible explanation is as follows. The martensite phase can be considered to be non-deformable. The fact that martensite does deform at higher strains in dual phase steels may indicate that the ferrite acts to confine the martensite helping to prevent fracture and hence allows a ductile response to develop. This behaviour should be contrasted to that of the conventional HSLA steels (ferrite and cementite structure). In this case no obvious deformation of the cementite phase is observed. When the ferrite phase is work hardened to its limit voids form preferentially at the ferrite-cementite interface, and fracture results. In dual phase ferritic-martensitic steels, void

formation only occurs when the harder phase has yielded and deformed, suggesting that the interfacial strength or coherency is critical to the formability performance. There are other possible explanations which will be outlined in the discussion. However, in practice, particles of slag and precipitates such as titanium carbo-nitrides may cause cavitation and subsequent failure.

A detailed consideration of the various deformation models and theoretical treatments describing the strength and ductility in plain carbon dual-phase steels is given by Korzekwa et at, 1980; Araki et al, 1977, and Öström, 1981.

In summary, the ferritic-martensitic dual phase alloys show remarkable strength, elongation and formability properties. This is due primarily to their continuous yielding behaviour which in turn is due to the micro-mechanical response. An important factor in the development of higher elongation is the degree of interface coherency, preventing premature fracture. The strength is controlled by the proportion of martensite which is determined by the correct choice of annealing temperature and quenching rate.

In the next chapter we shall consider how the dual phase alloy can be influenced by the addition of various alloying elements. These additions play a significant role in the development of the final microstructure and hence the ultimate mechanical and physical properties.

CHAPTER 3 : THE EFFECT OF ALLOYING ELEMENTS

Alloying elements have a profound effect upon the microstructure and hence mechanical and physical properties of a particular alloy. These elemental additions control the phase balance (the relative proportion and morphology of the different phases) and are thus critical to any metallurgical treatment. In the Fe - Cr steels, carbon, nitrogen and nickel act as austenitizers, expanding the γ- loop, while chromium and titanium stabilise the ferrite phase, reducing the extent of the γ- loop. To achieve the optimum alloy design by exploiting the dual phase characteristic, a balance between the austenite and ferrite formers will be required. Unlike many other systems, the ($\alpha + \gamma$) region of the Fe - Cr system is narrow and it is anticipated that care will need to be exercised in order to maintain this precise compositional balance. However, in addition to this alteration of the phase balance, alloying additions may influence both mechanical and physical properties, by for example, changing the grain size or interacting with impurity elements to form hard particles. Thus the judicious choice of alloying elements is of fundamental importance when considering the alloy systems and undesirable mechanical properties may result from a variety of sources. Unfortunately, there is little detailed work on the effect of alloying additions with

reference to dual phase alloys in the Fe - Cr system. It will be necessary to examine the Fe - Cr steels in a more general way to give a reasonable set of guidelines for the 12%Cr steel. The importance of the common elements is discussed below:

(i) Chromium acts as a ferrite stabilizer, but its most important characteristic is that it imparts corrosion resistance to the steel. It is generally accepted that a minimum addition of 11,5%Cr is required to render a steel "stainless". Increased chromium content raises the hardenability of the steel (Bee and Honeycombe, 1978).

(ii) In dual phase stainless steel, nickel stabilizes the austenite phase and increases both the strength and toughness (Snape, 1977; Pickering, 1978).

The percentage of ferrite in microduplex ferritic-martensitic steels can be varied by modifying the chromium and nickel content. It has been shown (Snape, 1977) that additions of nickel (2,8 - 5,5%) can depress the DBTT by as much as 147^{o}C for water quenched samples, and up to 257^{o}C for air cooled samples.

The way in which the phase diagram changes by nickel additions is shown in Figure 3.1 for various chromium contents.

To obtain a dual phase alloy at high chromium contents (>18%) requires large nickel additions (>5%). An important point to notice is that for chromium contents greater than approximately 12%, the low and high temperature dual phase regions are connected. Hence it is possible to heat treat these alloys at elevated temperatures (800°C) within the dual phase region and ensure that the subsequent quench results in the ferrite plus austenite transforming to ferrite plus martensite. A chromium content of greater than 12% is thus of critical importance to dual phase alloy fabrication.

Nickel is also important in that it retards corrosion (Bain and Aborn, 1939), and combined with chromium provides unusually superior corrosion resistance properties.

It is important to note that nickel is an exceptional alloying element, in that unlike other alloying elements it does not result in a decrease in toughness that is usually associated with an increase in strength (Pickering, 1978). However nickel is expensive, and therefore it is required to determine the minimum amount of nickel needed to impart the optimum properties to the steel.

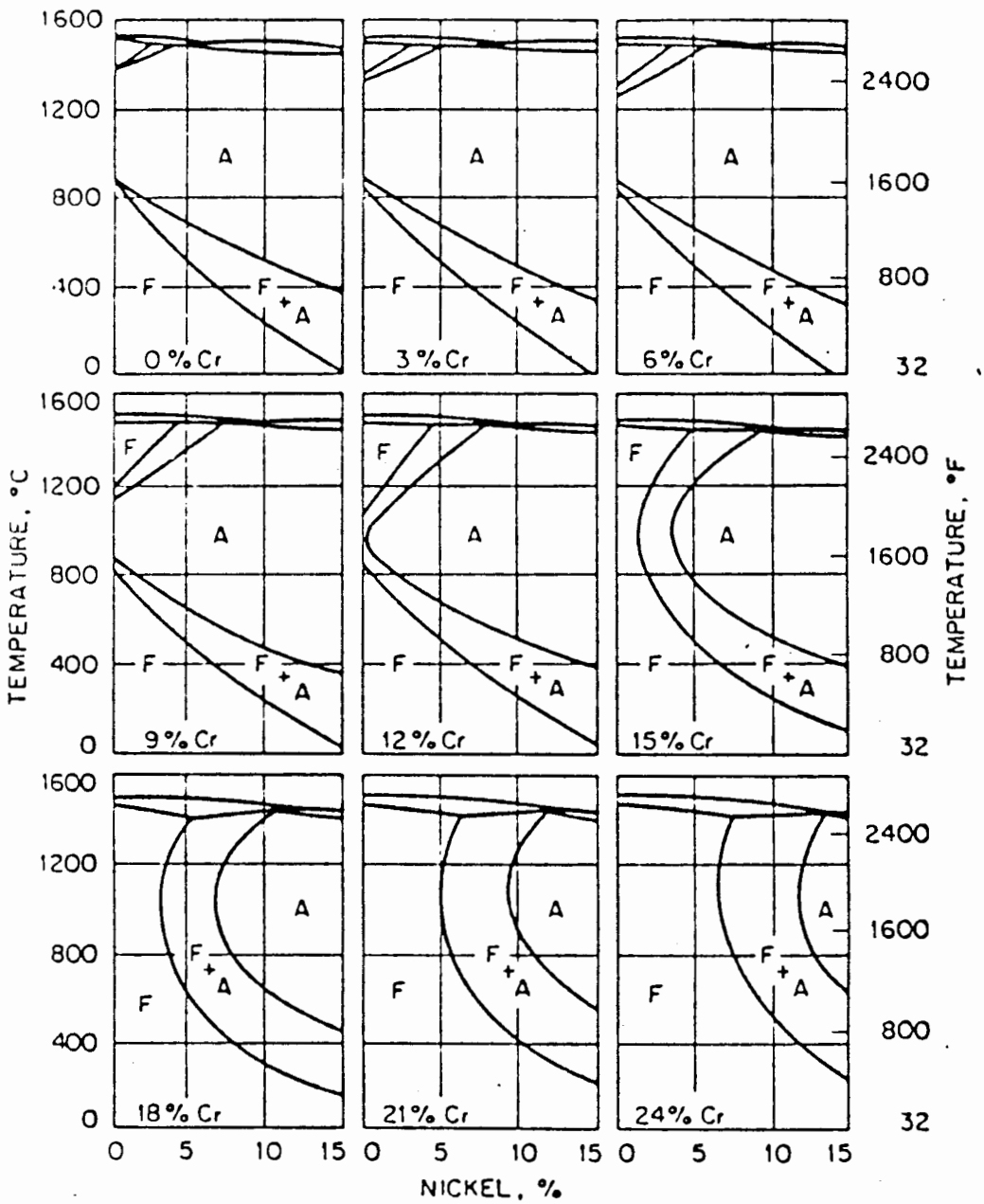

FIG. 3.1 The Fe-Cr-Ni diagram at chromium levels ranging from 0 to 24 percent. (Taken from Bain & Aborn, 1939)

A = austenite

F = ferrite

(iii) Silicon is an important alloying element in dual phase carbon steels and presents a complex interaction, or trade-off, between desired and undesired properties. Many of the influences are not fully understood. Silicon increases the activity of carbon promoting the migration of carbon from the ferrite matrix into the austentic phase. The ferrite becomes interstitial free or 'cleaner' and more ductile, (Thomas and Koo, 1979). However, the increased carbon content in the martensite may decrease the toughness of this phase. Silicon also inhibits carbide formation, particularly Fe_3C, at the ferrite- martensite interface (Thomas and Koo, 1979) and therefore suppresses the pearlite formation. A most significant effect of silicon in dual phase carbon steels (Koo and Thomas 1979[b]) is to increase the slope of the Ac_3 line (see Figure 3.2), thus allowing more flexibility in heat treatment procedures. It is probable that a similar effect occurs in dual phase stainless steel.

Silicon has also been reported to be effective in the grain refinement of the martensite dispersion promoting a fine fibrous micro-structure (Koo and Thomas, 1977).
This type of microstructure provides effective barriers to the motion of dislocations, thereby strengthening the alloy. In general, it has been found that silicon additions improve the ductility of dual phase steel at a given tensile strength level. (Davies, 1979{a}).

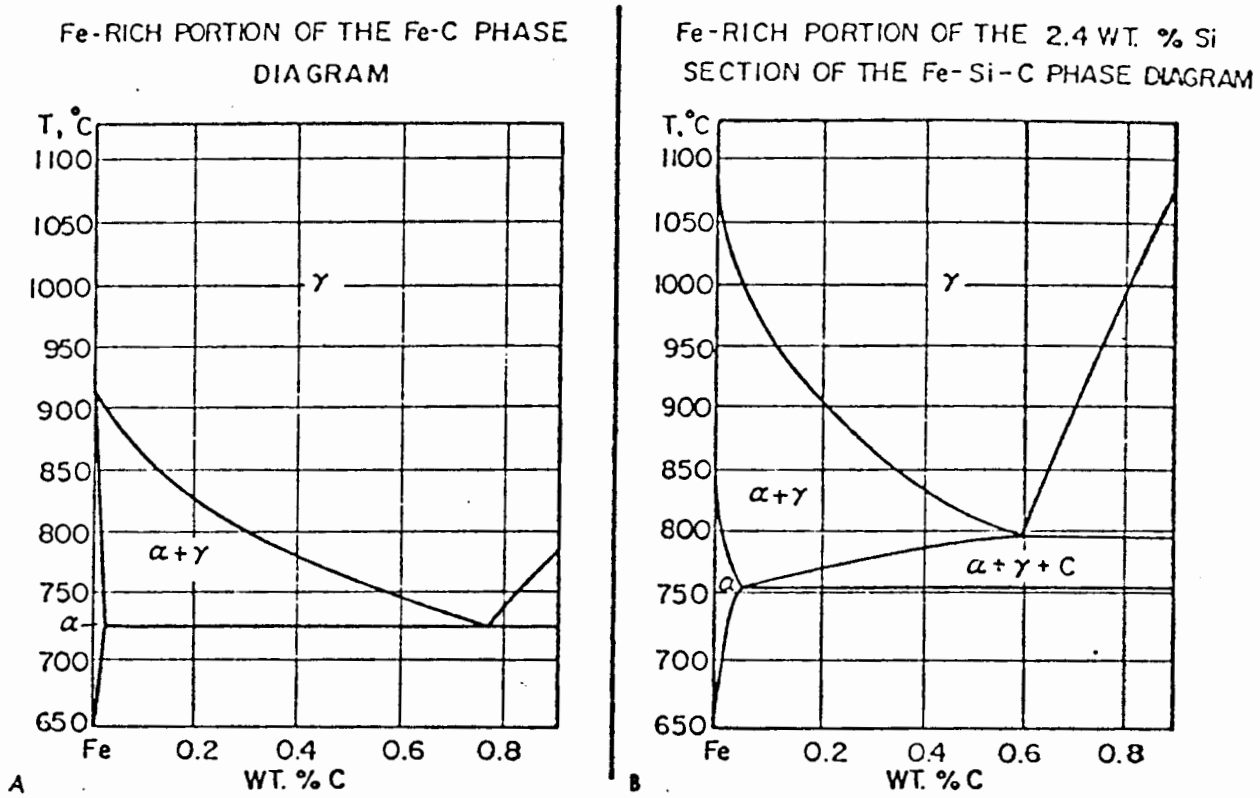

FIG. 3.2 Phase diagrams showing the expansion of the ($\alpha+\gamma$) range when silicon is added to the Fe-C system. (Taken from Koo and Thomas, 1979[b]).

(iv) Manganese partitions preferentially to the austenite, and hence increases the hardenability of the alloy (Rashid, 1981). In general, manganese stabilizes the austenite and lowers the Ms temperature. Manganese may also play a vital role in the steel in 'gettering' the sulphur and forming manganese sulphide stringers.

(v) The role of titanium is to stabilize the stainless steel against intergranular corrosion. Titanium has a greater affinity for carbon and nitrogen, forming titanium carbo-nitride precipitates, and thereby avoids the deleterious formation of chromium carbide ($Cr_{23}C_6$) and chromium nitride precipitates at grain boundaries. The chromium then remains in solution, maintaining the corrosion resistance of the steel. However, the titanium carbo-nitride precipitates are brittle and hard, and can nucleate cleavage cracks and cavities in the ferrite phase (Thomas, 1981), an obviously deteriorating effect which may need careful practical assessment of its significance. The removal of carbon and nitrogen which are strong austenitizers from solution by the 'gettering' action of titanium has a powerful effect on the phase structure.

(vi) Vanadium has a high solubility in the ferrite matrix (Rashid, 1981), and may remain in

solution during anealing, promoting martensite formation, and an increased strength. In non-chromium dual phase steels vanadium is preferred to titanium since it does not as readily form precipitates. However, in the case of Fe-Cr steels, as mentioned in the previous section, it is preferential to allow the formation of titanium carbo-nitride precipitate to prevent loss of chromium from the matrix, and the use of vanadium in these steels is not recommended.

(vii) The effects of carbon have previously been mentioned; carbon levels must be kept as low as possible (<0,1%) in order to maintain the high toughness value of the martensite. Low carbon martensite has a tough lath-type morphology (Krauss and Marder, 1971) while high carbon martensite is twinned and brittle.

In structural applications where welding is necessary, a low carbon content is advantageous in order to prevent sensitisation ($Cr_{23}C_6$ formation) and the formation of intergranular cracks in the heat affected zone (HAZ).

(viii) Nitrogen is also a strong austenitizer and has similar effects to carbon. Nitrogen content must also be kept low to prevent chromium nitride precipitate formation and subsequent intergranular cracking.

Kaltenhauser (1971) has shown that it is possible to construct an empirical formula which takes into account the various percentage alloying element and determines whether the steel will be austenitic (martensitic), ferritic, or dual phase. This formula gives the so-called ferrite factor (FF), and may provide a convenient guideline for alloy design.

$$FF = \%Cr + 6(\%Si) + 8(\%Ti) + 4(\%Mo) + 2(\%Al) + 4(\%Nb) - 2(\%Mn) - 4(\%Ni) - 40[\%(C + N)]$$

An indication of the phases present in a stainless steel is also given as a function of the ferritizing and austenitizing elements in the well known Schaeffler diagram. The diagram (Fig. 3.3) was initially used to predict the microstructure of welds. It can be seen that the composition of 3CR12 has been chosen to lie in the ferrite plus martensite region.

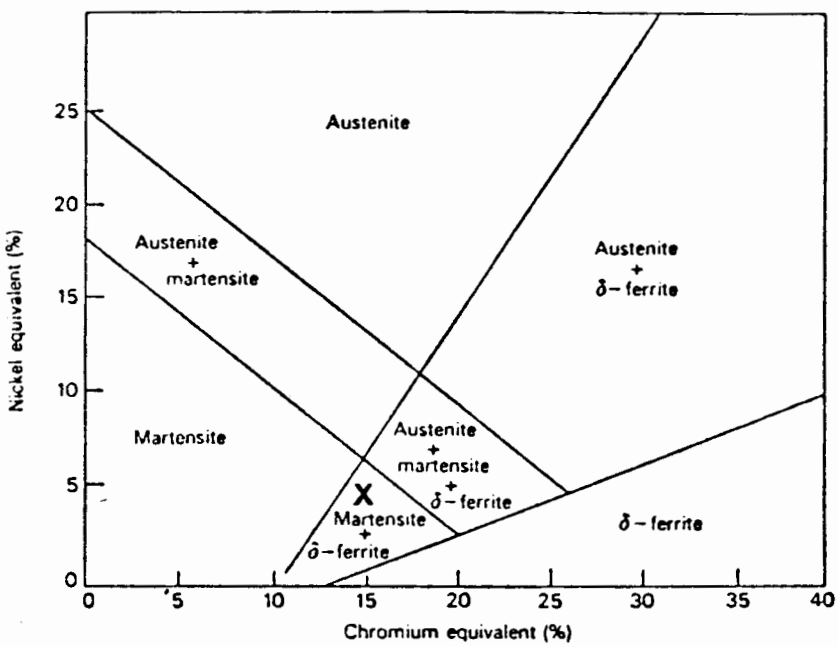

FIG. 3.3 Modified Schaeffler diagram (taken from Honeycombe, 1981).
X = Position of 3CR12 (ie. in ferrite plus martensite region) on Schaeffler diagram.

Cr equivalent = (Cr) + 2(Si) + 1,5(Mo) + 5(V) + 5,5(Al) + 1,75(Nb) +1,5(Ti) +0,75(W)

Ni equivalent = (Ni) + (Co) + 0,5(Mn) + 0,3(Cu) + 25(N) + 30(C)

CHAPTER 4 : EXPERIMENTAL TECHNIQUES

4.1 ALLOY COMPOSITIONS

Alloys of nineteen compositions were supplied by Middelburg Steel and Alloys (Pty) Ltd. The composition of the alloys for two different chromium contents, ie. 11,5% Cr and 14,3% Cr are listed below in Table 4.1 and Table 4.2 respectively, together with their ferrite factors (FF). The formula given by Kaltenhauser (1971) (see previous chapter) was used to determine the ferrite factor, viz:

$$FF = \%Cr + 6(\%\,Si) + 8(\%Ti) - 2(\%\,Mn) - 4(\%\,Ni) - 40[\%(C+N)]$$

All samples were received in the as-rolled condition and a homogenizing treatment was given at 1000°C for one hour followed by slow cooling in the furnace. Specimens suitable for dilatometry, metallography and hardness testing were prepared from the nineteen samples.

The above-mentioned heat treatment was considered necessary in order to relieve the effects of the hot-rolling procedure on the resultant microstructure. For instance, in the AHR condition, the microstructure depicts a banded dual phase structure (see Fig. 4.1(a)). However, after a heat

treatment of one hour at 1000°C followed by a furnace cool, the micrograph (Fig. 4.1(b)) depicts a more homogeneous duplex structure. This homogeneous (as opposed to a banded) structure is preferred when investigating the phase transformation characteristics of an alloy.

11,5% CHROMIUM									
ALLOY	% C	% S	% P	% Mn	% Si	% Ti	% N	% Ni	FF
A	0,03	0,02	0,02	0,83	0,45	0,32	0,03	0,27	11,62
B								0,49	10,74
C								0,85	9,30
D								1,19	7,94
E								1,34	7,34
F								1,77	5,62
G								1,84	5,34
H								2,71	1,86
I								3,50	-1,30

TABLE 4.1 Chemical composition (in weight percent) of 3CR12 alloys containing 11,5%Cr. The ferrite factor for each alloy is also included.

14,3% CHROMIUM									
ALLOY	% C	% S	% P	% Mn	% Si	% Ti	% N	% Ni	FF
1	0,03	0,02	0,02	0,85	0,46	0,31	0,03	0,62	12,96
2								0,98	11,52
3								1,41	9,80
4								1,80	8,24
5								2,40	5,84
6								2,80	4,24
7								3,90	-0,16
8								4,70	-3,36
9								5,60	-6,96

TABLE 4.2 Chemical composition (in weight percent) of 3CR12 alloys containing 14,3% Cr. Included also is the ferrite factor for each alloy.

FIG. 4.1(a) Micrograph of Alloy B (11,5%Cr; 0,49%Ni) in the as-hot-rolled (AHR) condition, depicting a banded, dual phase ferritic-martensitic microstructure.

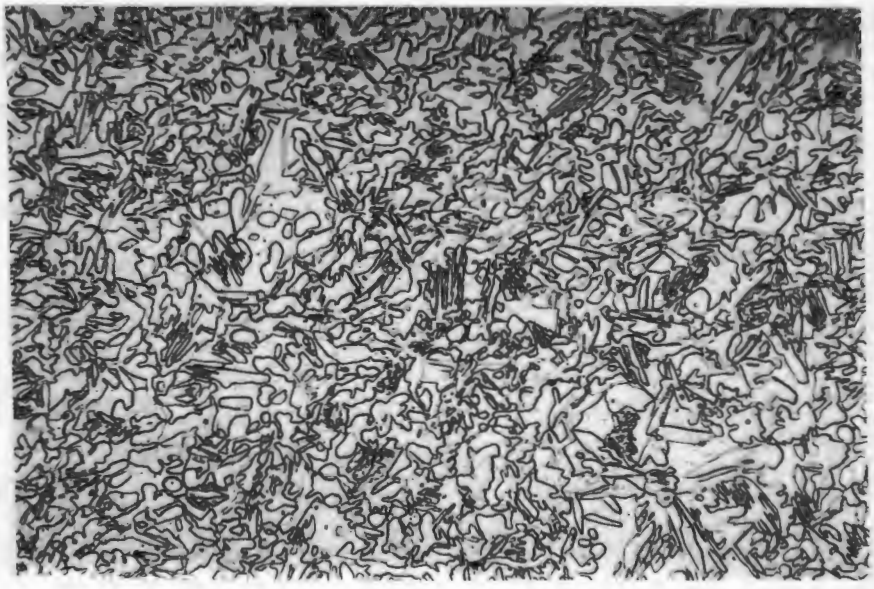

FIG. 4.1(b) Micrograph of Alloy B (11,5%Cr; 0,49%Ni), depicting a duplex ferritic-martensitic microstructure. Heat treatment consisted of 1 hour at 1000°C followed by a slow cool (furnace cool).

Prior heat treatment : AHR

100 μm

4.2 DILATOMETRY

The X-ray, thermal and microscopical methods are the most useful for the investigation of phase changes in the solid state, but in some cases it is necessary to supplement or replace these by other methods. Any physical property which changes at a phase boundary may be used, but the method of dilatometry described in this chapter is more suitable than others.*

Dilatometry is a well established technique (Hume-Rothery et al, 1952) in the determination of equilibrium phase diagrams. The dilatometric method utilizes the change in volume associated with nearly all phase changes. It is usually applied by measuring the change in length (or volume) of a specimen heated or cooled at a given rate. Curves of length versus temperature and (temperature versus time) may usually be simultaneously obtained.

A Leitz dilatometer (Model UBV) (see figure 4.1) was used in order to obtain the transformation temperatures under slow heating and cooling conditions.

---

* *It was not possible to use the x-ray method in order to distinguish between the various phases due to the very low carbon content (0,03%) of this steel, (Roberts, 1953). Consequently the distortion of the ferritic and martensitic lattice parameters is minimal.*
(Refer to Fig. B.1 in Appendix B).

FIG. 4.2 The Leitz dilatometer (Model UBV) used in this investigation to obtain the transformation temperatures of an alloy under slow heating and cooling conditions.

Since the work involved the determination of phase transformation characteristics, it was desirable to use as slow a heating and cooling rate as possible (with the equipment available of course). For this reason, a preliminary investigation into the effect of a range of heating rates (from 3°C/min up to 7,5°C/min) in the transformation temperatures of a few selected alloys was carried out.

No significant differences were observed in the transformation temperatures for the heating rates in the range of 3°C/min to 5,5°C/min. However, at slightly higher heating rates (5,5°C/min to 7,5°C/min) slight variations in transformation temperature were observed (differences of approximately 15- 25°C). It should be mentioned here that for the determination of so-called 'equilibrium' phase diagrams, very slow heating and cooling rates are required in order to ensure (as far as possible) that equilibrium conditions are attained or else at least are approached. For this reason, a heating rate of 3°C/min was selected in order to determine the temperatures at which phase transformations may occur in these alloys.

In a similar dilatometric study of the phase transformation characteristics in a high purity iron-chromium (9.6% Cr) alloy, Bee and Honeycombe (1978) employed a heating rate of 1°C/min using a commercial Netzch dilatometer. Moreover, this type

of dilatometer had facilities for programmed heat treatment with a range of heating and cooling rates up to 20°C/min.

The question then arises whether the heating rate (3°C/min) used in this investigation is indeed slow enough in order to allow sufficient time for the system to 'equilibrate.' At the outset of this investigation, no information concerning the kinetics of transformation in these particular alloys was available. Thus, there was no idea whether equilibrium conditions were actually being attained. For this reason, it is important to stress that the phase diagrams as presented in this thesis are not intended to represent phase equilibrium diagrams, but rather should be considered as phase transformation diagrams under the conditions specified. Nevertheless, useful information on the phase transformation characteristics may still be obtained, and is presented in this thesis.

A serious problem was encountered when it came to selecting an appropriate cooling rate. Unfortunately it was not possible to use a programmed cooling rate with the equipment available. However, it was possible to employ two cooling rates - a furnace cool (which is generally considered as a very slow cooling rate) (Reed-Hill, 1973; Cottrell, 1975) and an air cool (intermediate cooling rate).

Specimens (dimensions 50mm x 4mm x 4mm) of each alloy composition were thus heated at an average rate of 3°C per minute in a furnace over the high temperature range of 20°C to 1500°C. For experiments above 1000°C argon was flushed over the sample to prevent oxidation and spurious results.

At the maximum desired temperature, the dilatometer was switched off, allowing the specimens to furnace cool.*

At least four dilatation versus temperature curves were obtained for each alloy composition. The curves for the lower temperature experiments ($T<1000°C$) were analyzed as follows (see fig. 4.3). The upper curve is obtained on heating, with a transformation occurring at a temperature T_1, where the curve deviates from linearity. A volume contraction accompanies this change up to a certain temperature T_2, whereupon the transformation is largely complete. (A volume contraction on heating is due to the transformation of a BCC phase → FCC phase). A small amount of the starting phase remaining is finally converted in the temperature range from T_2 to T_4.

---

* *Since it was possible to effectively remove the furnace and allow the specimen to air cool, a preliminary investigation into the effects of cooling rate ie FC as opposed to AC; was also conducted.*
Note: This was only possible with the low temperature experiment since air cooling from 1 400°C posed a problem with severe oxidation of the samples tested. This in turn would not allow for the accurate interpretation of the dilatometric traces obtained.

During cooling, the high temperature phase transforms at a temperature T_5. This reaction is complete at T_6 (Volume expansion, FCC → BCC)

To construct the phase diagram the following procedure was used (Figure 4.4).

Using temperature and percentage nickel as graph axes, transformation temperatures T_1 and T_2 were plotted for the particular alloy contents*.

---

* *The temperatures T_1 and T_2 may be referred to as the Ac_1 and Ac_3 temperatures respectively. Also T_5 and T_6 may be referred to as the Ms and Mf respectively.*

Curves were then drawn through the T_1 points to determine the phase boundary. Similarly, points T_2 were joined to indicate the higher temperature phase boundary*. Thus, three phase regions can be described (A, B and C). It is anticipated that region A is the fully ferritic structure, B is the dual phase ($\alpha + \gamma$) region and C is the fully austenitic region.

For the high temperature experiments (T>1000°C) additional phase transformations can and are expected to occur (refer to Figure 3.1 in Chapter 3). Figure 4.5 is a typical dilatometer trace of this higher temperature phase. The following sequence of events is occurring.

A transformation occurs at T_1 which is near completion at T_2. From T_3 to T_4 an additional high temperature transformation takes place which involves an increase in volume. Upon cooling, a reverse transformation between T_5 and T_6 occurs. At T_7 the final low temperature transformation takes place, which is complete at T_8.

---

* *It should be noted from Figure 4.3 that T_2, T_3 or T_4 may be referred to as the temperature at which transformation is complete. The T_2-T_4 transformation of the low temperature experiment (T<1000°C) was not observed on the traces obtained for all the alloys tested; for example in Fig. 5.1 (ii) and (iii), the dilatometric traces for a low nickel and a high nickel alloy (11,5%Cr) do not depict the T_2-T_4 transformation which is observed in Fig. 4.3. Furthermore, this latter transformation was not observed in the dilatometric traces obtained from the high temperature experiment (for example see Figs. 4.5 and 5.23). For this reason, T_2 was chosen as the temperature at which the transformation is largely complete.*

Figure 4.6 shows how the transformation temperatures T_3 and T_4 determined by dilatometry are plotted to derive the phase diagram. Clearly seen now is the additional region D at elevated temperatures.

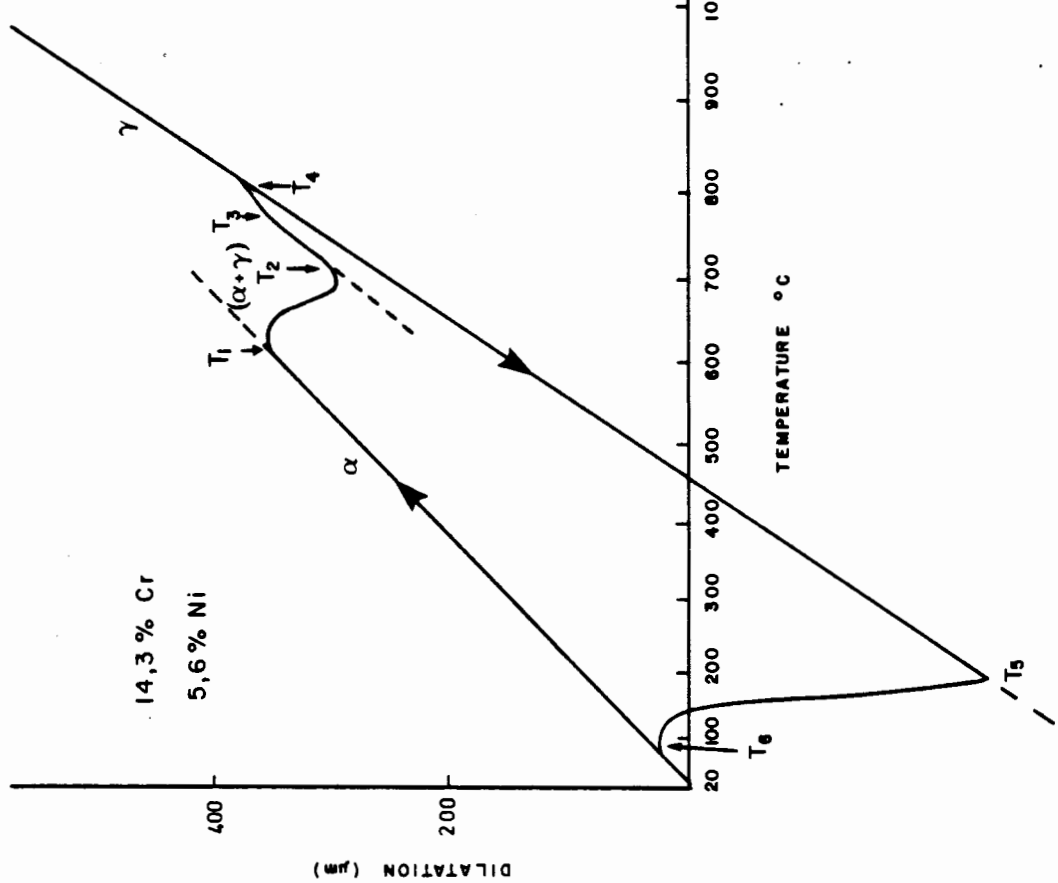

FIG. 4.3 Typical Low temperature (ie T<1000°C) dilatometer trace indicating temperatures at which phase changes occur, for both heating and cooling cycle.

NOTE: Arrows indicate heating and cooling cycle.

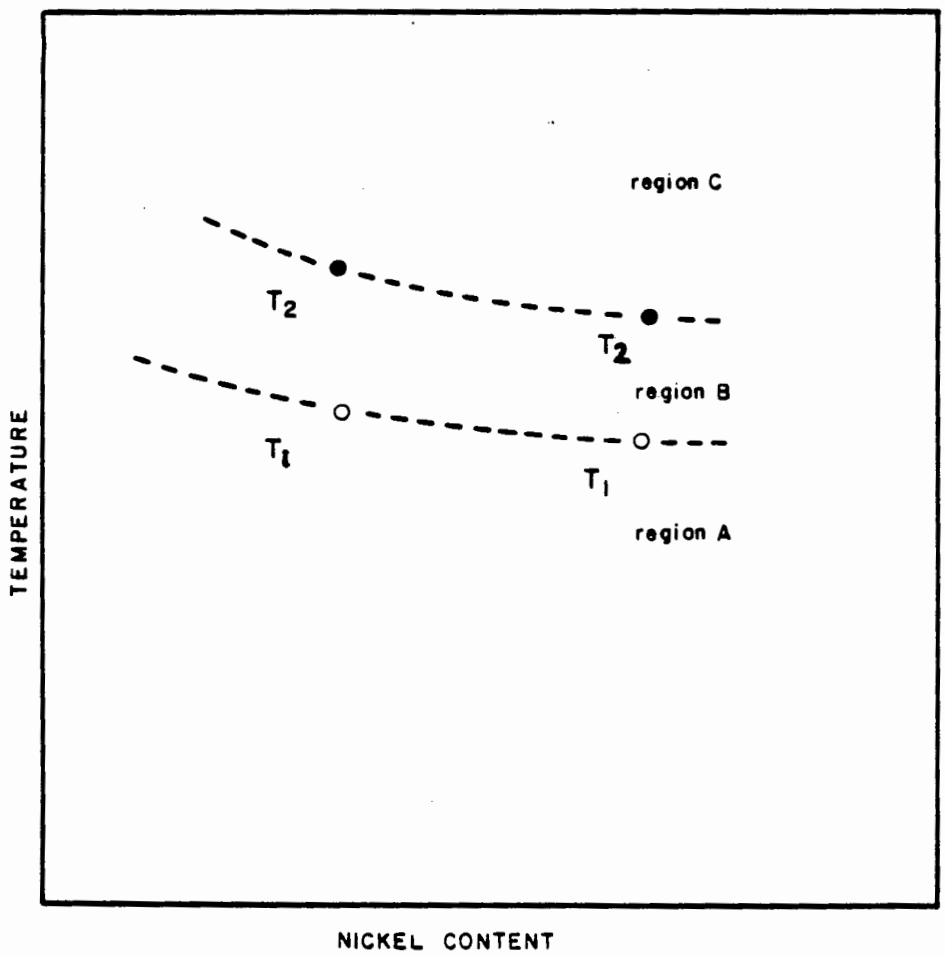

FIG. 4.4 Schematic diagram showing the construction of phase diagram including using T_1 and T_2 temperatures obtained from Figure 4.3

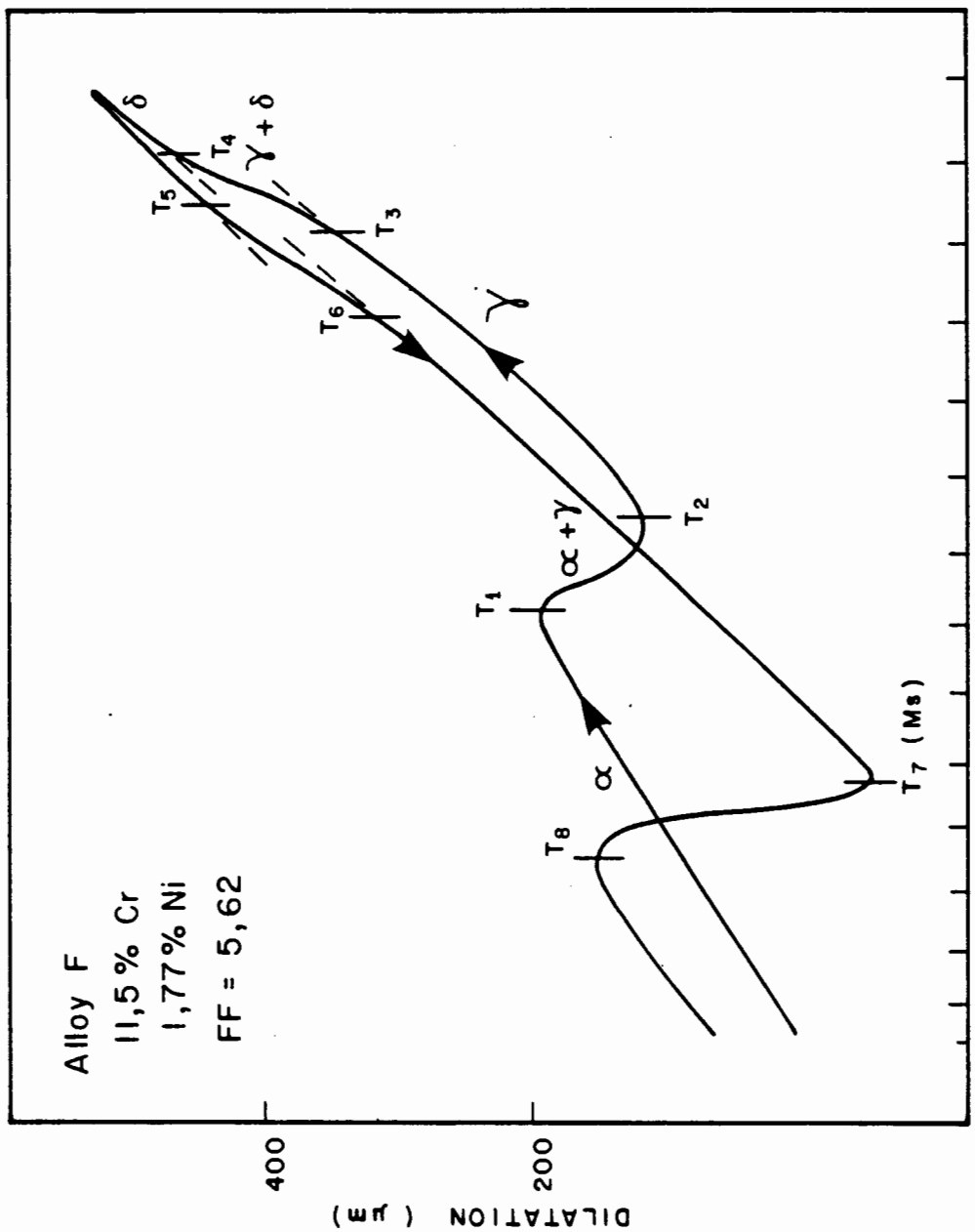

FIG. 4.5 Typical dilatometer trace for the high temperature (T>1000°C) experiment. Transformation temperatures, T_i, indicating phase changes are shown.

Note: Arrows indicate heating and cooling cycle.

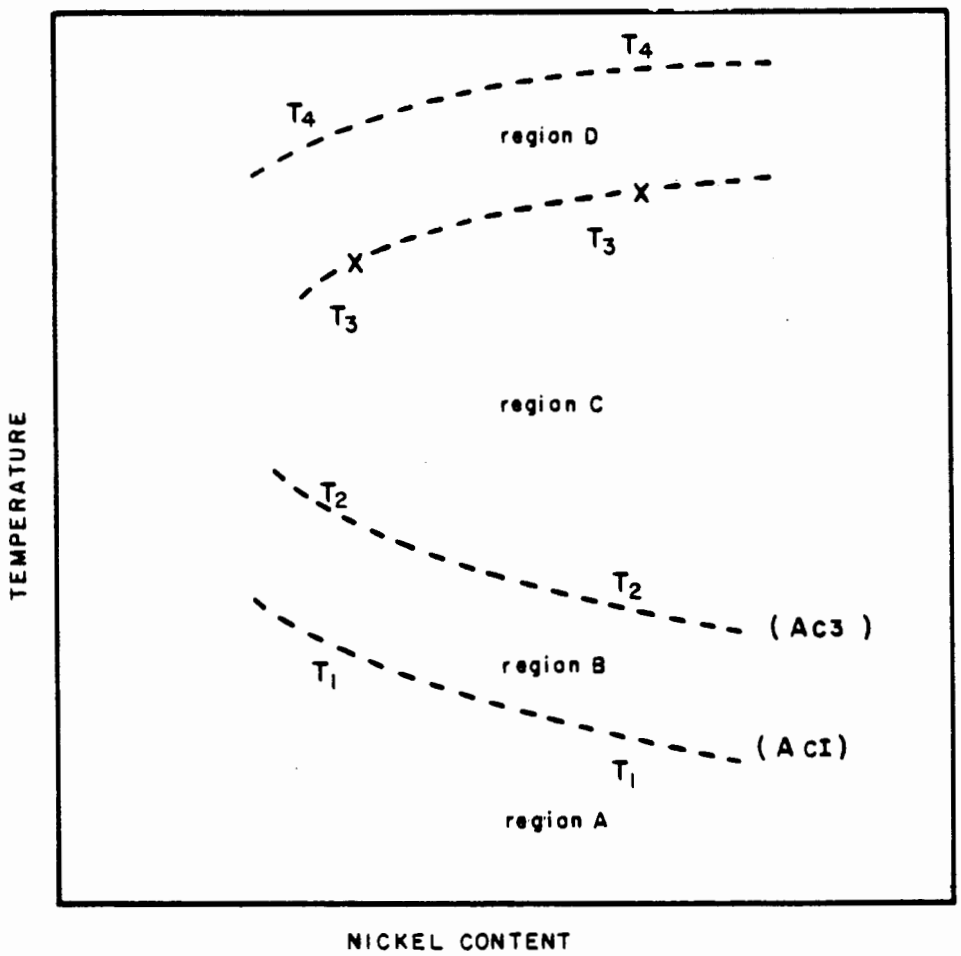

FIG. 4.6 Schematic diagram showing the construction of phase diagram including high temperature transformation T_3 and T_4 (obtained from Figure 4.5)

4.3 METALLOGRAPHY

In order to examine the phases present at different temperatures, various heat treatments were carried out in the temperature range 700°C-1000°C. Specimens of each alloy composition were held at temperature for one hour followed by quenching into water. Each sample was then mechanically polished on alumina grit paper to a fineness of 1000 μm after which they were diamond polished to a 0,25 μm finish. A 10 percent oxalic acid solution was used to electro-etch the samples at a potential of 10V for times ranging between one minute to three minutes depending on the nickel content.

Micrographs were taken of the various microstructures using a Reichert microscope.

In addition, optical metallography was performed on all the alloys in the as-hot-rolled (AHR), ie. as-received condition. Micrographs were also recorded for the alloys after being heat treated at 1000°C (one hour) and subsequently furnace cooled (annealing treatment).

---

* *Since the kinetics of transformation in these alloys was still unkown, the time required at a particular temperature for equilibrium conditions to be attained was also not known. However, since this work is intended as a preliminary investigation into the microstructure and phase transformation characteristics of these alloys, the selected annealing time of one hour seemed adequate at that stage. Furthermore, an annealing time of one hour may be related to acceptable industrial annealing schedules.*

An attempt was made to qualitatively investigate the effect of a wide range of cooling rates on the resultant microstructure. The various cooling rates ranged from: a furnace cool or 'full anneal' and represents very slow cooling; (Reed-Hill, 1973); an air cool or 'normalizing' heat treatment representing an intermediate cooling rate; and oil quench (fast cooling rate); and finally a water quench indicating a very rapid cooling rate.

4.4 T.E.M.

It is possible to differentiate phases using transmission electron microscopy. Thin foils were prepared from bulk specimens of the samples used for the metallographic examination and observed in a JOEL 200 CX electron microscope operating at 200 keV. Samples were prepared as follows:

1. Rolling to reduce the thickness of the alloy to 1mm.

2. Heat treatment at temperature (675°-860°C) for various times (60 mins to 300 mins). The specimens were annealed in a vacuum furnace at better than 133×10^{-4} pascals in order to prevent oxidation.

3. Subsequent to heat treatment, the specimens were oil quenched.

4. Electropolishing was carried out using a 10% perchloric acid solution in butanol at -30°C. This process thins the sample without introducing any damage.

5. Thin ($<1\mu m$) areas of the electropolished specimen were selected and carefully partitioned into a microscope grid assembly.

6. The prepared specimens were kept free from contamination by immersion in alcohol.

4.5 HARDNESS MEASUREMENTS

An indication of the nature and proportion of the various phases present may be assessed by hardness measurements. Specimens of each alloy composition were heat treated at various temperatures between 700°C-1000°C; held at temperature for one hour, followed by quenching into water. Using a load of 300 newtons, hardness values (in Vickers or VPN) were recorded. These hardness values recorded at RT may provide a useful guide as to the strength of the alloy.*

---

*NOTE: *To avoid any possible confusion, the hardness values quoted in this work, for instance the hardness value at 900°C does not imply a hot hardness measurement, but the hardness value measured at RT after quenching from a high temperature anneal.*

4.6 TEMPERING CHARACTERISTICS

In order to determine the tempering characteristics of 3CR12, alloys with a low, medium and high nickel content were investigated. These alloys were chosen to determine the effect of nickel content. The following procedure was carried out:

1. The alloys were heat treated at 1000°C for one hour followed by an oil quench.

2. After quenching, the alloys were tempered for one hour at various temperatures between 300°C-700°C and then quenched.

The effect of these various temperatures was monitored by the use of hardness tests, and optical metallography.

CHAPTER 5 : RESULTS

5.1 THE 11,5% Cr-Ni ALLOYS

5.1.1 Dilatometry

5.1.1.1 Low Temperature Experiments (T<1000°C)

Typical dilatometer traces for the 11,5%Cr alloys are shown in Fig. 5.1. The effect of an increased nickel content is to decrease the transformation temperatures on heating and on cooling to decrease the low temperature transformation temperature. With increased nickel content a considerable hysteresis effect is noted, delaying the start of the reverse transformation on the cooling cycle. For comparison purposes, a typical trace for a single phase alloy (AISI 409) undergoing no transformation whatsoever is also included.

5.1.1.2 High Temperature Experiment (T>1000°C)

By heating the alloys to elevated temperatures (1400°C) it was possible to distinguish the dual phase ($\gamma+\delta$) and δferrite region which exist at high temperatures. A typical trace is shown in Fig. 4.5 (Chapter 4).

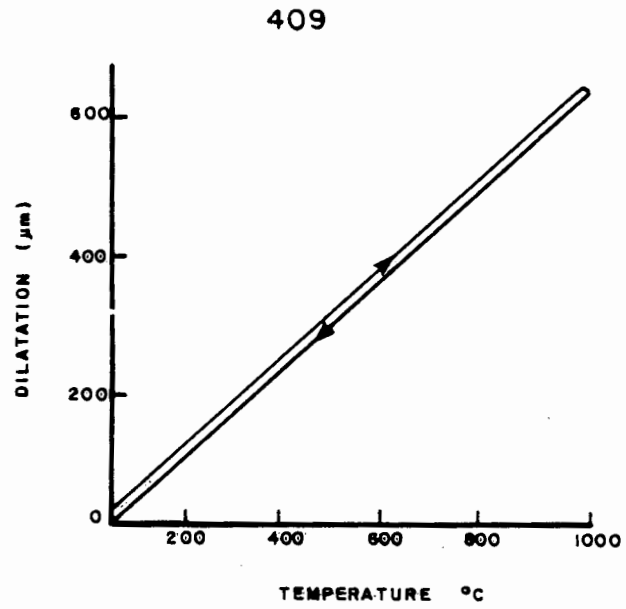

(i) A typical trace obtained for a single phase alloy (AISI 409) undergoing no transformation.

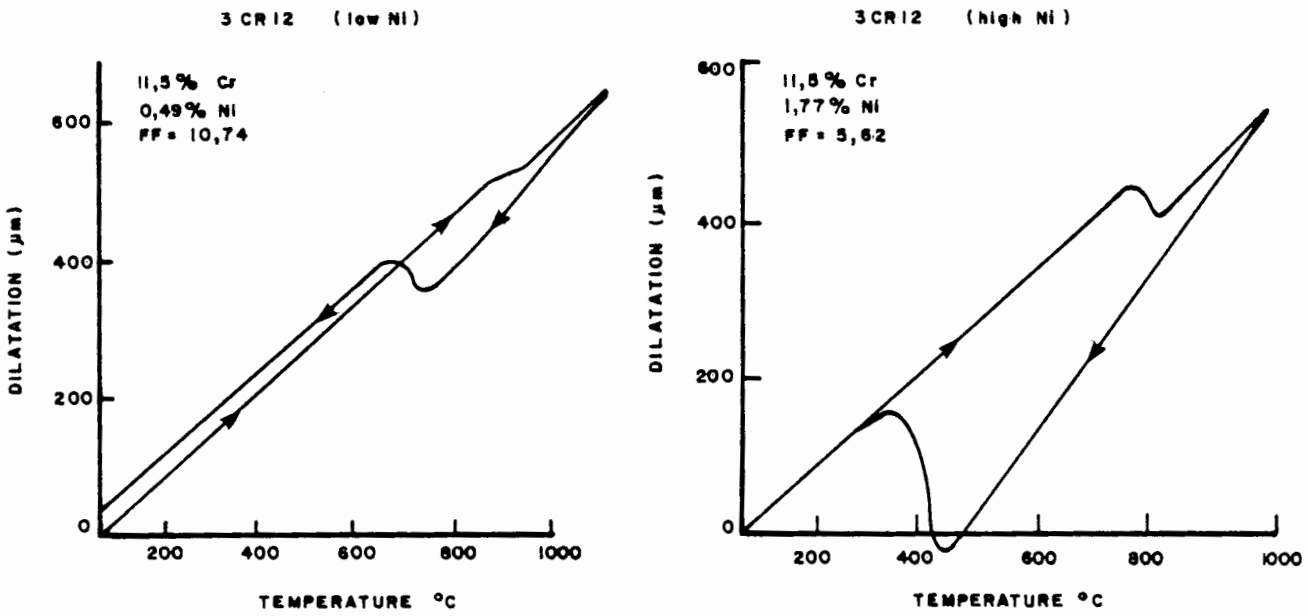

Typical trace obtained for (ii) a low nickel and (iii) a high nickel alloy.

FIG. 5.1 Typical dilatometric trace obtained for (ii) a low nickel alloy compared to (iii) a high nickel alloy and (i) a single phase alloy (409).

It will be noted that there is a slight hysteresis in the high temperature transformation i.e. $(\gamma + \delta) \rightarrow \delta$ and the reverse transformation.

5.1.2 The Phase Transformation Diagram

The transformation temperatures obtained in the low temperature experiments ($T<1000°C$) for both the heating and cooling cycle are tabulated in Table 5.1. The transformation temperatures obtained during the heating cycle are plotted as a phase transformation diagram in Fig. 5.2. In Fig. 5.3 the transformation temperatures obtained during the cooling cycle are also included. Note that at this stage we cannot identify the exact nature of the phases but by analogy with the Fe-Cr-Ni phase diagram of Fig. 3.1, we can speculate that dual phase $(\alpha+\gamma)$ regions are present. It should be noted here that although martensite is not an equilibrium phase, the importance of this constituent, especially when discussing dual phase ferritic-martensitic steels should not be underestimated.

In the alloys investigated in this work, the martensite, although it is metastable, happens to be the phase which is present at

RT. For these reasons, the martensitic transformation temperatures are also included in some of the 'phase transformation diagrams', remembering that these diagrams are not intended to represent equilibrium phases.

The transformation temperatures obtained from the high temperature (T>1000°C) experiments are tabulated in Table 5.2, and the transformation temperatures obtained during the heating cycle are plotted in Fig. 5.4. Also included in Fig. 5.5 are the transformation temperatures obtained during the cooling cycle (T>1000°C).

For comparison purposes, both the transformation temperatures that were obtained in the low temperature experiment (T<1000°C) and those that were obtained during the high temperature (T7 1000°C) experiment (heating cycle only) are plotted in Fig. 5.6; and in Fig. 5.7, the transformation temperatures obtained during cooling are also included in the phase diagram.

A comparison of the transformation temperatures obtained from the low temperature experiments (T<1000°C) with the

values obtained from the high temperature experiments (T>1000°C) (heating cycle only) may be seen in Table E.1 of Appendix E. According to this table the discrepancy between T_1 (T<1000°C) and T_1 (T>1000°C) ranged from approximately 5°C to a maximum of 65°C while the average difference between T_1 (T<1000°C) and T_1 (T>1000°C) is approximately 20°C. However, the average difference between T_2 (T<1000°C) and T_2 (T>1000°C) is approximately 46°C.

Table E.2 (Appendix E) shows a comparison of transformation temperatures obtained from the low temperature experiments (T<1000°C) with the values obtained from the high temperature experiments (T>1000°C) (cooling cycle only). The average difference between T_7 (T>1000°C) and T_5 (T<1000°C) is approx. 40°C and for T_8 (T>1000°C) and T_6 (T<1000°C) is approx 30°C.

However, no direct correlation between these discrepancies in transformation temperatures and nickel content is evident.

It appears from Fig. 5.6 that the temperature range T_1 to T_2 obtained from the high temperature experiments (T>1000°C) is slightly larger than the T_1 - T_2 temperature

range observed from the low temperature experiments (T<1000°C). Initially this might seem to suggest that the transformation temperature, T_3 and T_4 of the (T<1000°C) experiments may be a more accurate indication of the temperature at which transformation is complete (as opposed to T_2). However, T_3 and T_4 was not observed in all the alloys tested and for this reason T_2 is taken as the temperature at which transformation is complete. Furthermore, the metallographic results shown in Fig. 5.11 seem to suggest that the Ac_3 for the high nickel alloys, ie alloy H (2,71% Ni) and alloy I (3,5% Ni) should be much lower.

It should be noted from Fig. 5.7 that the M_s temperature range extends from approximately 550°C to $\sim$350°C and the M_f temperature range from $\sim$450°C to $\sim$230°C.

It is generally agreed that this reaction is the martensite reaction because of the characteristic low temperature range in which this reaction is occuring and also because bainite is not normally observed in the 12% Cr alloys "even at very slow cooling rates" (Pickering, private communication). Evidence that this is the martensite reaction occuring at low temperatures is further provided by metallography and TEM.

However, it will be noted from Fig. 5.3 and Fig. 5.7 that for alloy B (0,49% Ni) the reverse transformation upon cooling begins at approximately 750°C and is complete at $\sim$ 680°C. It is very unlikely that this is the martensite reaction occuring at such high temperatures and it is probable that a ferritic-type reaction is occuring. It can be seen from Fig. 5.11 that the metallographically obtained micrograph for alloy B does indeed indicate a ferritic structure.

In a kinetic and microstructural study into the formation of ferrite from austenite in a high purity Fe-7% Cr - 2% Ni alloy, Ricks et al, 1981, observed two separate reaction kinetic characteristics which implied that two different ferrite reactions occured in the temperature range between 550°C - 760°C. The high temperature reaction (600°C - 760°C) was shown to produce a mixture of equiaxed and Widmanstätten ferrite.

However it should be noted that the reverse transformation upon cooling for alloy B which is observed in Fig. 5.3 and Fig. 5.7 is not observed in the high temperature experiment, for instance see Fig. 5.5.

Clearly more information is required on the isothermal transformation characteristics of these alloys.

11,5% Cr		TRANSFORMATION TEMPERATURES			
Alloy	% Ni	Heating (°C)		Cooling (°C)	
		$T_1(A_{c1})$	$T_2(A_{c3})$	$T_5(M_s)$	$T_6(M_f)$
A	0,27	900	*	*	*
B	0,49	870	950	760	680
C	0,85	810	907	560	455
D	1,19	775	860	480	460
E	1,34	755	840	450	340
F	1,77	750	820	430	325
G	1,84	725	830	425	320
H	2,71	655	770	360	255
I	3,50	630	760	340	230

* No transformation temperature observed on dilatometric trace

TABLE 5.1: Transformation temperatures obtained during the heating and cooling cycle from the low temperature experiment ($T<1000^{o}C$) for the 11,5%Cr Alloys.

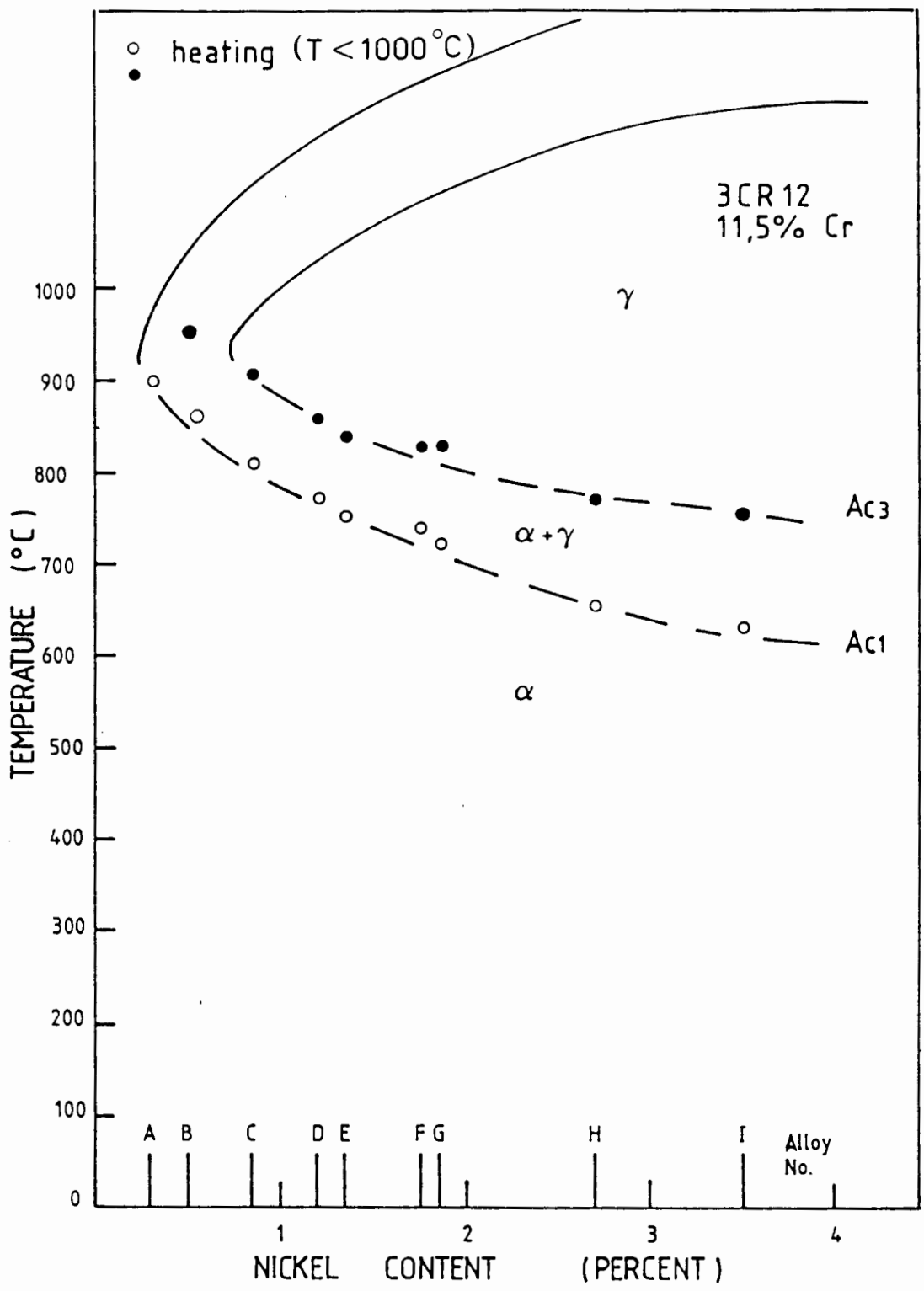

FIG. 5.2 Transformation temperatures obtained during the heating cycle of the low temperature ($T<1000^{o}C$) experiments plotted as a 'phase transformation diagram' for the 11,5%Cr alloys.

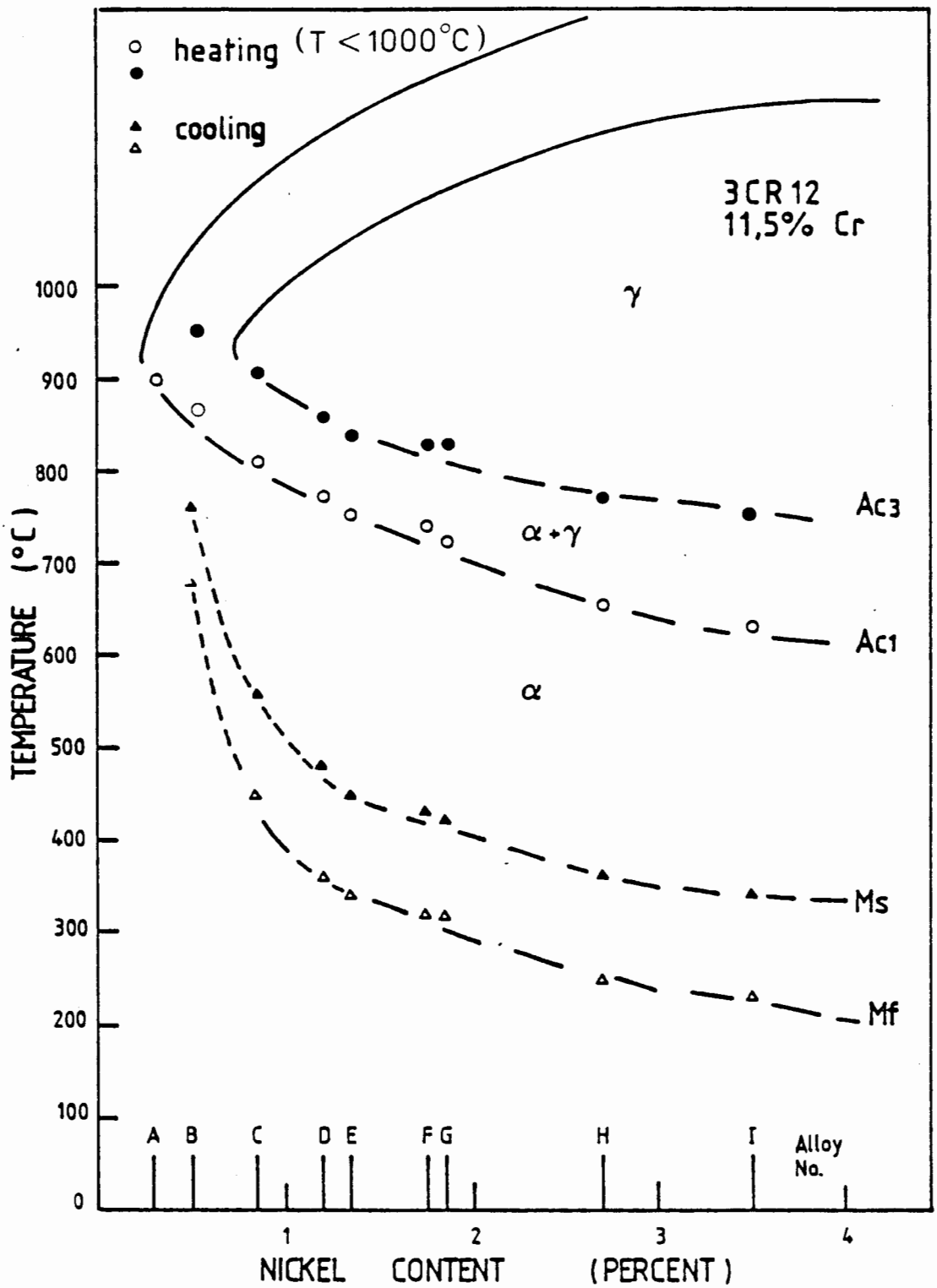

FIG. 5.3 The 'Phase Transformation diagram' of the 11,5%Cr alloys showing transformation temperatures obtained during the heating and cooling cycle in the low temperature experiments ($T<1000^{o}C$).

11,5% Cr		TRANSFORMATION TEMPERATURES							
Alloy	% Ni	Heating (°C)				Cooling (°C)			
		$T_1(A_{c1})$	$T_2(A_{c3})$	T_3	T_4	T_5	T_6	$T_7(M_s)$	$T_8(M_f)$
A	0,27	940	1000	1100	1240	*	*	*	*
B	0,49	840	975	*	*	*	*	*	*
C	0,85	820	980	1195	1270	1185	1080	550	450
D	1,19	780	920	1190	1245	1185	1090	540	420
E	1,34	760	920	1210	1245	1180	1090	520	400
F	1,77	730	850	1210	1320	1240	1120	455	360
G	1,84	660	830	1220	1330	1320	1230	*	*
H	2,71	665	850	1210	*	*	*	420	270
I	3,50	630	800	1210	*	*	*	350	225
* No transformation temperature observed on dilatometric trace									

TABLE 5.2 : Transformation Temperatures obtained during the heating and cooling cycle (T>1000°C) for the 11,5%Cr alloys.

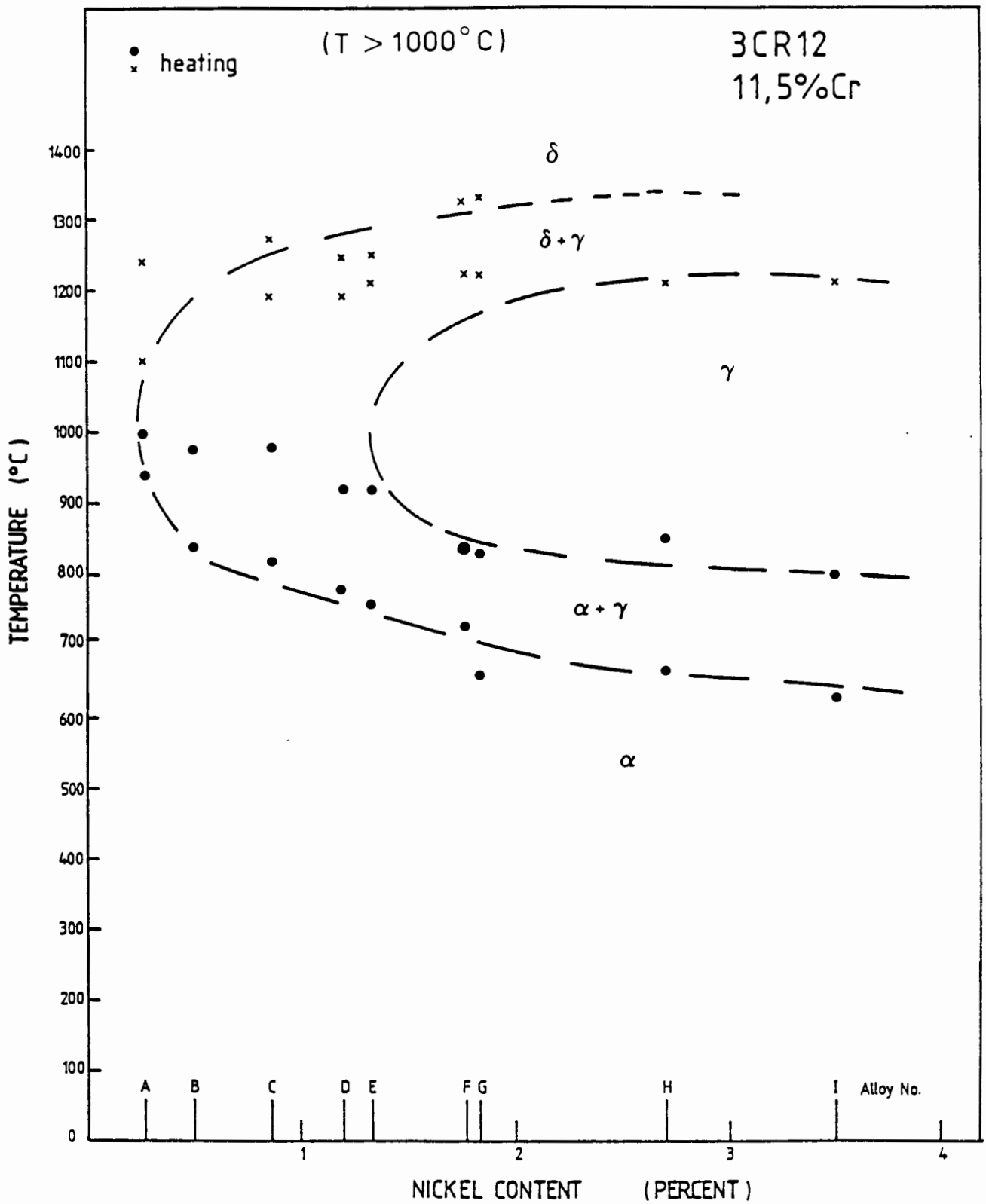

FIG. 5.4 Transformation temperatures obtained during the heating cycle of the high temperature (T>1000°C) experiments plotted as a 'Phase Transformation Diagram' for the 11,5%Cr alloys.

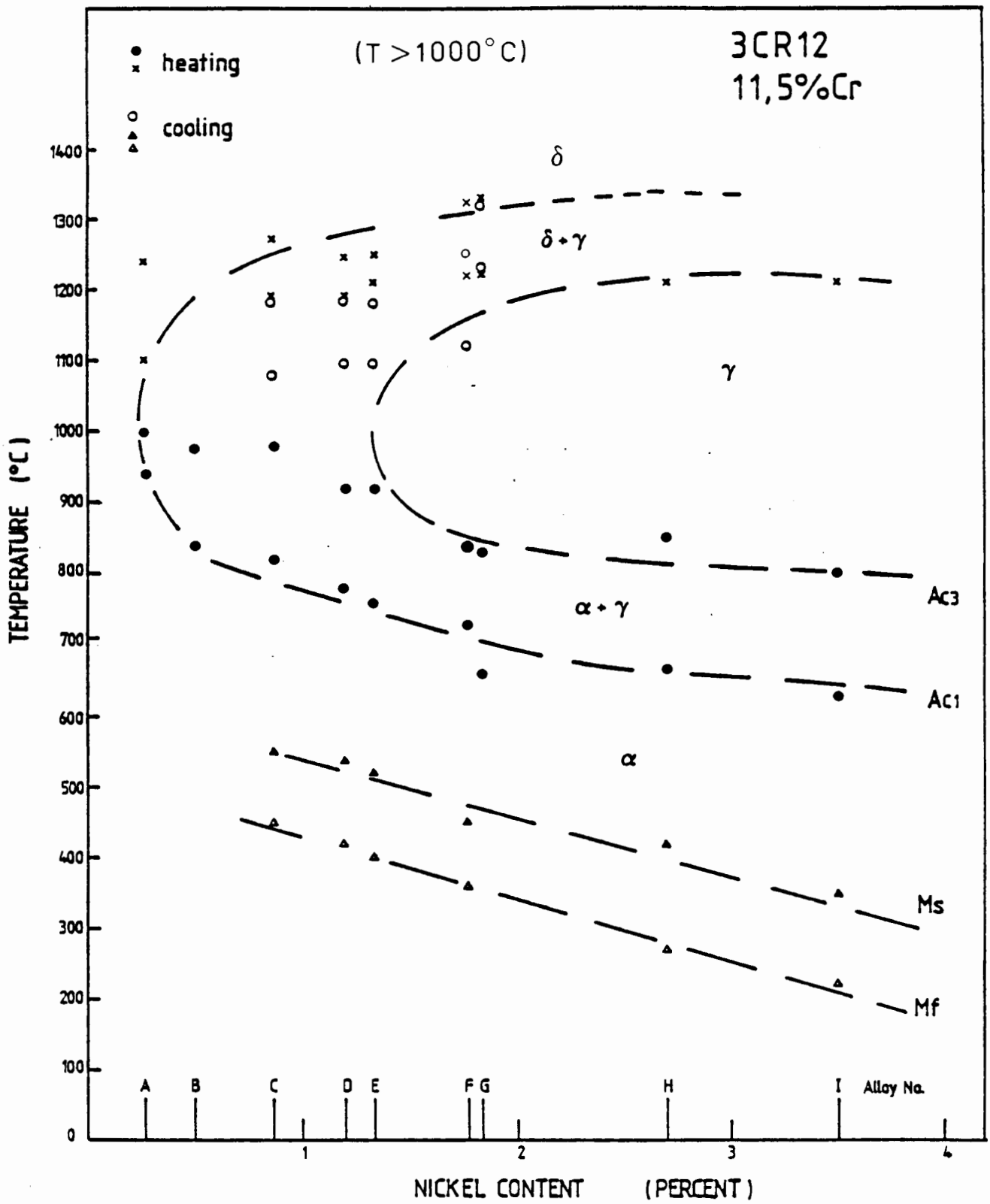

FIG. 5.5 The 'Phase Transformation Diagram' for the 11,5%Cr alloys showing transformation temperatures obtained during the heating and cooling cycle (T>1000°C).

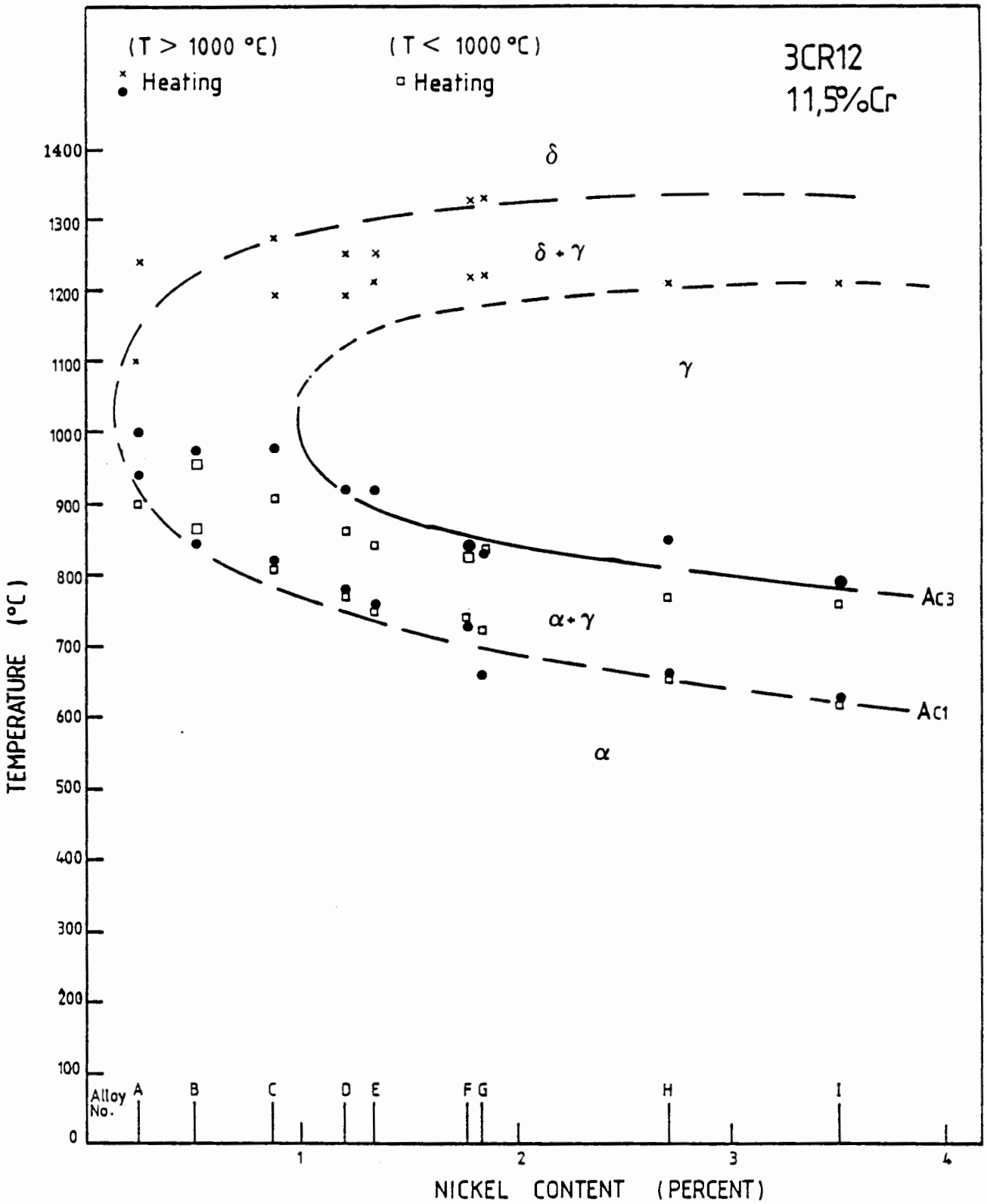

FIG. 5.6 Transformation temperatures obtained during heating cycle for both low temperature ($T<1000^{o}C$) and high temperature ($T>1000^{o}C$) experiments plotted as a 'Phase Transformation Diagram' for the 11,5% Cr alloys.

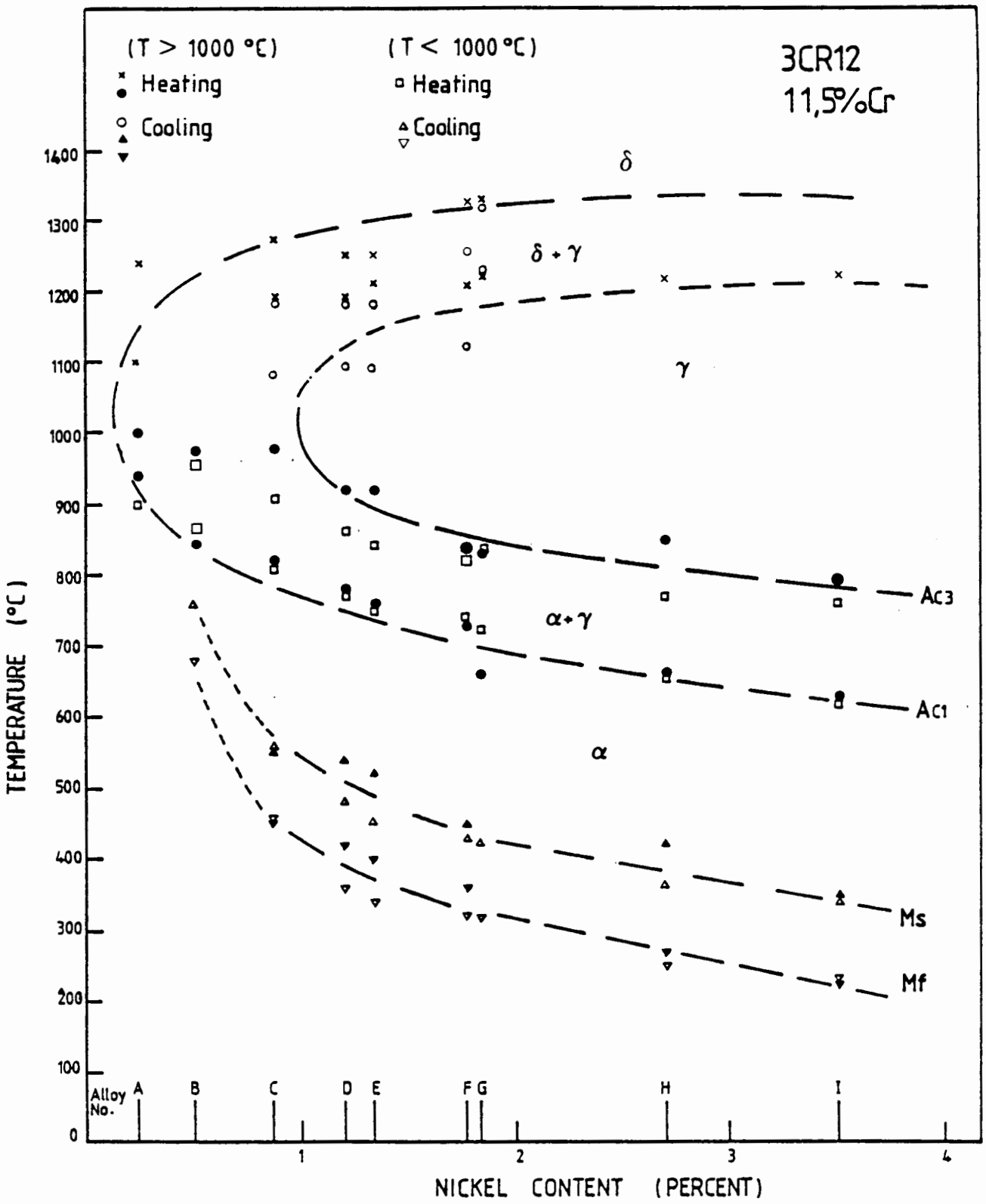

FIG. 5.7 The Phase Transformation Diagram for the 11,5%Cr alloys showing both heating and cooling transformation temperatures obtained in the (T<1000°C) and (T>1000°C) experiments.

5.1.3 Metallography

To identify the phases present at different temperatures, optical metallography was used. For example, for identical anneals at 800°C, Figure 5.8 shows a single phase fully ferritic structure (Alloy A; 0,27%Ni); Figure 5.9 is a dual phase ferritic-martensitic structure (Alloy E; 1,3%Ni), while Figure 5.10 is predominantly martensitic (Alloy H; 2,7%Ni).

On Figure 5.11, the phases identified optically are plotted on the combined 'Phase Transformation Diagram'. This diagram shows both the heating and cooling transformation temperatures obtained in the (T<1000°C) and (T>1000°C) experiments. The results predicted by the dilatometer are, to a certain degree, confirmed.

However, some of the results that are obtained metallographically do not coincide with that predicated by the phase transformation diagram on Fig. 5.11. For example, at 700°C, alloys C (0,85% Ni); D (1,19% Ni), and alloy E (1,34% Ni) should, according to the diagram be fully ferritic. However, after a one hour anneal at 700°C followed by a water quench, the micrographs

revealed a duplex structure for alloys C, D and E. In addition, alloys H (2,71% Ni) and I (3,5% Ni) should be dual-phase ferrite-austenite (martensite) at 700°C but the metallographically obtained results indicate a predominantly martensitic structure for these two alloys. It appears that the agreement between the dilatometrically obtained results and those obtained by metallography is not very good, especially at low temperatures, ie at 700°C.

There are various reasons why the phases predicted by the dilatometer are not those observed metallographically. The transformation kinetics of these alloys was still unknown at the time of testing and the annealing time of one hour might not have been sufficient time for the reaction occuring to go to completion. Another possible explanation may be that the heating rate of 3°C/min used in this investigation is not slow enough. For instance at a heating rate of say, 0,1°C/min, (which was not possible with the equipment available), the transformation temperatures T_1 and T_2 may change and allow for better agreement. However, it will be noted, that at higher temperatures, for example, from 800°C → 1000°C, agreement is rather good. This is

probably due to the more rapid diffusion and transformation kinetics at the higher temperature (ie 800°C - 1000°C) as opposed to the lower temperature (ie 700°C).

Figs. 5.12 (a) → (d) show micrographs depicting the effect of increasing nickel additions on the morphology ie shape, size and distribution of the second phase (martensite) in a ferritic matrix. The specimens had all received identical heat treatments. These microstructures will be discussed in more detail in Chapter 6.

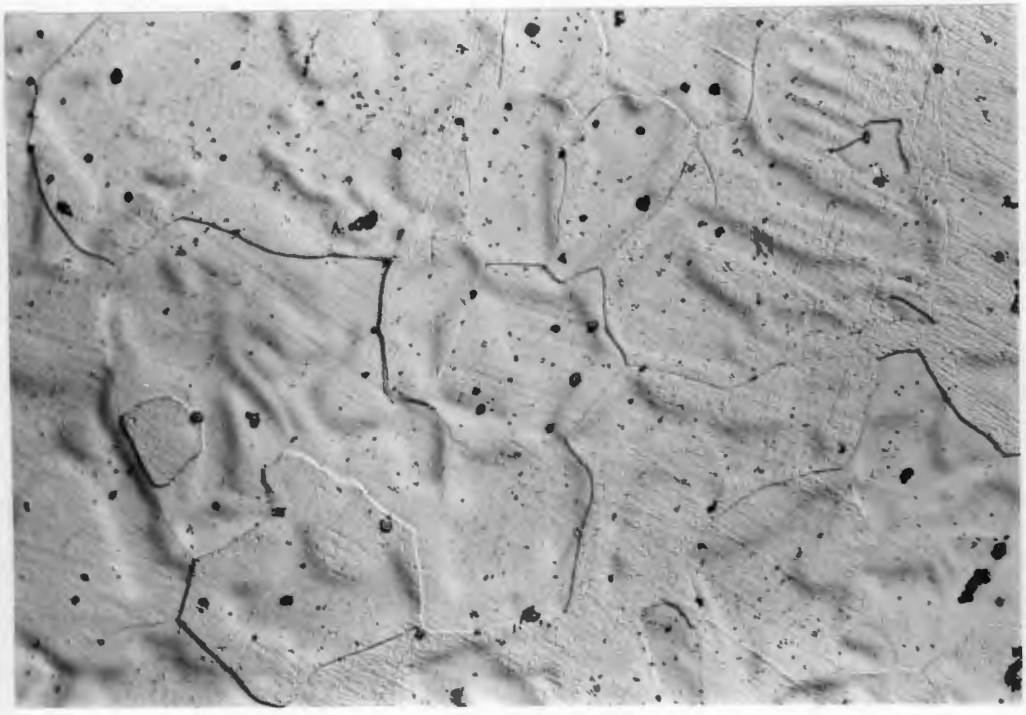

FIG. 5.8

Alloy A: (11,5%Cr; 0,27%Ni)
depicting fully ferritic microstructure

Heat Treatment: Held at temperature (800°C) for 1 hour followed by quenching into water

Prior Heat Treatment:
i) Alloy received in as-hot-rolled condition
ii) A homogenizing treatment at 1000°C (1 hour) followed by a furnace cool

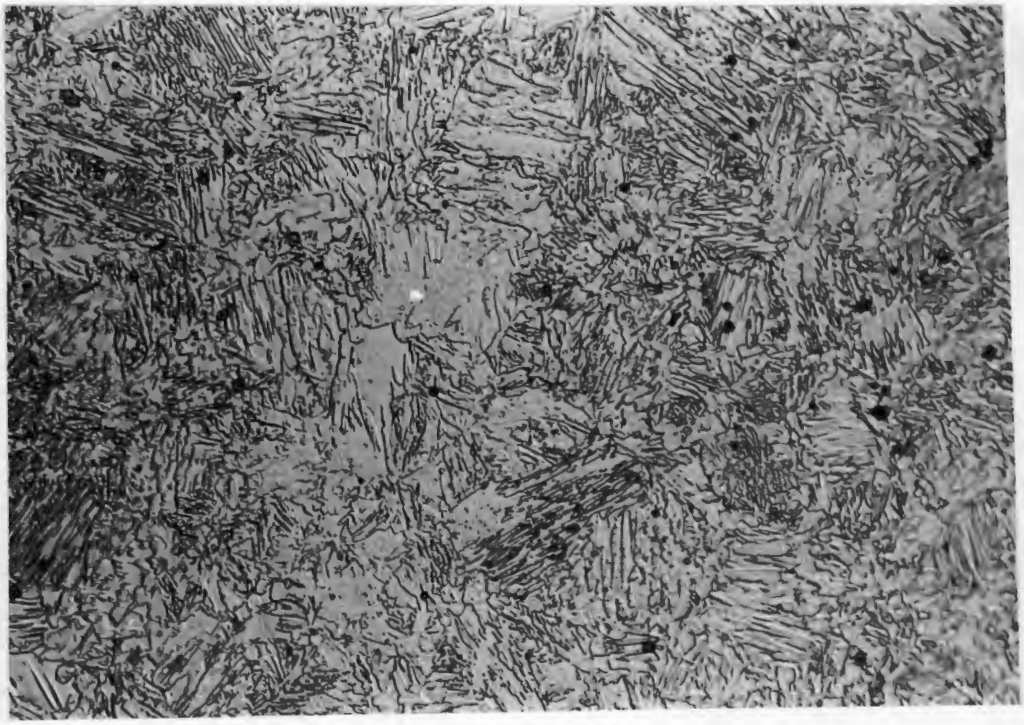

FIG. 5.9

Alloy E: (11,5%Cr; 1,3%Ni)
depicting ferritic-martensitic duplex structure

Heat Treatment: Held at temperature (800°C) for 1 hour followed by a water quench

Prior Heat Treatment:
i) Hot-rolled condition (as received) followed by a
ii) homogenizing treatment at 1000°C (1 hour) plus furnace cooling

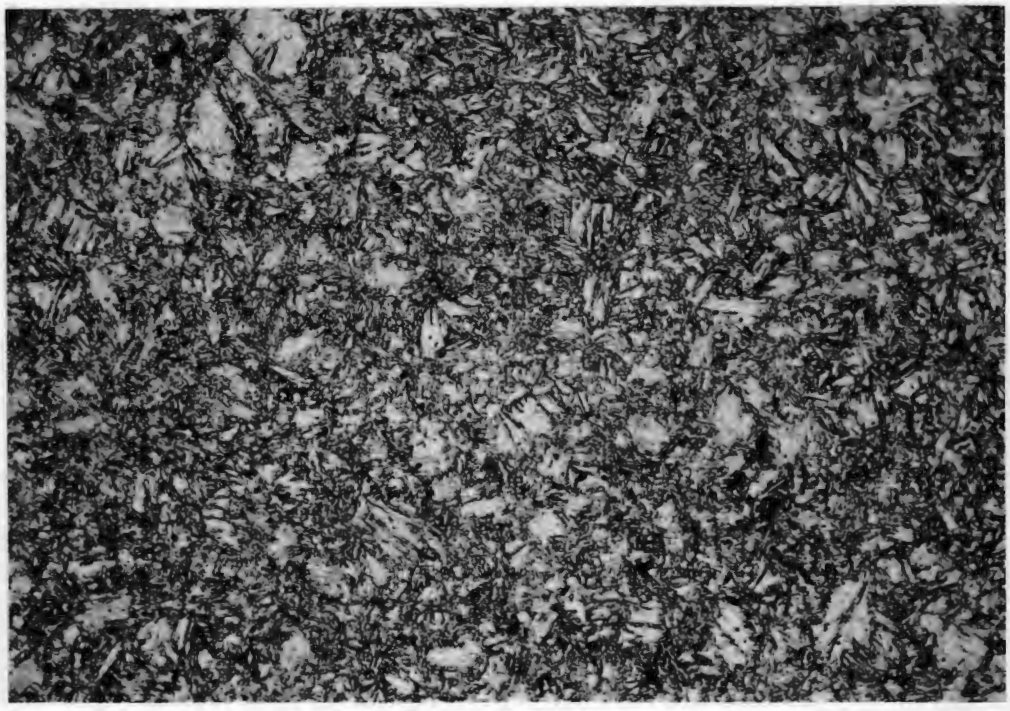

FIG. 5.10

Alloy H: (11,5%Cr; 2,71%Ni)
showing predominantly martensitic structure with traces of ferrite.

Heat Treatment: Held at temperature (800°C) for 1 hour followed by a water quench

Prior Heat Treatment:
i) Alloy received in as-hot-rolled condition
ii) A homogenizing treatment at 1000°C (1 hour) followed by a furnace cool

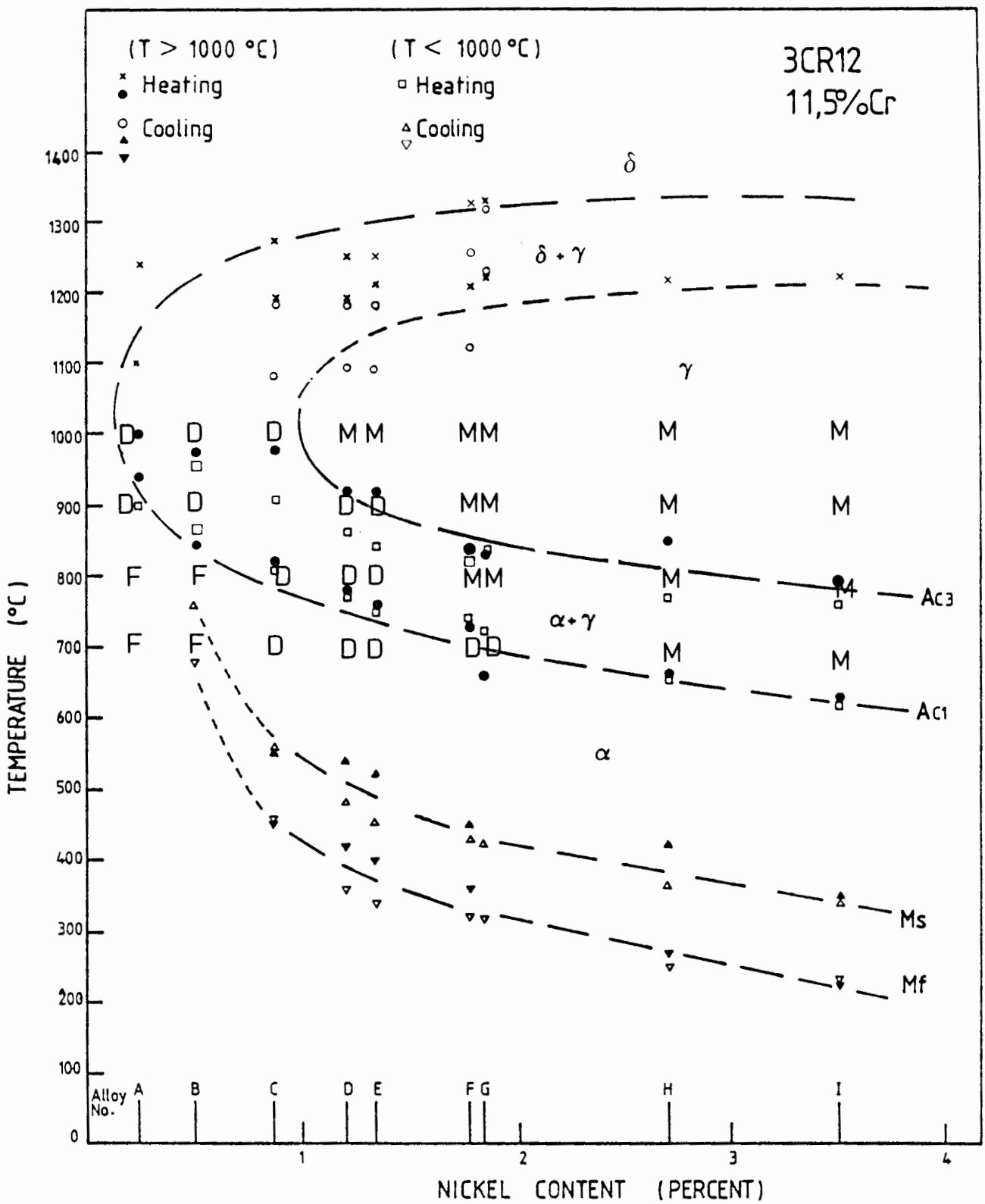

FIG. 5.11 The 'Phase Transformation Diagram' for the 11,5%Cr alloys indicating the phases present at a particular annealing temperature.
F= ferrite: D= duplex ferritic-martensitic and M= martensitic microstructure.

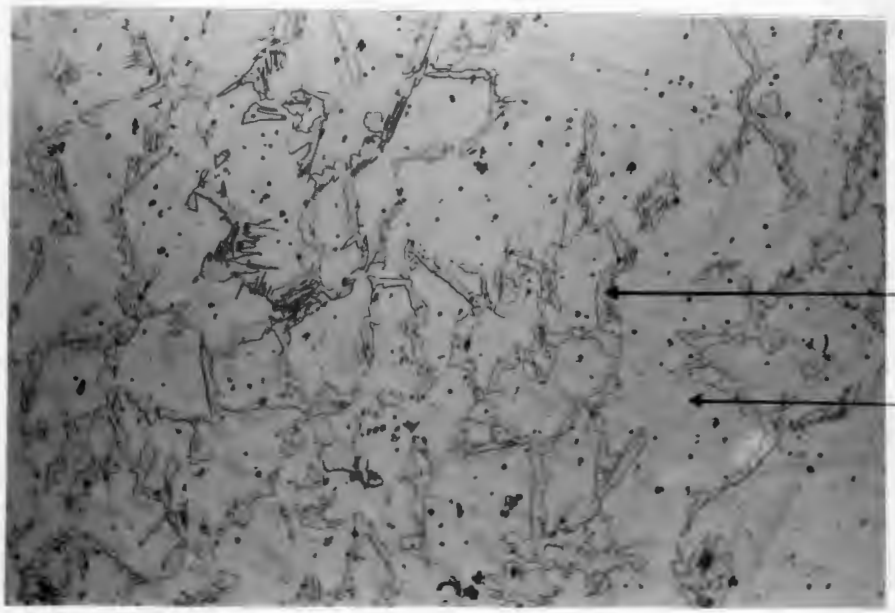

(a) Alloy A : (I‡,5%Cr; 0,27%Ni)

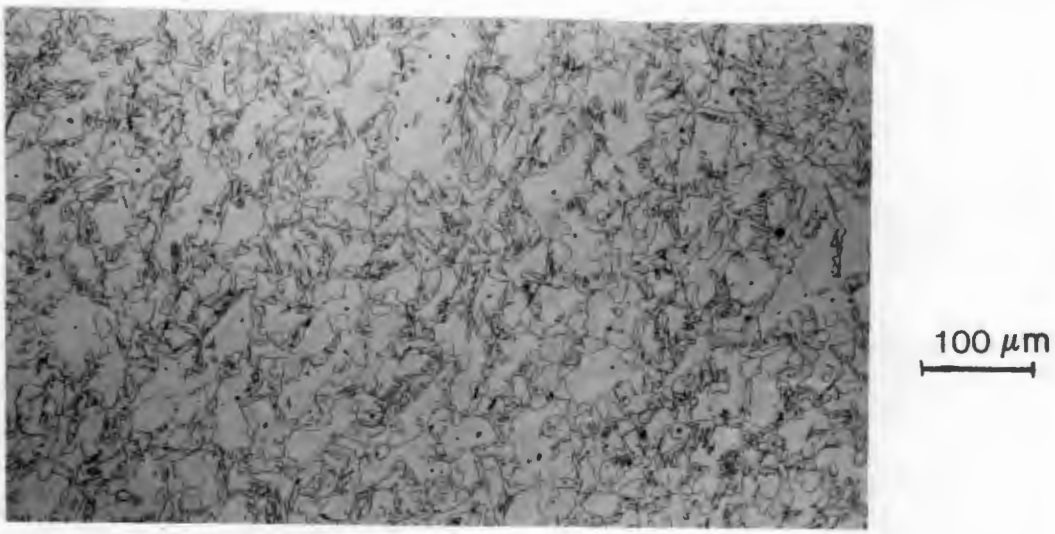

(b) Alloy B : (11,5%Cr; 0,49%Ni)

Heat Treatment : Water quenched from 900°C (1 hour)

Prior Heat Treatment: i) AHR condition, then
ii) Anneal at 1000°C (1 hour) followed by a furnace cool

FIG. 5.12(a+b) Micrographs depicting effect of increasing nickel additions on the morphology (shape, size and distribution) of the second phase (martensite) in a ferrite matrix.

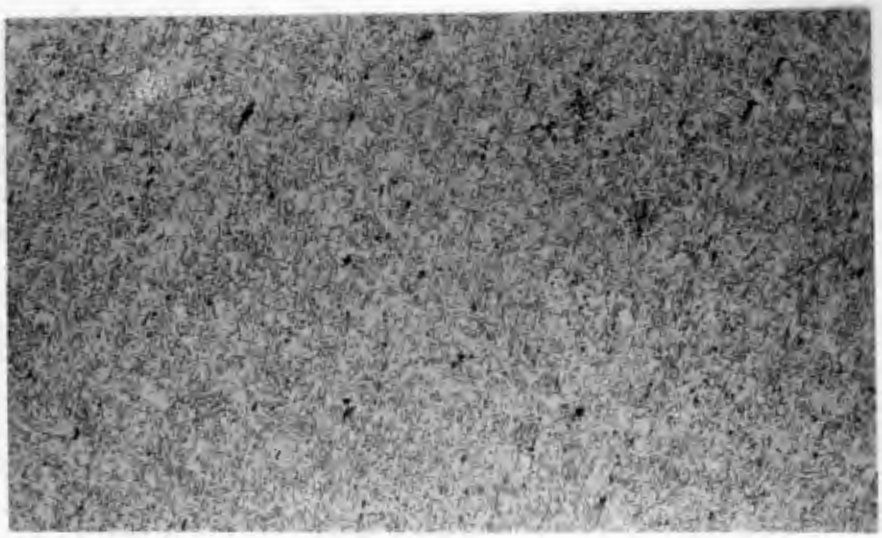

(c) Alloy C : (11,5%Cr; 0,85%Ni)

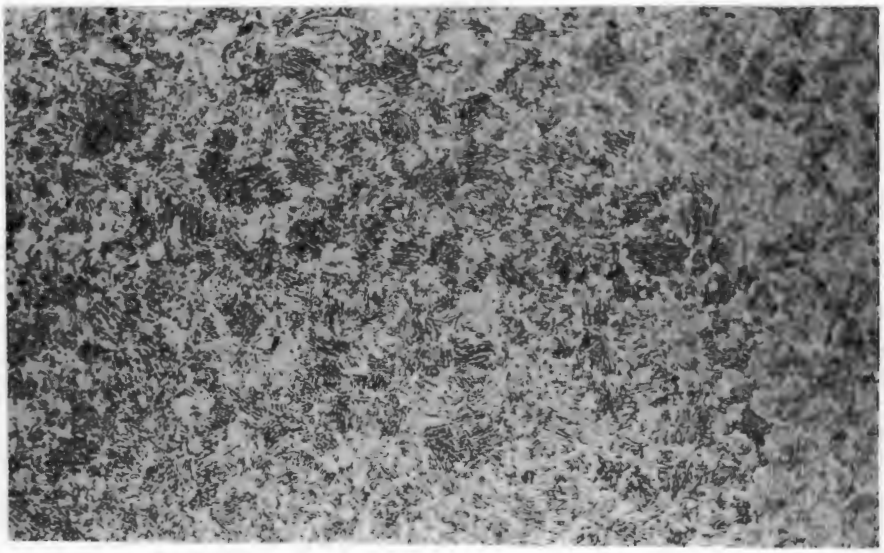

(d) Alloy D : (11,5%Cr; 1,19%Ni)

Heat Treatment : Water quenched from 900°C (1 hour)

Prior Heat Treatment: i) AHR condition, then
ii) Anneal at 1000°C (1 hour) followed by a furnace cool.

FIG. 5.12(c+d) Micrographs depicting effect of increasing nickel additions on the morphology (shape, size and distribution) of the second phase (martensite) in a ferrite matrix.

5.1.4 T.E.M.

Transmission electron microscopy can be used to differentiate between the various phases present.

Figures 5.13, 5.14 and 5.15 are typical micrographs obtained for Alloy F, heat treated for 3 hours at 860°C, 800°C and 675°C respectively.

At 860°C, Fig. 5.13 indicates an almost fully martensitic structure, again consistent with optical microscopy. It should be noted that the "lath" martensite is internally dislocated and not twinned.

At 800°C, the dual phase nature of the steel is apparent. Fig. 5.14 depicts predominantly dislocated grains of the ferrite matrix surrounded by some islands of martensite. Note the high dislocation density at the grain boundaries of the ferrite as compared with the ferrite grain interiors. It has been suggested (Matlock et al, 1979) that in order to produce good combinations of strength and ductility (in dual-phase plain carbon steels), the microstructures must contain non-uniform distributions and low densities of mobile

dislocations in the ferrite. The high density of dislocations that is observed is a result of the volume expansion and shear accompanying the austenite to martensite reaction upon cooling

At 675°C we expect the fully ferritic phase and the electron micrograph of Fig. 5.15 shows some of the ferrite grains of this structure. A cuboid titanium carbo-(nitride) precipitate is clearly observed in the micrograph. Small islands of martensite remain at the grain boundaries of the ferrite because the transformation will be very slow at these low temperatures.

1 μm

FIG. 5.13

Alloy F: (11,5%Cr; 1,77%Ni)
depicting the "lath" type martensite which is tough and is characteristic of low carbon alloys

Heat Treatment: Held at temperature (860°C) for 3 hours and then oil quenched

Prior Heat Treatment: i) In as-hot-rolled condition then
ii) homogenized at 1000°C (1 hour) then furnace cooled

FIG. 5.14

Alloy F: (11,5%Cr; 1,77%Ni)
showing predominantly dislocated ferrite with martensite islands on grain boundaries. Note the high dislocation density at the grain boundaries of the ferrite as compared with the ferrite grain interiors.

Heat Treatment: Held at temperature (800°C) for 3 hours and then oil quenched.

Prior Heat Treatment: i) In as-hot-rolled condition then
ii) homogenized at 1000°C (1 hour) then furnace cooled

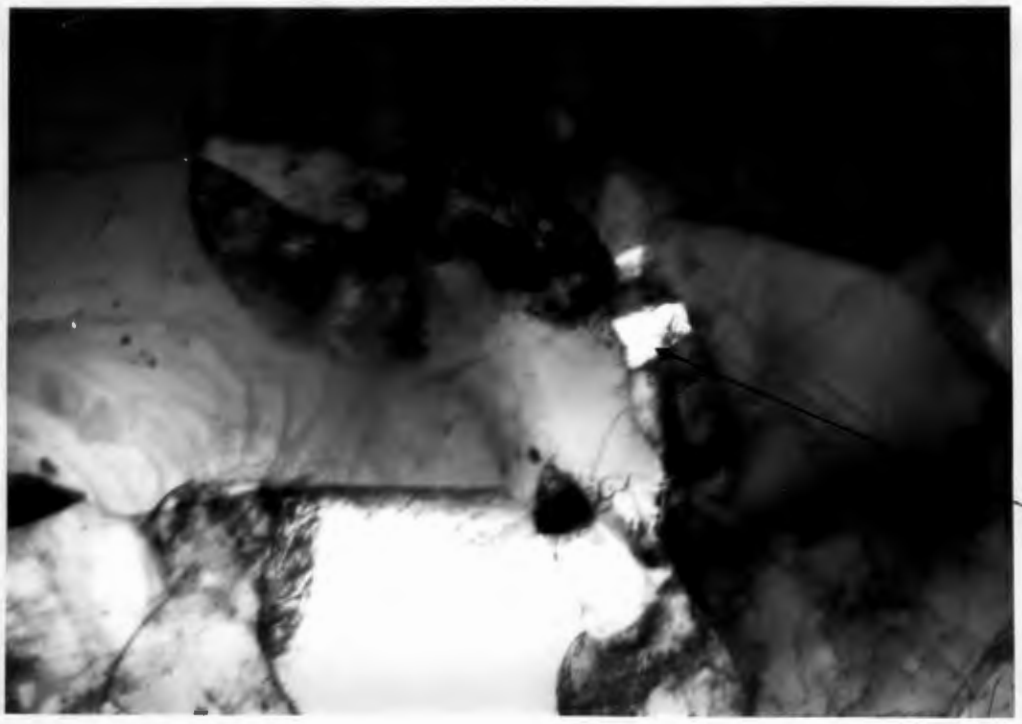

FIG. 5.15

Alloy F: (11,5%Cr; 1,77%Ni)
showing predominantly ferritic structure
note also cuboid titanium carbide precipitate

Heat Treatment: Held at temperature (675°C) for 3 hours and then oil quenched

Prior Heat Treatment: i) In as-hot-rolled condition then
ii) homogenized at 1000°C (1 hour) then furnace cooled

5.1.5 Hardness

The hardness values obtained as a function of nickel content and annealing temperature for the 11,5%Cr base alloys is shown in Fig. 5.16.

Alloys with increasing nickel content displayed an increasing hardness for a given annealing temperature. This increase in hardness was continuous through the ferrite, dual phase and austenitic (martensitic) regions, but becomes less marked for fully martensitic structures. This effect is also illustrated in Fig. 5.17 (for the alloys quenched at 700°C) and in Fig. 5.18 (for the alloys quenched at 950°C).

It should also be noted from the above figures that the hardness of a particular alloy increases with increasing annealing temperature.

For example, the hardness value for Alloy C with 0,85%Ni at 700°C is 140VPN (Fig. 5.16) and at 1000°C the hardness is increased to a value of 270VPN. For a higher nickel content, such as Alloy I (3,50%Ni) a hardness measurement of 225VPN is obtained at 700°C, and at 1000°C the hardness is increased to 310VPN.

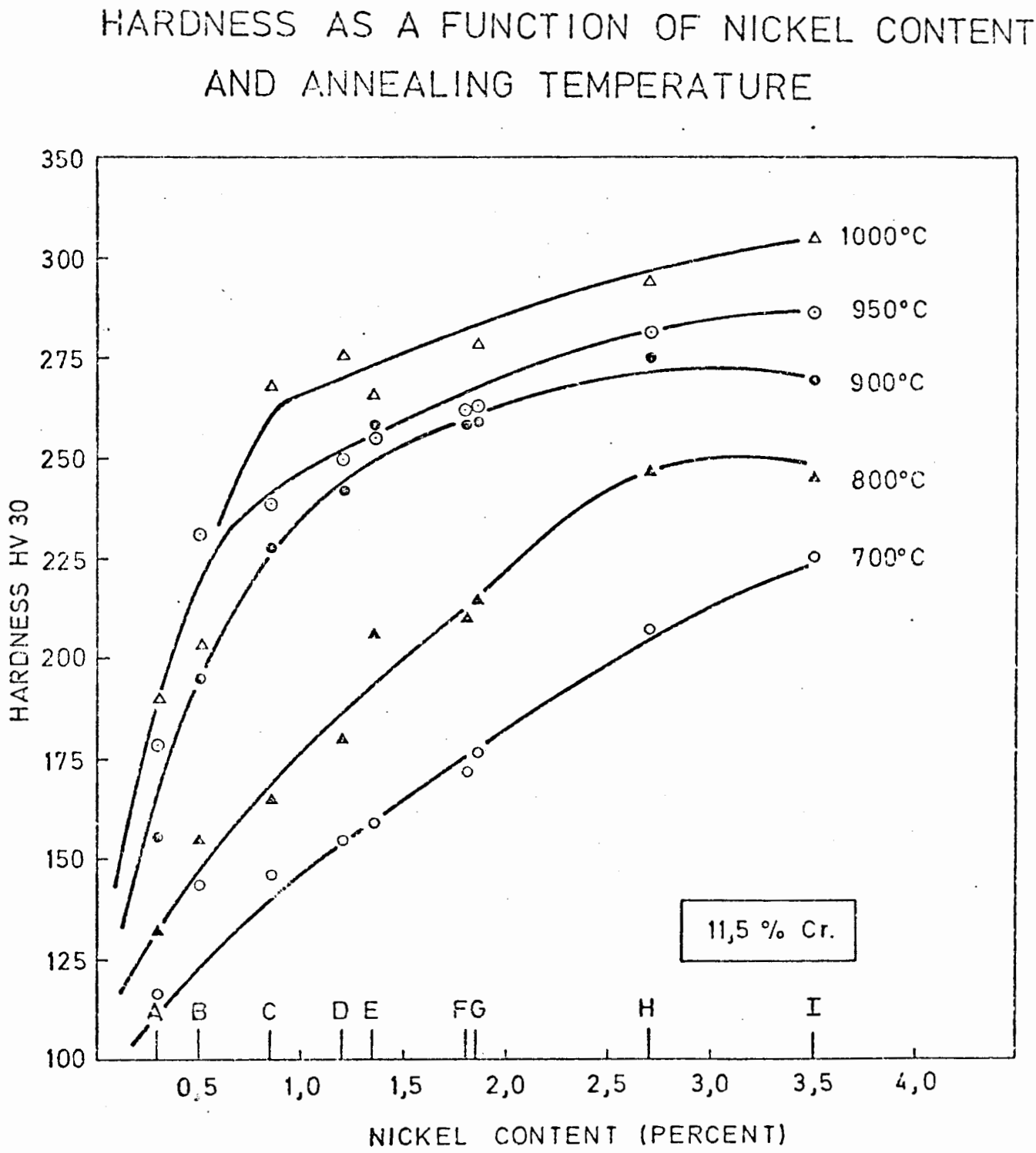

FIG. 5.16 Vickers Hardness measurements (recorded at RT) as a function of nickel content and annealing temperature (11,5%Cr alloys).

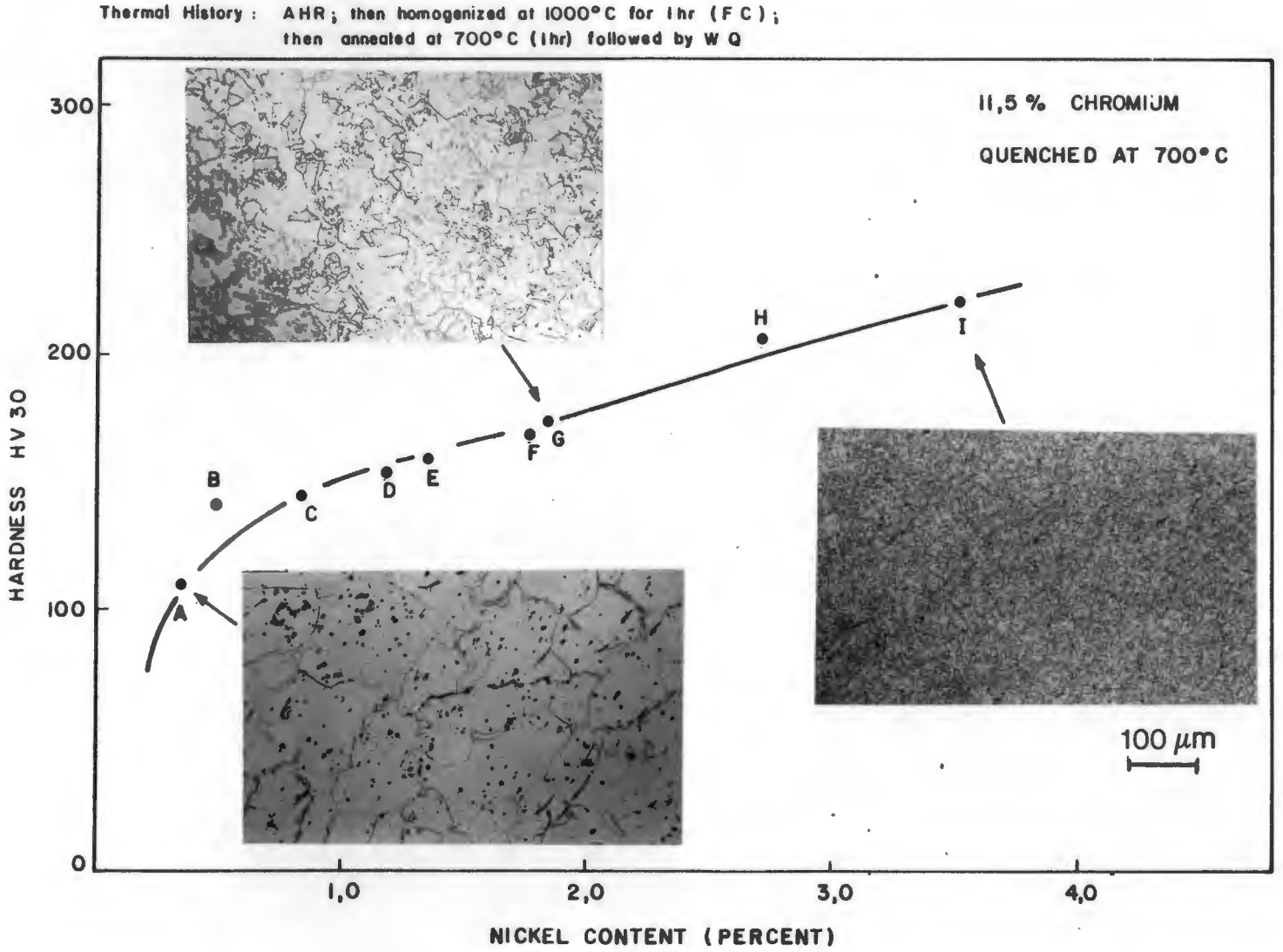

FIG 5.17 Vickers Hardness as a function of nickel content (at 700°C) for the 11,5%Cr Alloys. Also included are typical micrographs for various alloys.

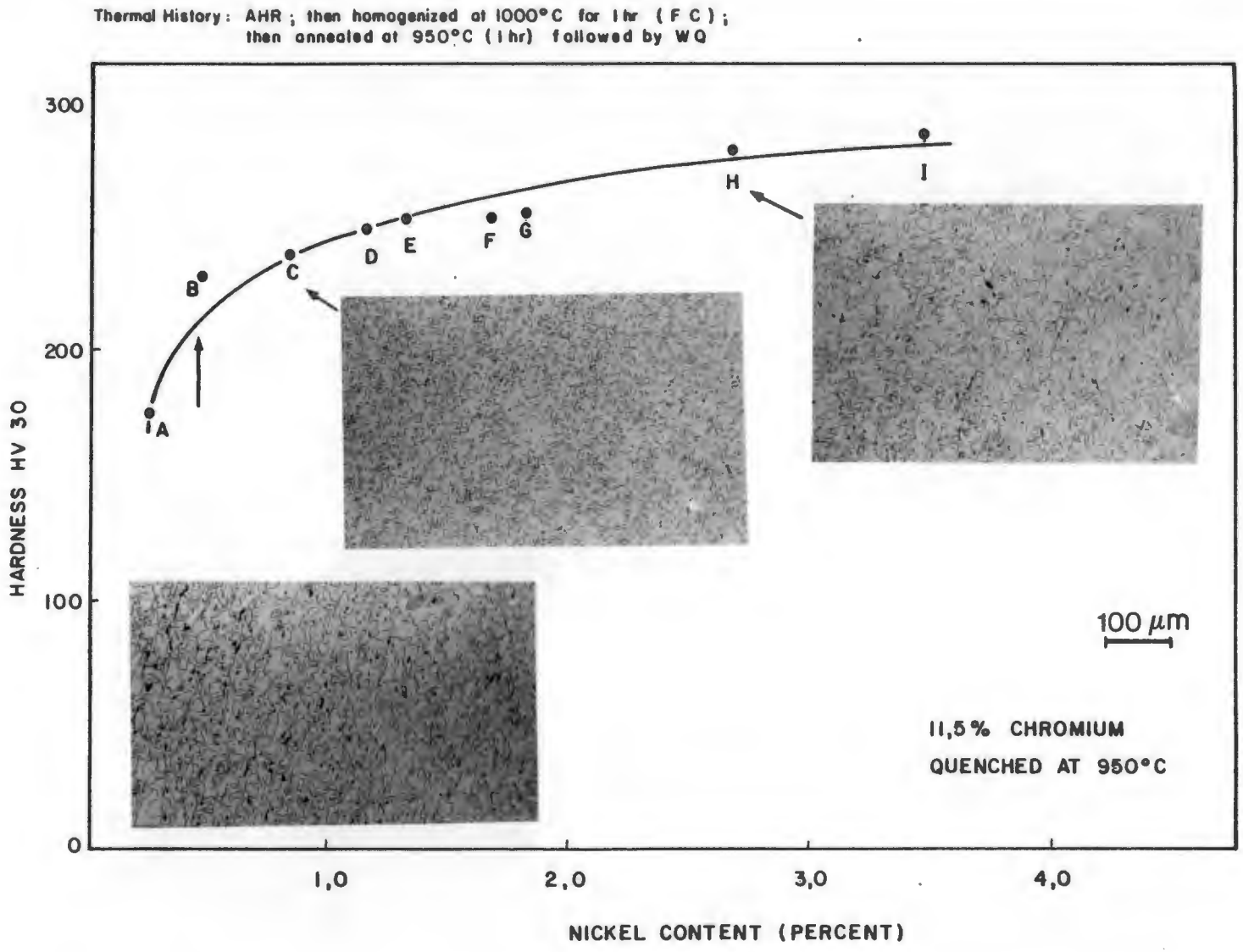

FIG 5.18 Vickers Hardness as a function of nickel content (at 950°C) for the 11,5%Cr Alloys. Also included are typical micrographs for various alloys.

5.1.6 Tempering Characteristics

The tempering characteristics of alloy C (0,85%Ni), alloy E (1,34%Ni) and alloy G (1,84%Ni) which had been previously held at 1000°C for one hour and oil quenched were investigated. After the various heat treatments, micrographs were taken (Fig. 5.19) and hardness measurements recorded. Fig. 5.20 shows the change in hardness as a function of temperature. The main feature of this graph is the 25% decrease in hardness over the temperature range 500°-700°C. It is also apparent that the nickel content has little effect up to 500°C; at temperatures in excess of 500°C there are slight variations although these are thought to be insignificant.

There is no optical evidence (See Fig. 5.19) of any real change in the temperature range 300°C- 500°C. However, at 600°C and especially at 700°C the micrographs display very fine carbide or nitride precipitates randomly distributed throughout the matrix. It is assumed that this decomposition of the martensite is also responsible for the drop in hardness observed in the temperature range (500-700°C).

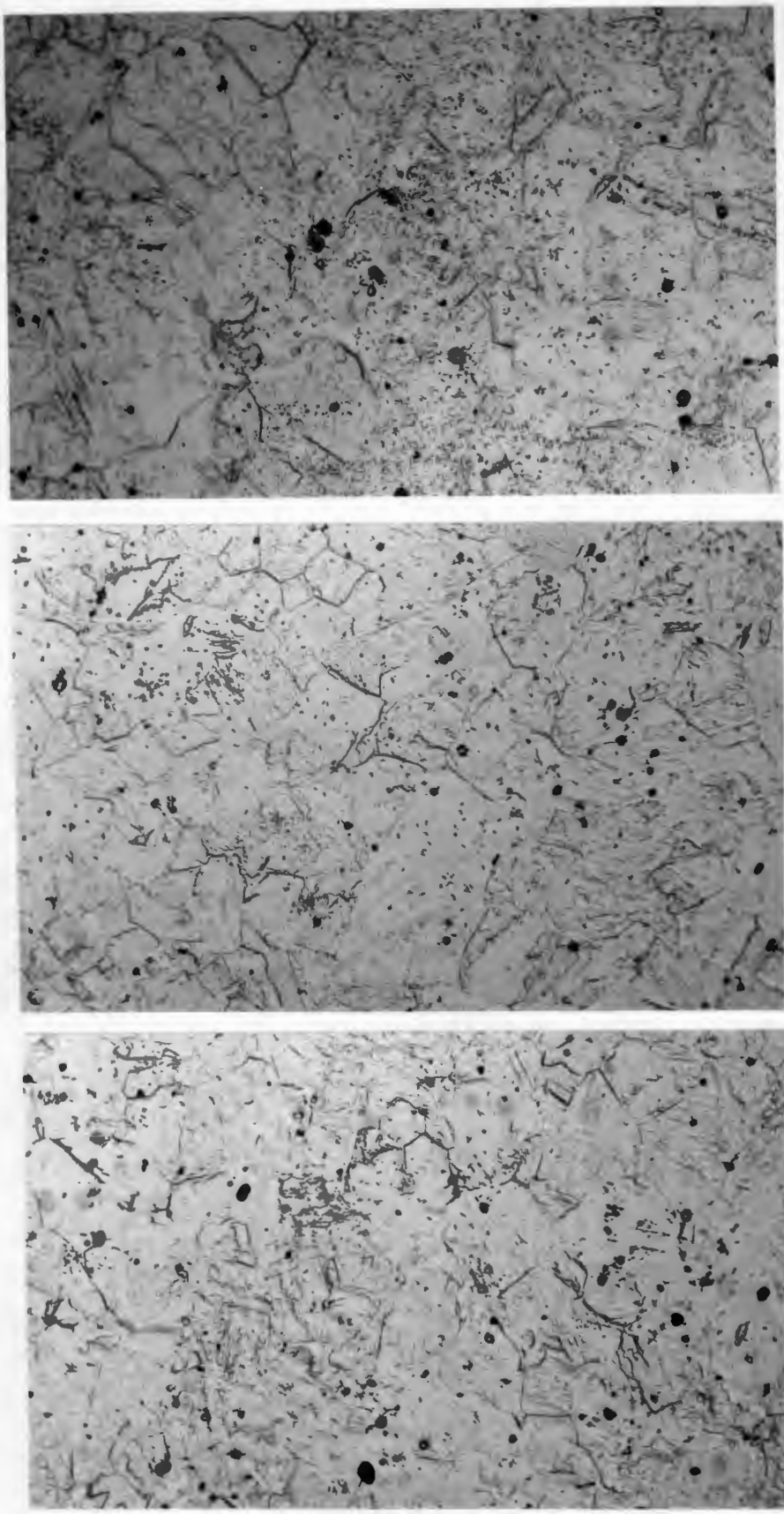

FIG. 5.19 Microstructure of Alloy E (1,84%Ni) after tempering at a temperature, T (^{o}C) for 1 hour, followed by an oil quench.

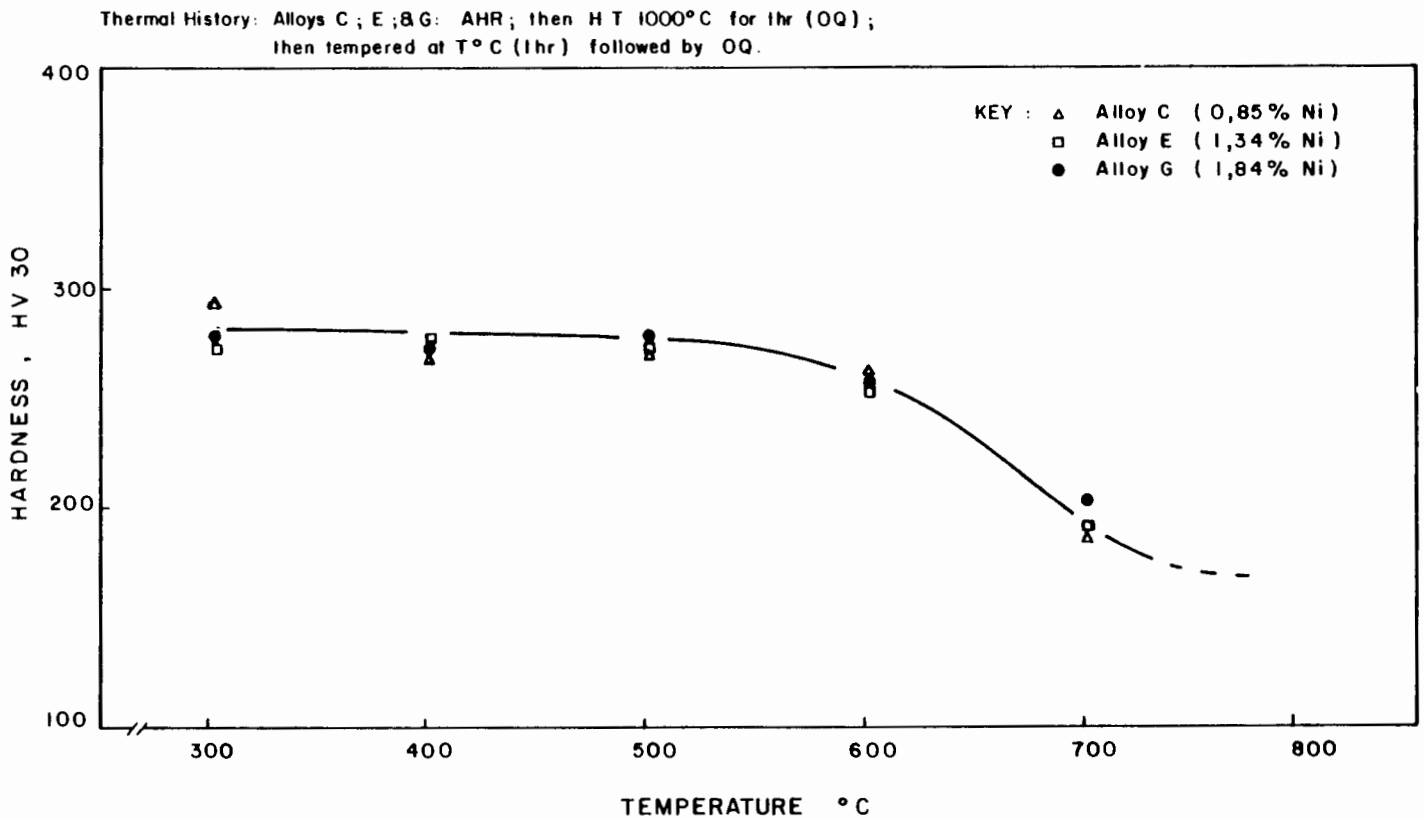

FIG 5.20 Vickers Hardness measurements versus tempering temperatures for Alloys C, E and G.

5.2 THE 14,3%Cr-Ni ALLOYS

5.2.1 Dilatometry

5.2.1.1 Low Temperature Experiments (T<1000°C)

Dilatometer traces for the 14,3%Cr alloys are similar to those obtained for the 11,5%Cr alloys (shown in Fig. 5.1). With increasing nickel content, there is a decrease in the transformation temperatures during the heating and cooling cycle. The 'hysteresis' effect is also increased with increasing nickel content.

5.2.1.2 High Temperature Experiment (T>1000°C)

In these experiments a high temperature phase transformation was found to occur for the alloys with a nickel content of greater than approximately 0,8 percent.

A typical trace is shown in Fig. 4.5 (see Chapter 4). However, it should be noted that the interpretation of these high temperature dilatometric traces is sometimes difficult as in the case where no reverse high temperature phase change is observed. An example of such a trace is shown in Fig. 5.21. Whether this is due to insensitivity of the apparatus or has some other significance is not yet clear.

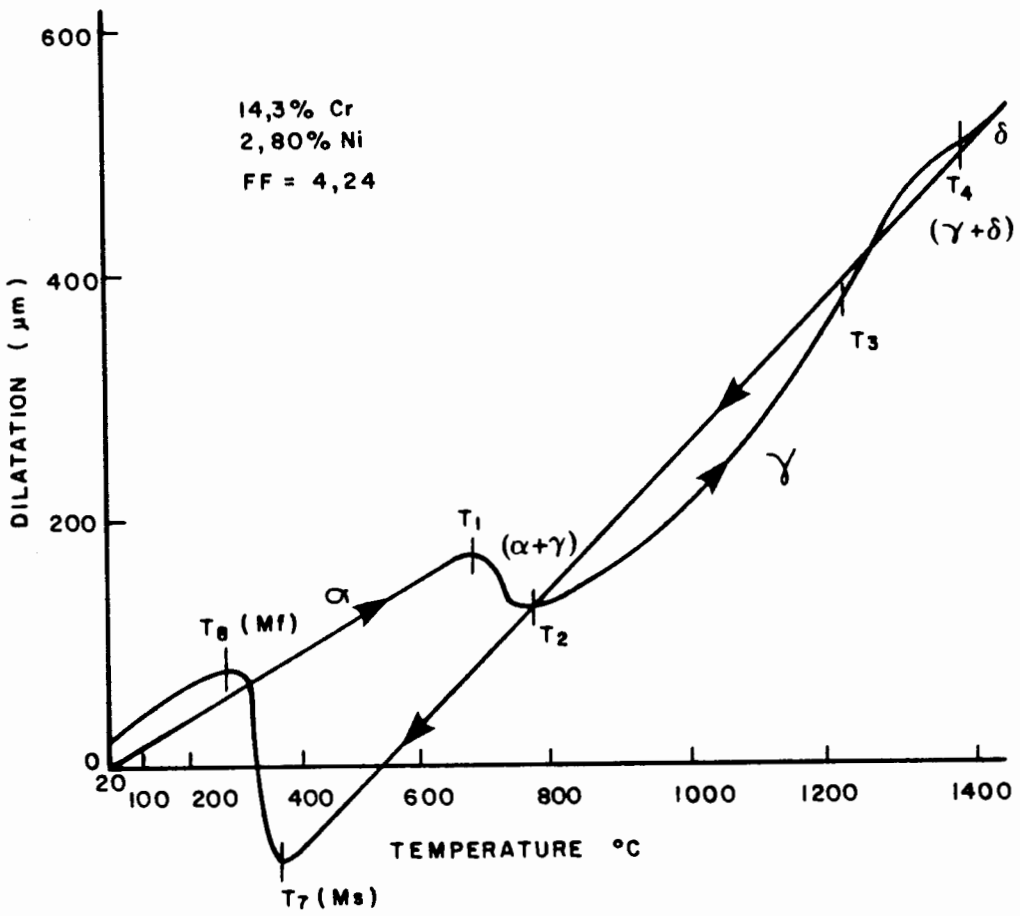

FIG. 5.21 A dilatometric trace obtained for a 14,3%Cr alloy (T>1000°C)

Note: arrows indicate heating and cooling cycle.

---

* *Interpretation of the dilatometric trace is sometimes difficult in the high temperature experiment. Results may be obtained such as the Fig. 5.21 above, where no reverse high temperature phase change is observed. Whether this is due to experimental error or has some other significance is not yet clear.*

5.2.2 The Phase Transformation Diagrams

The transformation temperatures obtained in the low temperature experiments (T<1000°C) are tabulated in Table 5.3. These values, for the heating cycle only, were plotted as a phase transformation diagram in Fig. 5.22 and in Fig. 5.23, the values obtained during the cooling cycle are also included in the diagram.

Similarly, the transformation temperatures obtained from the high temperature (T>1000°C) experiments are tabulated in Table 5.4 and the values obtained from the heating cycle are plotted as a phase diagram in Fig. 5.24. In Fig. 5.25 the cooling transformation temperatures are also included.

In order to compare the low temperature results and the values obtained from the high temperature experiment a 'combined' phase transformation diagram is shown in Fig. 5.26 (heating cycle transformation temperatures only).

The 'complete' phase transformation diagram for the 14,3%Cr alloys is shown in Fig. 5.27. Included in this diagram are the transformation temperatures of the heating

and cooling cycle for the combined ($T<1000°C$) and ($T>1000°C$) experimental results.

It should be noted that there are two dual phase regions: the ($\alpha+\gamma$) which is present between 620°C and 800°C, and the ($\gamma+\delta$) region which is present over the temperature range 1150°C to 1400°C. The ferritic (α), austenitic (γ) and martensitic regions are also shown.

The importance of including the martensitic regions in some of the phase transformation diagrams has previously been mentioned.

It is evident that Fig. 5.27 that the Ms temperature range is from approximately 450°C - 200°C and the Mf temperature range extends from approximately 350°C - 50°C. The Ms and Mf both decrease as the nickel content is increased.

A comparison of the transformation temperatures obtained from the low temperature experiments ($T<1000°C$) with the values obtained from the high temperature experiments ($T>1000°C$) (heating cycle only) may be seen in Table E.3 of Appendix E. According to this table the discrepancy

between T_1 (T>1000°C) and T_1 (T<1000°C) varied from a few degrees (5°C) for alloy 7 and up to (25°C) for alloy 6. A rather large difference (75°C) is observed for the T_2 (T<1000°C) and T_2 (T>1000°C) for alloy 5. The average difference between T_1 (T<1000°C) and T_1 (T>1000°C) is approximately 12°C and the average difference between T_2 (T<1000°C) and T_2 (T>1000°C) is approximately 18°C.

Table E.4 (Appendix E) shows a comparison of the transformation temperatures obtained from the low temperature experiments (T<1000°C) with the values obtained from the high temperature experiments (T>1000°C) (for the cooling cycle only). The average difference between T_7 (T>1000°C) and T_5 (T<1000°C) is approx. 40°C and for T_8 (T>1000°C) and T_6 (T<1000°C) is $\sim$42°C.

However, it will be noted that there is no evidence for a correlation between the observed differences in transformation temperatures and nickel content.

14,3 % Cr		TRANSFORMATION TEMPERATURES			
Alloy	% Ni	Heating (°C)		Cooling (°C)	
		$T_1(A_{c1})$	$T_2(A_{c3})$	$T_5(M_s)$	$T_6(M_f)$
1	0,62	*	*	*	*
2	0,98	780	*	420	330
3	1,41	740	*	410	325
4	1,80	735	835	360	280
5	2,40	680	800	340	260
6	2,80	655	775	320	225
7	3,90	635	750	300	195
8	4,70	630	740	230	150
9	5,60	620	735	200	125

* No transformation temperature observed on dilatometric trace

TABLE 5.3: Transformation temperatures obtained during the heating and cooling cycle (T<1000°C) for the 14,3%Cr alloys.

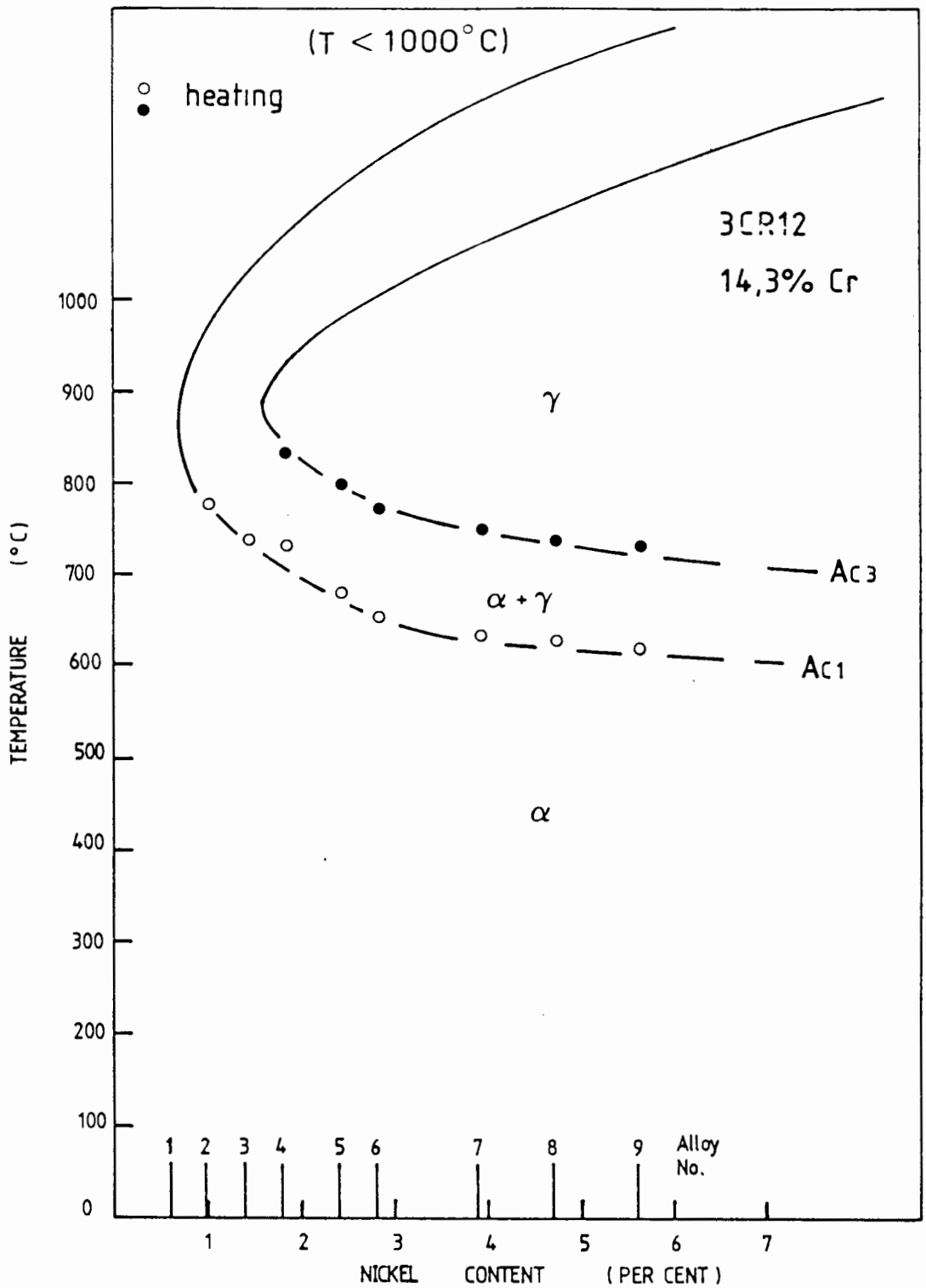

FIG.5.22 Transformation temperatures obtained during the heating cycle (T<1000°C) and plotted as a phase transformation diagram for the 14,3%Cr alloys.

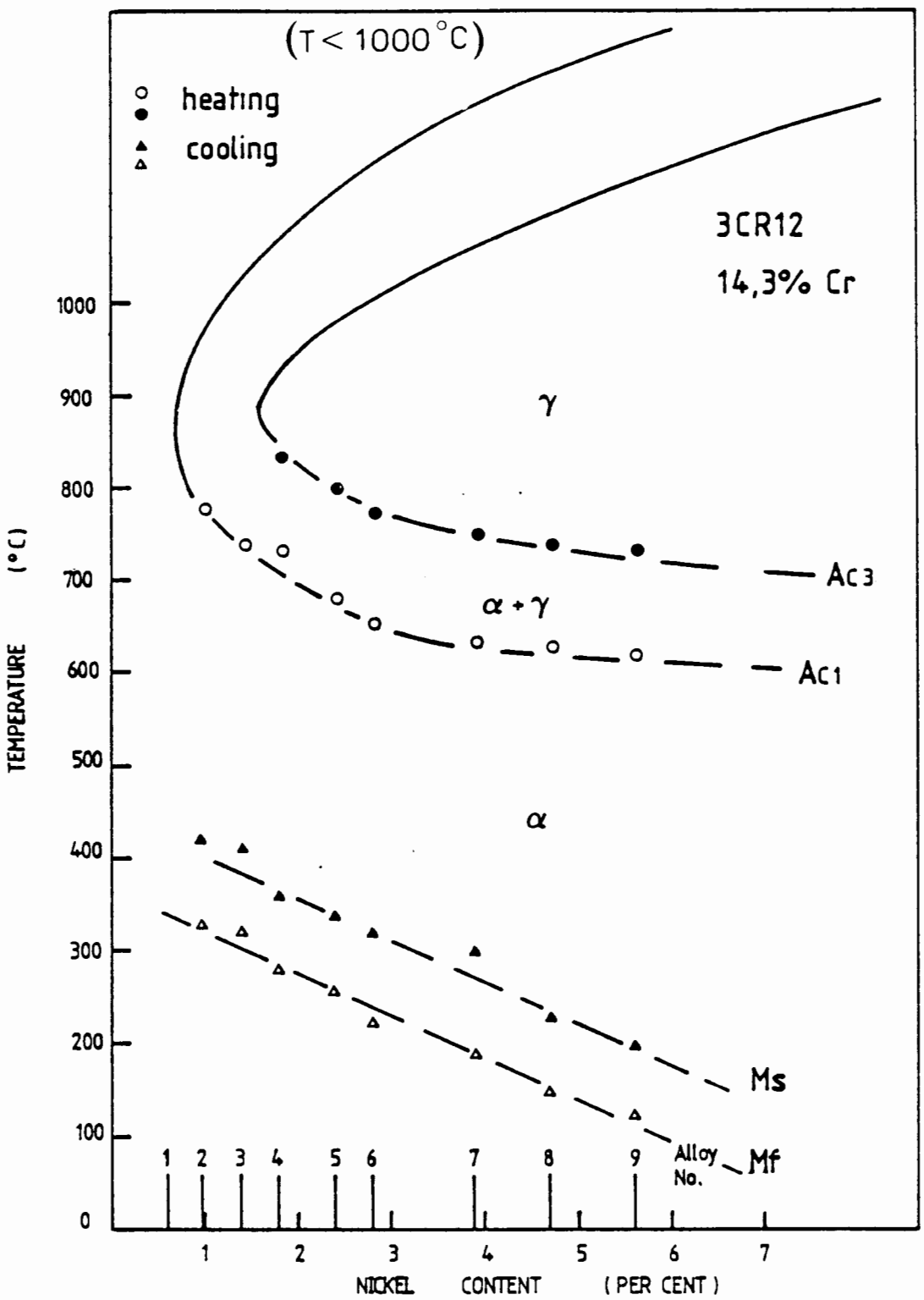

FIG. 5.23 Phase Transformation Diagram showing transformation temperatures obtained during heating and cooling cycle of (T<1000°C) experiments (14,3% Cr alloys).

14,3% Cr		TRANSFORMATION TEMPERATURES (°C)							
Alloy	% Ni	Heating (°C)				Cooling (°C)			
		$T_1(A_{c1})$	$T_2(A_{c3})$	T_3	T_4	T_5	T_6	$T_7(M_s)$	$T_8(M_f)$
1	0,62	*	*	*	*	*	*	*	*
2	0,98	800	890	*	*	*	*	420	370
3	1,41	*	900	*	1200	*	*	460	*
4	1,80	*	850	*	1240	*	*	400	310
5	2,40	690	875	1160	1280	1080	940	420	320
6	2,80	680	780	1220	1380	*	*	360	250
7	3,90	630	745	1240	1335	1300	1155	275	150
8	4,70	620	730	1320	1380	1350	1250	250	100
9	5,60	620	735	1340	1390	1280	1220	200	50

* No transformation temperature observed in dilatometric trace

TABLE 5.4: TRANSFORMATION TEMPERATURES OBTAINED DURING THE HEATING AND COOLING CYCLE (T>1000°C) FOR THE 14,3% Cr ALLOYS.

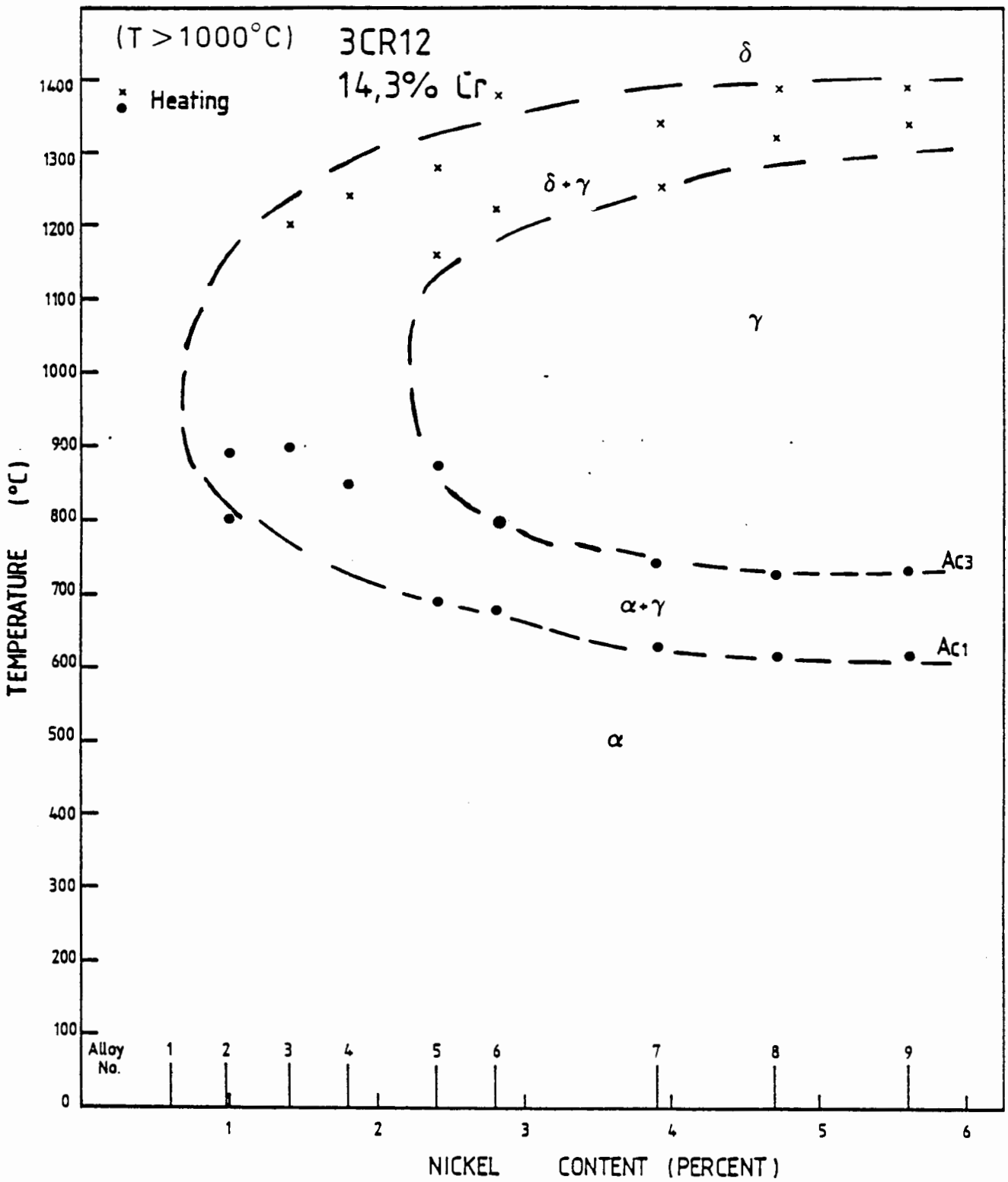

FIG. 5.24 Transformation temperatures obtained during the heating cycle (T>1000°C) and plotted as a phase transformation diagram for the 14,3%Cr alloys.

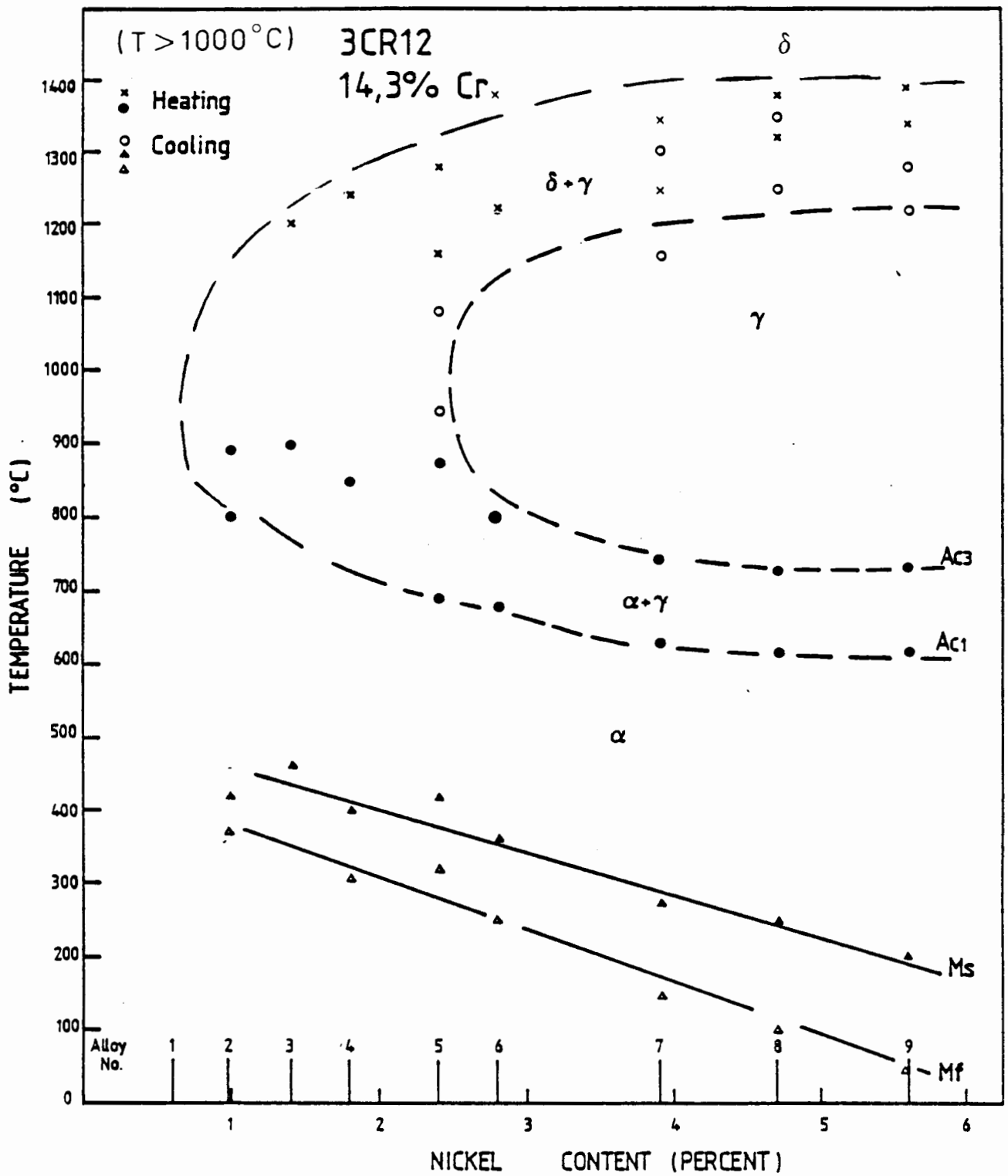

FIG. 5.25 Phase Transformation Diagram showing transformation temperatures obtained during the heating and cooling cycle from (T>1000°C) experiments. (14,3%Cr alloys)

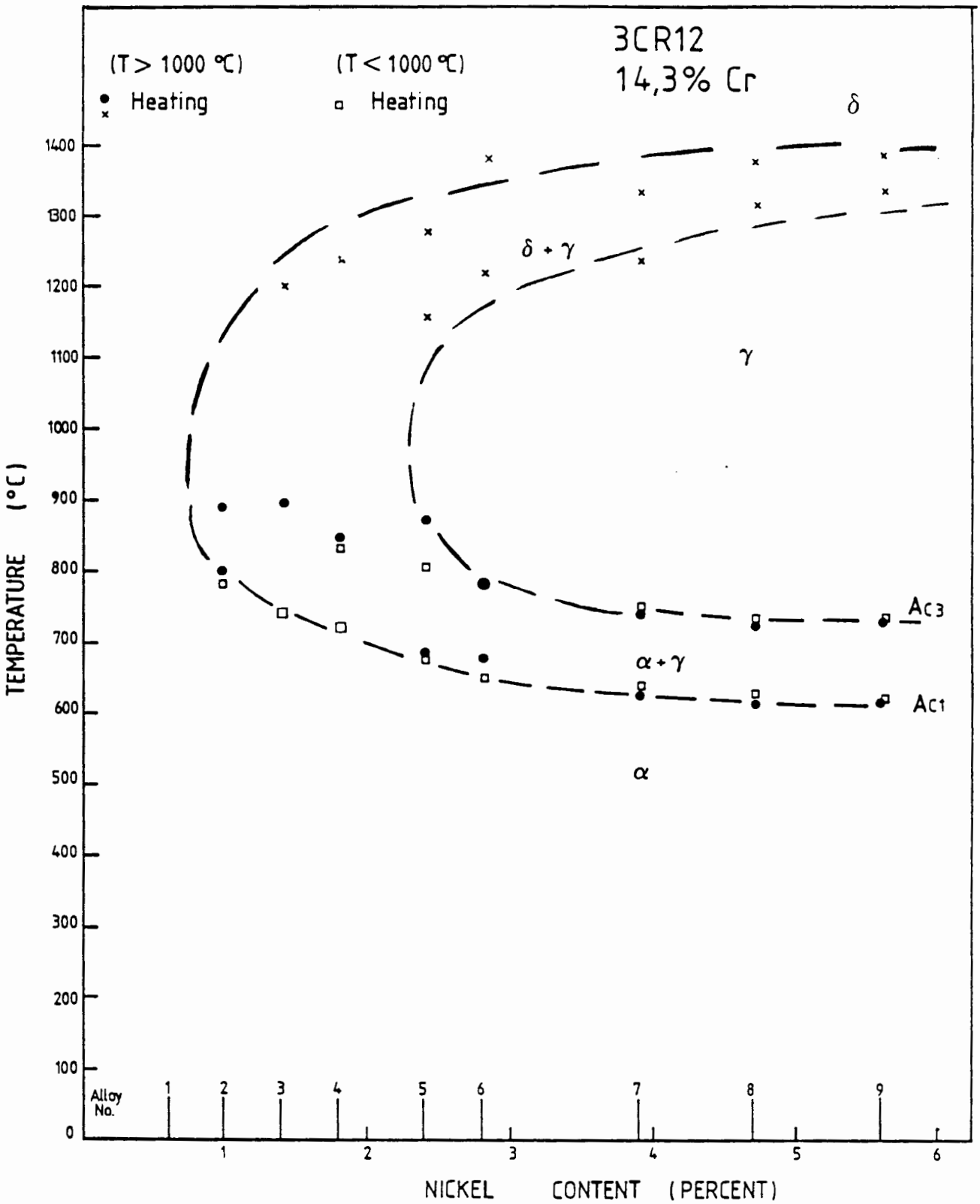

FIG. 5.26 Transformation termperatures obtained during the heating cycle from the (T<1000°C) and (T>1000°C) experiments plotted as a phase transformation diagram. (14,3%Cr alloys)

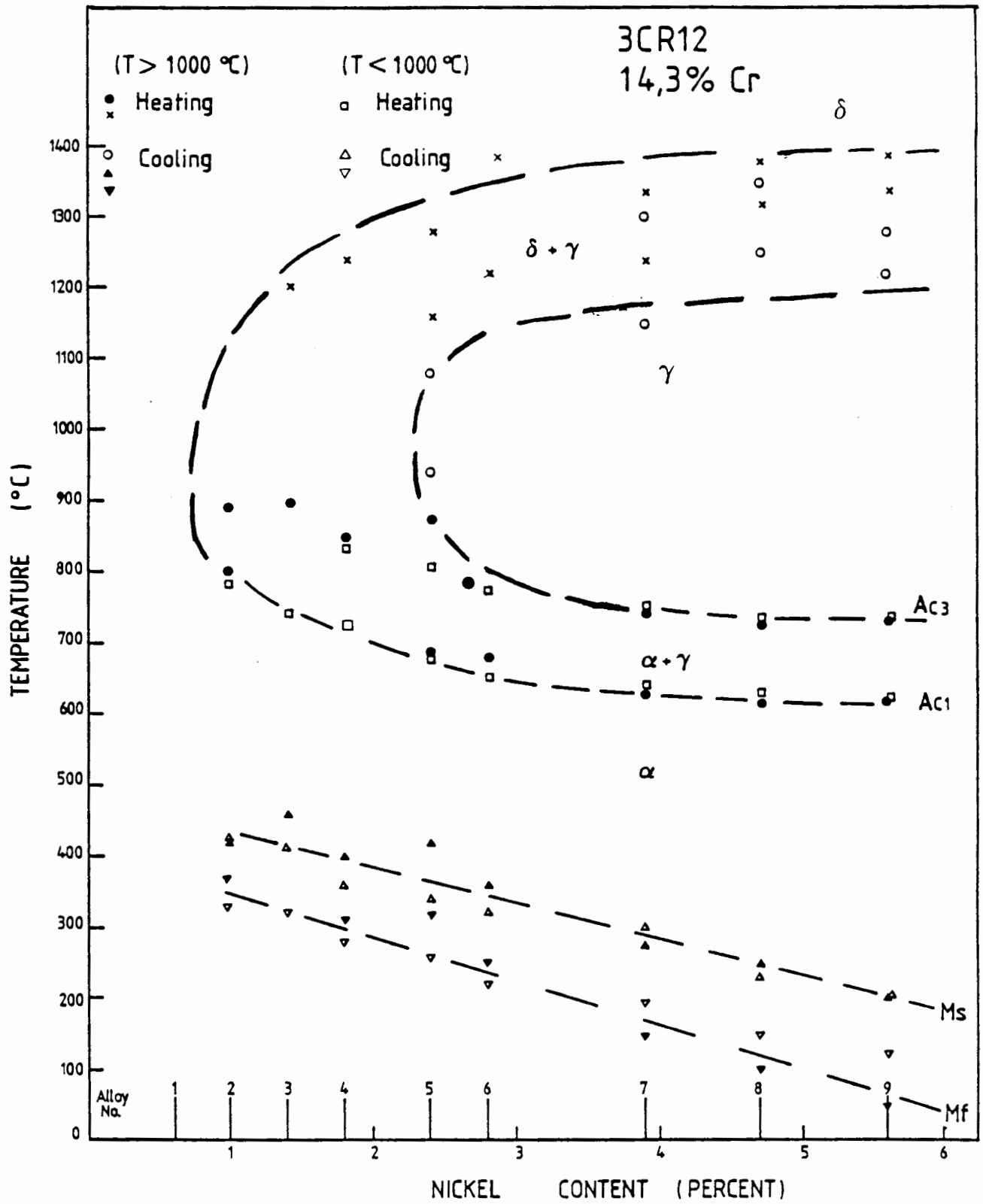

FIG.5.27 The Phase Transformation Diagram for the 14,3%Cr alloys showing heating and cooling transformation temperatures obtained from both (T<1000°C) and (T>1000°C) experiments.

5.2.3 Metallography

Optical metallography was used to differentiate the various phases present at different temperatures. For example, at 800°C, Fig. 5.28 shows a predominantly ferritic structure (Alloy 1; 0,62%Ni); in Fig. 5.29 (Alloy 3; 1,4%Ni) the dual phase ferrite-martensite structure is apparent and in Fig. 5.30 (Alloy 7; 3,9%Ni) depicts a martensitic structure. The phases that are identified optically (after heat treatment at various annealing temperatures) are plotted in Fig. 5.31.

It will be noted from Fig. 5.31, that certain phases predicted by the dilatometer are not those observed metallographically. For instance, alloys 2 (0,98% Ni); and 3 (1,41% Ni) at 700°C should according to the phase transformation diagram be fully ferritic, although it should be noted that alloy 3 is rather close to the phase boundary separating the fully ferritic region from the duplex ferrite-austenite regime. However, after a one hour anneal at 700°C, followed by a water quench the micrographs for these alloys depict a duplex ferrite-martensite structure.

Similarly alloys 7 (3,90% Ni); 8 (4,70% Ni) and alloy 9 (5,60% Ni) should according to Fig. 5.31 be duplex ferrite-austenitic at 700°C. However after a one hour anneal at 700°C followed by a water quench the micrographs obtained depict a predominantly martensitic structure for these alloys.

There are various reasons for the discrepancies mentioned above and these have been mentioned in section 5.1.3.

However it should be noted that at higher temperatures, ie 800°C - 1000°C the agreement between the phases predicted by the phase transformation diagram in Fig. 5.31 and those obtained metallographically is rather good.

The phase transformation diagram in Fig. 5.31 suggests that alloy 1, containing 0,62%Ni is rather close to the phase boundary separating the single phase ferritic region from the duplex ferrite-austenite region. Upon closer examination of Fig. 5.28 it will be noted that the structure is not entirely ferritic. A small amount of second phase austenite (now martensite) appears to nucleate at the grain boundaries of the primary phase. This is evidence to suggest that alloy 1 is indeed very close to the 'nose' of the curve as presented in Fig. 5.31.

Fig. 5.29 depicts the duplex ferritic martensitic microstructure obtained for alloy 3 (1,4% Ni). It will be noted from this micrograph that the ferrite phase is not very 'clean', ie a very fine distribution of titanium carbo-nitrides is dispersed throughout the ferrite matrix. A larger cuboid titanium carbide precipitate may also be observed in the ferrite phase. These fine precipitates may affect the ductility of the ferrite phase (Thomas and Koo, 1979; Davies, 1979{b}) and this effect requires further investigation.

The grain refining effect which nickel has on the microstructure is shown in Fig. 5.32. Alloy 1 containing 0,6 percent nickel and alloys 2 (0,98%Ni); 5 (2,4%Ni) and alloy 6 (2,8%Ni) had all received the same heat treatment comprising of a one hour anneal at 1000^{o}C followed by a water quench. After this heat treatment, a fully ferritic structure is indicated for alloy 1, and the large, polygonal ferrite grains of this structure are depicted in Fig. 5.32 (a). However, for alloy 2 with 0,98 percent nickel a fine-grained duplex ferritic-martensitic structure is observed (see Fig. 5.34 (b)). An extremely fine-grained microstructure is depicted for alloy 5 (2,4%Ni) in Fig. 5.32 (c).

According to the phase diagram in Fig. 5.31, alloy 5 at 1000°C still lies within the duplex region although it is very close to the phase boundary separating the duplex ($\alpha + \gamma$) region from the austenitic (γ) region.

A marked difference is observed in the microstructure of alloy 6, (Fig. 5.32 (d)), containing only slightly more nickel (2,8 percent) than alloy 5 (2,4 percent). The extremely fine-grained structure which is well-defined in alloy 5 is not observed in alloy 6. Rather, the structure appears to be predominantly martensitic, in accordance with the structure predicted by the diagram in Fig. 5.31.

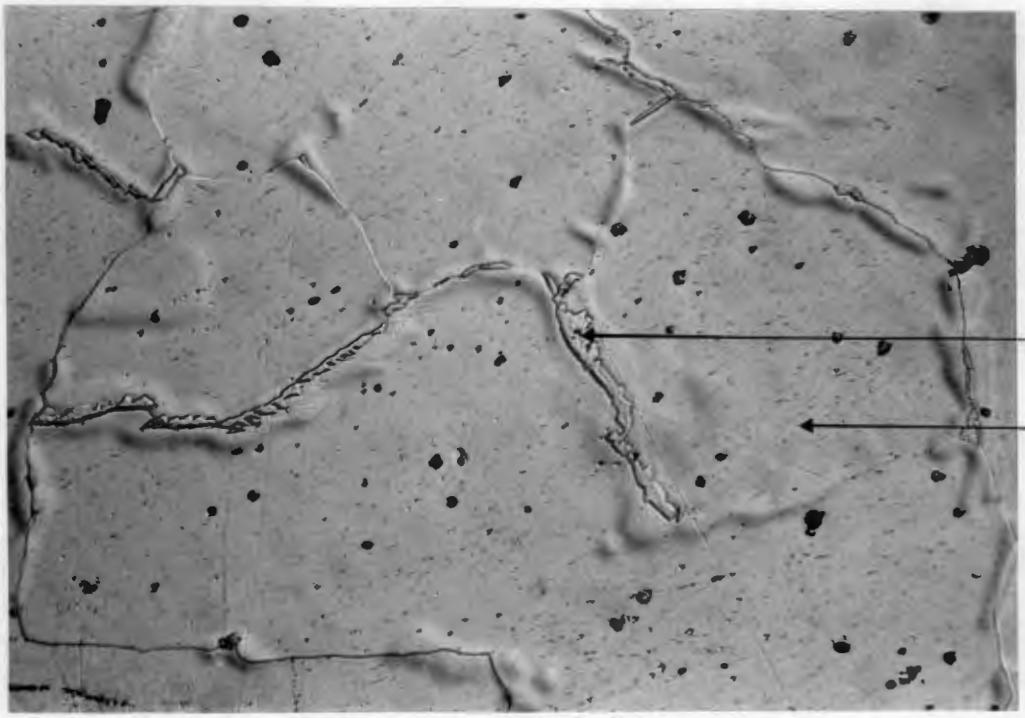

FIG. 5.28

Alloy 1; (14,3%Cr; 0,62%Ni)
depicting ferritic microstructure
Note also the second phase austenite
(now martensite) nucleating at the grain
boundary of the primary phase ferrite

Heat Treatment: Held at temperature (800°C) for
1 hour followed by a water quench

Prior Heat Treatment: i) AHR, then
ii) homogenized at 1000°C (1 hour)
followed by furnace cool.

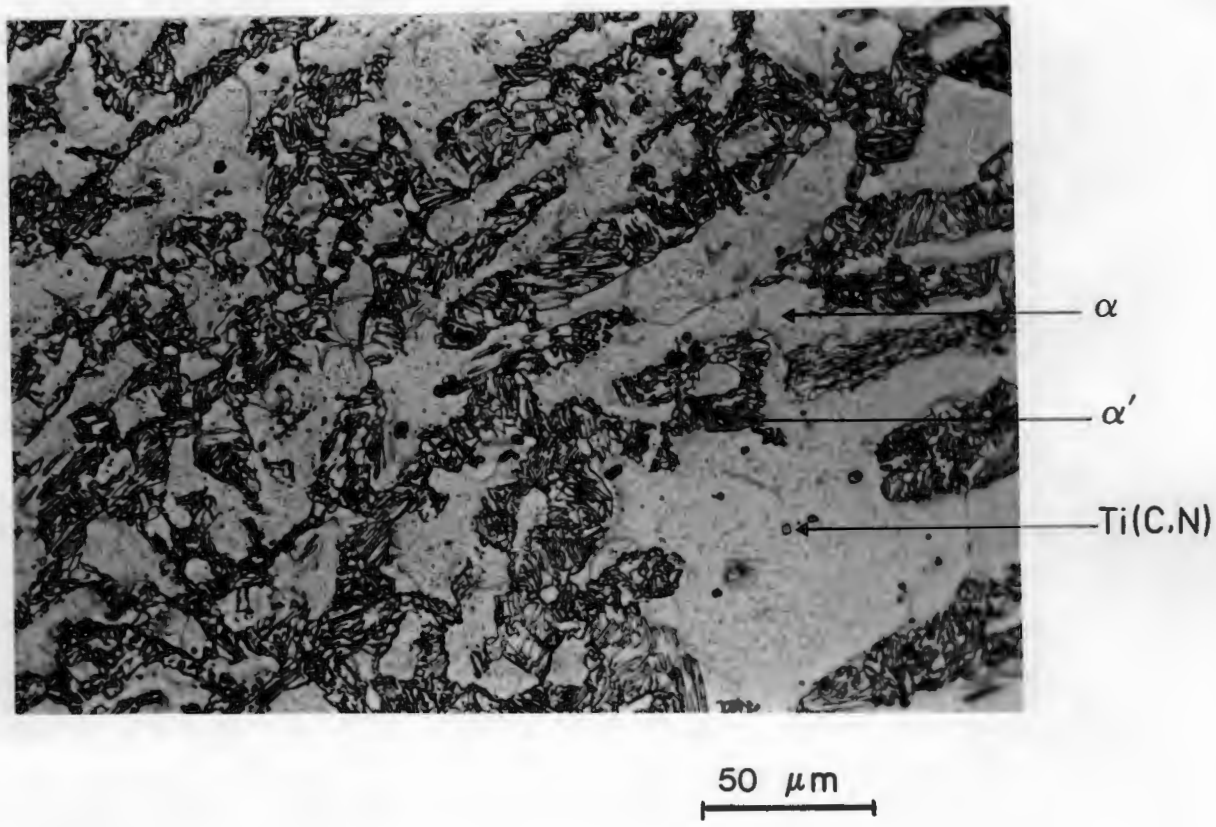

FIG. 5.29

Alloy 3 ; (14,3%Cr; 1,4%Ni)
showing a ferritic-martensitic microstructure
Note also the cuboid titanium carbide
precipitate as well as the very fine titanium
carbo-nitride precipitates in the ferrite matrix

Heat Treatment: Held at temperature (800°C) for
1 hour then quenched into water.

Prior Heat Treatment: i) AHR, then
ii) homogenized at 1000°C (1 hour)
followed by furnace cool.

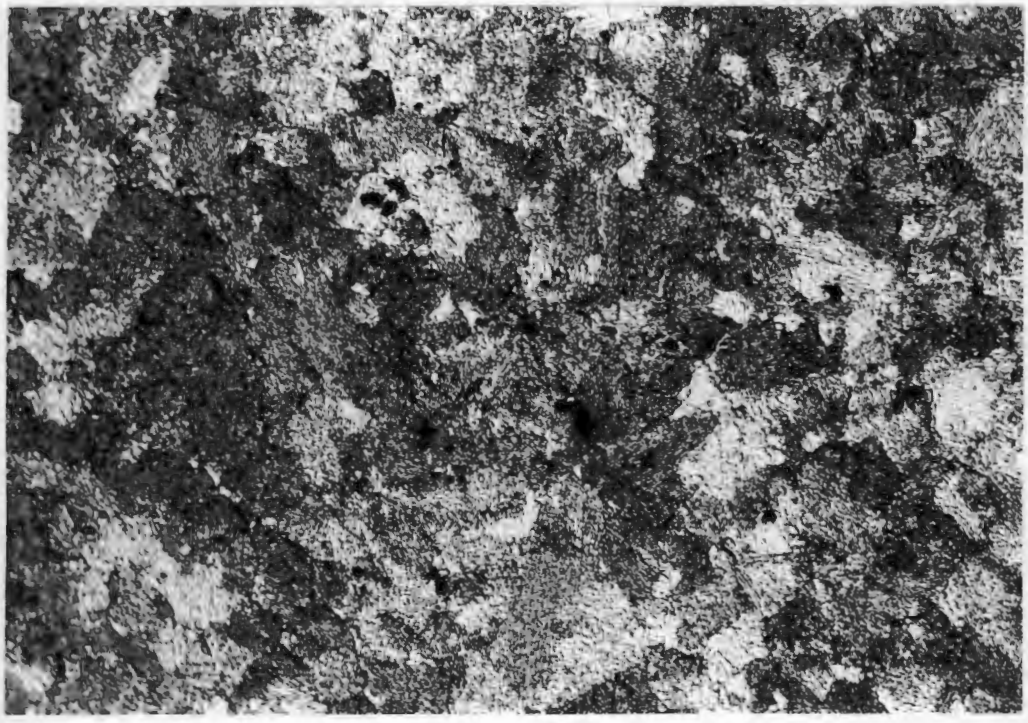

FIG. 5.30

Alloy 7 : (14,3%Cr; 3,9%Ni)
showing martensitic microstructure

Heat Treatment: Held at temperature (800°C) for 1 hour followed by a water quench

Prior Heat Treatment:
i) Received in the as-hot-rolled condition
ii) then homogenized at 1000°C and allowed to furnace cool

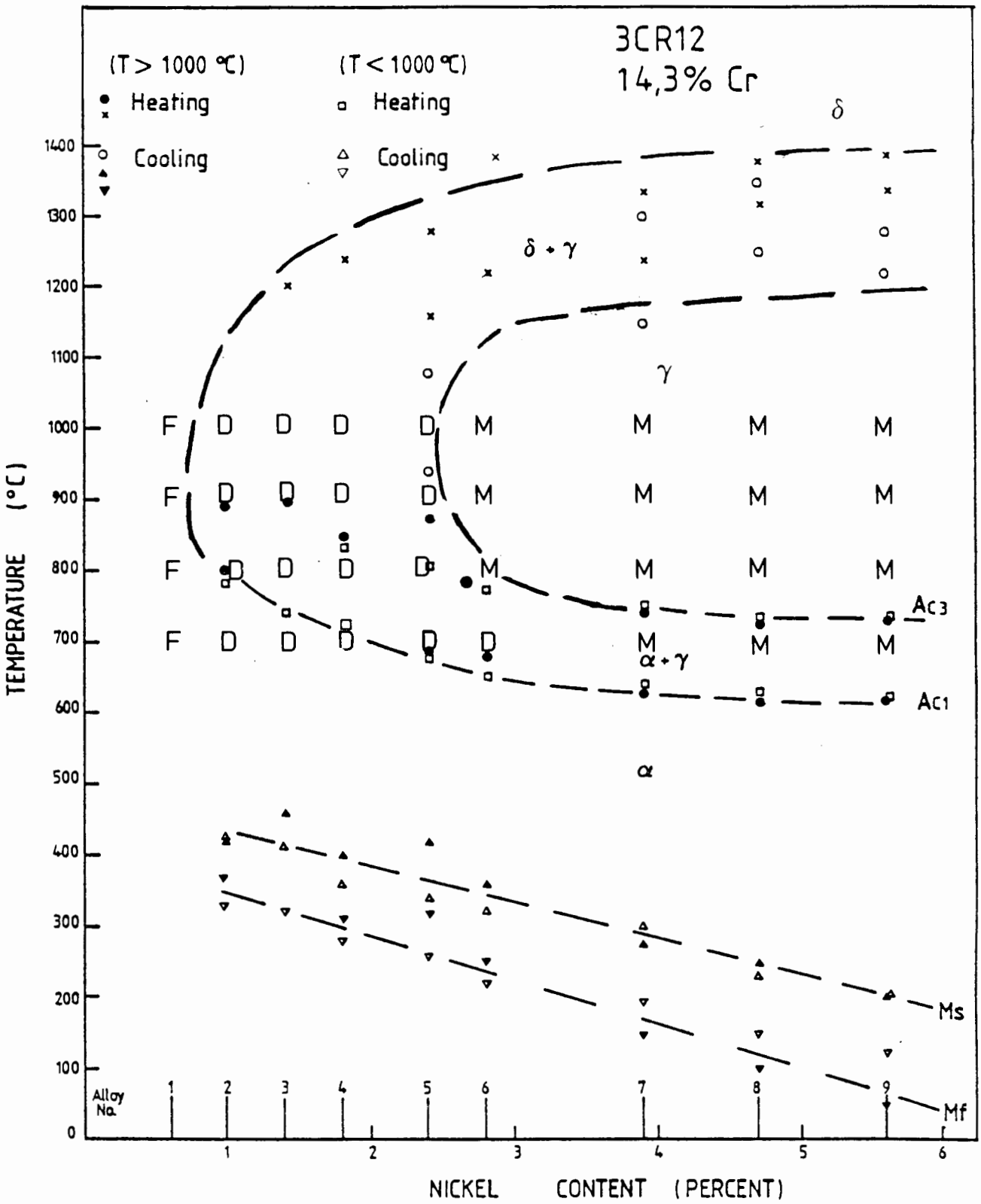

FIG. 5.31 The Phase Transformation Diagram for the 14,3%Cr alloys indicating the phases present at a particular temperature.
F = Ferrite; D = Duplex ferritic-martensitic; and
M = Martensitic microstructure.

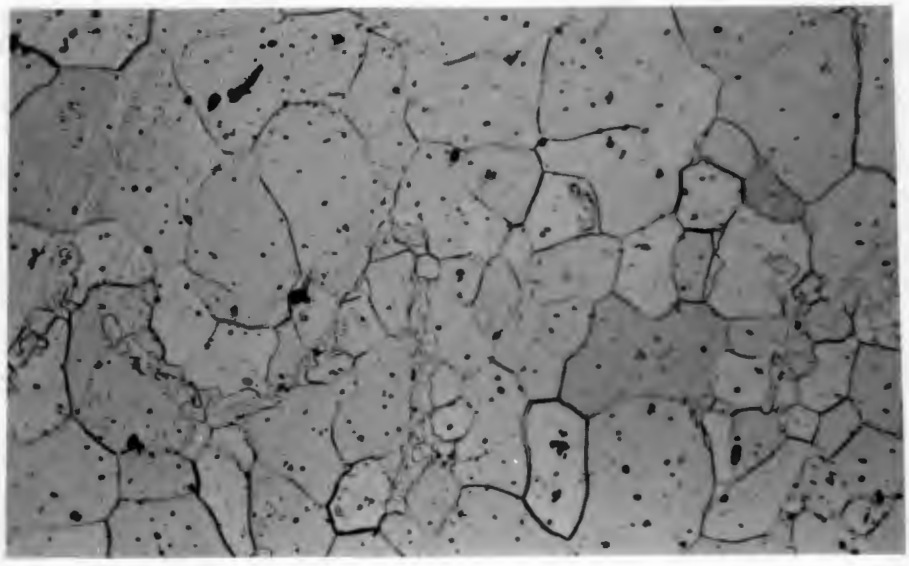

(a) Alloy 1 : 14,3%Cr: 0,62Ni

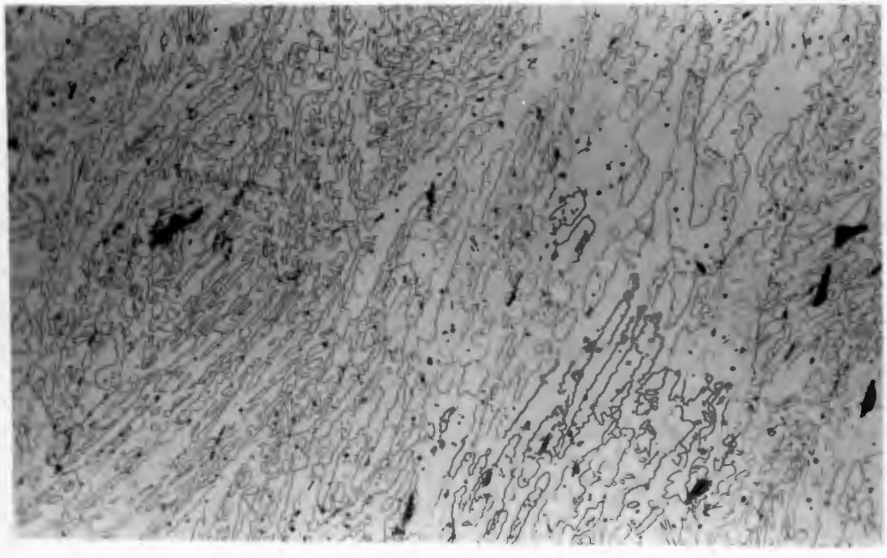

(b) Alloy 2 : 14,3%Cr; 0,98%Ni

Heat Treatment: Water quenched from 1000°C (1 hour)

Prior Heat Treatment: i) AHR condition, then
ii) Anneal at 1000°C (1 hour) followed by a furnace cool

FIG. 5.32(a) and (b): The grain refining effect of increasing nickel additions on the 14,3% Cr alloys.

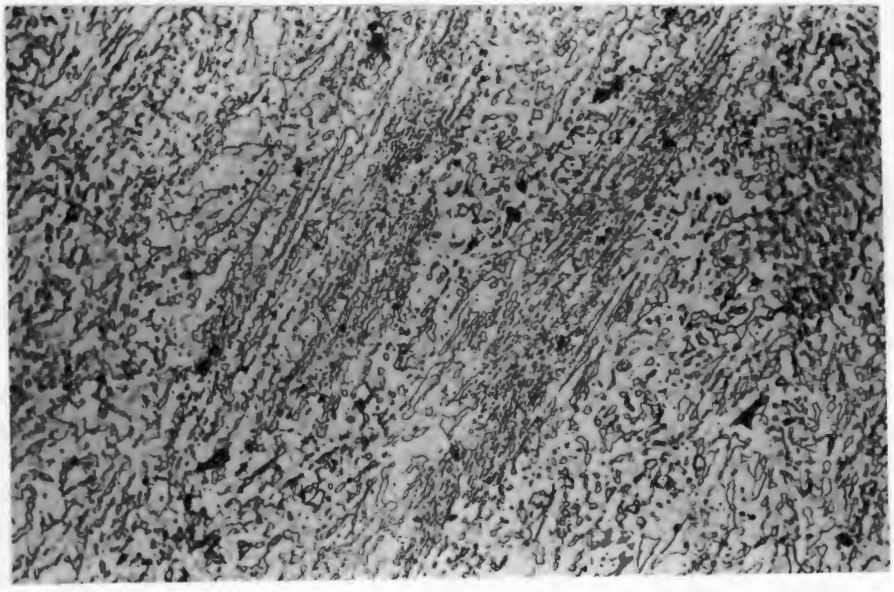

(c) Alloy 5 : 14,3%Cr; 2,4%Ni

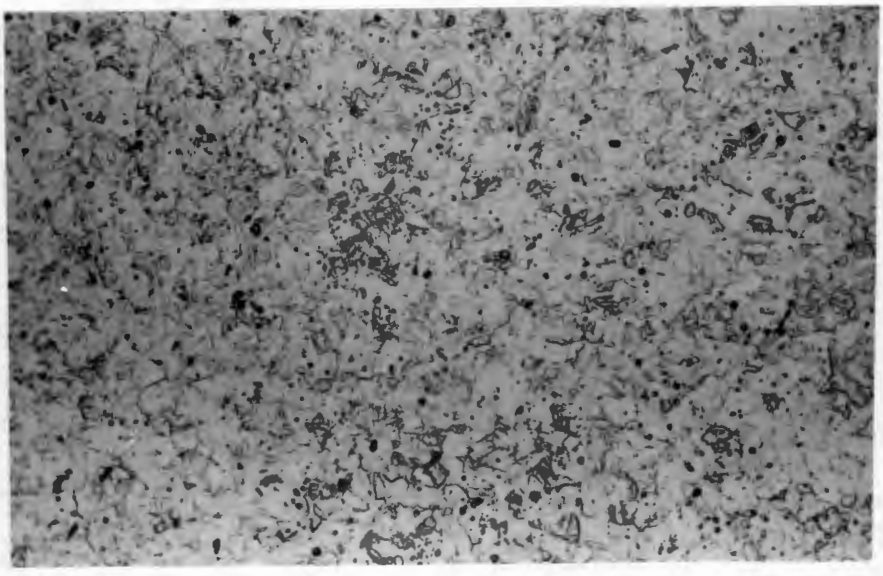

(d) Alloy 6 : 14,3%Cr; 2,8%Ni

Heat Treatment: Water quenched from 1000°C (1 hour)

Prior Heat Treatment: i) AHR condition, then
ii) anneal at 1000°C (1 hour) followed by a furnace cool

FIG. 5.32(c) and (d): The grain refining effect of increasing nickel additons on the 14,3% Cr alloys.

5.2.4 T.E.M.

In order to distinguish between the various phases present, transmissionn electron microscopy was used. Figs. 5.33, 5.34 and 5.35 are typical micrographs obtained for Alloy 6, heat treated for 3 hours at 840°C, 800°C and 707°C respectively.

Fig. 5.33 depicts the micrograph obtained for alloy 6 (2,8% Ni) after a heat treatment consisting of a 3 hour anneal at 840°C and then oil quenched. The 'lath' type martensite which is typical of low carbon steels is clearly depicted in this micrograph. It is anticipated that this type of martensite (within a fine grained ferrite matrix) will be responsible for the improved toughness and formability properties which is characteristic of these steels. It will be noted that according to the phase transformation diagram in Fig. 5.31 alloy 6 with 2,8 percent nickel should be martensitic at 840°C and this structure is confirmed by transmission electron microscopy, as well as by metallography.

The micrograph obtained for alloy 6 (2,8% Ni) after a 3 hour anneal at 800°C (followed by OQ) is depicted in Fig. 5.34. According

to the phase transformation diagram in Fig. 5.31, a duplex ferrite-austenite (martensite) is evident in Fig. 5.34. However, it will be noted that the metallographically obtained microstructures at 800°C indicates a martensitic structure. This could possibly be as a result of the one hour anneal at temperature (for metallography samples) as opposed to the three hour anneal for the TEM samples.

It should be emphasized again that since the kinetics of transformation in these alloys was still unknown the different annealing times used in this investigation may only indicate whether a certain phase or phases exist at a particular temperature, for the conditions specified.

After a three hour anneal at 707°C (followed by OQ), alloy 6 (2,8% Ni) depicts a predominantly ferritic structure in Fig. 5.35 According to Fig. 5.31, a duplex ferrite-austenite (martensite) structure is expected at 707°C, which is evident after a one hour anneal at 707°C (followed by WQ) in the metallography samples. However, at 700°C, alloy 6 is rather close to the phase boundary separating the fully ferritic region from the duplex ferrite-austenite region.

Clearly further work is required in order to determine the transformation kinetics of these alloys.

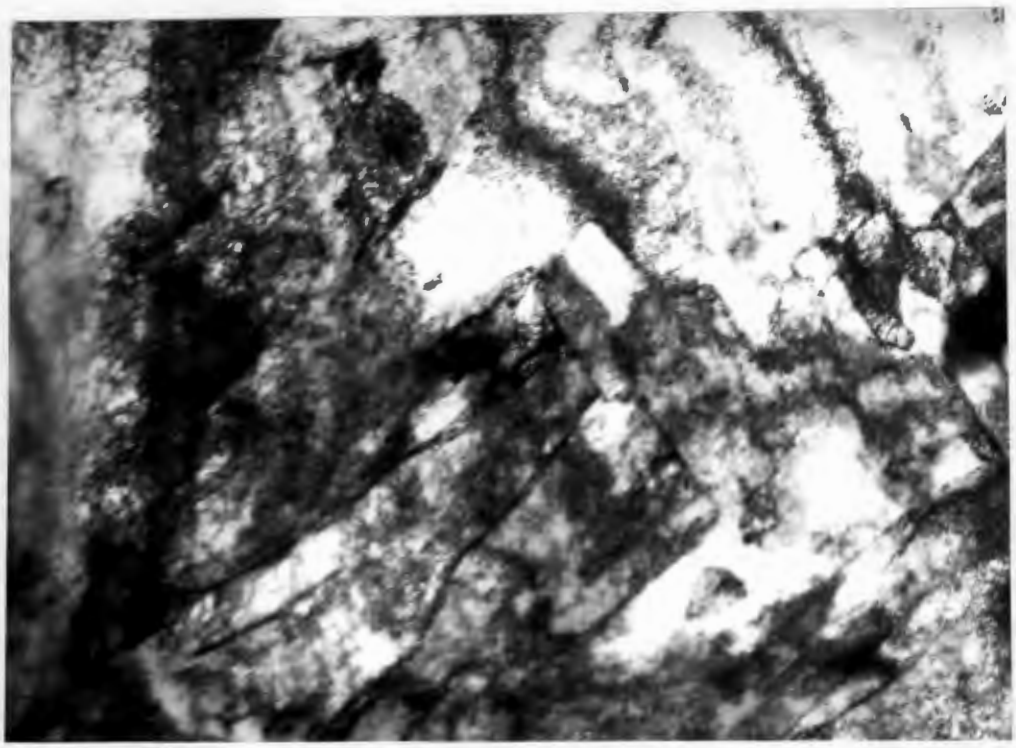

FIG. 5.33

Alloy 6: (14,3%Cr ; 2,80%Ni)
depicting "lath" type martensitic structure

Heat Treatment: Held at temperature 840°C for 3 hours and then oil quenched

Prior Heat Treatment : i) AHR condition, then
ii) homogenized at 1000°C for 1 hour followed by FC

0,5 μm

FIG. 5.34

Alloy 6: (14,3%Cr ; 2,80%Ni)
showing duplex ferritic-martensitic structure

Heat Treatment: Held at temperature 800°C for 3 hours and then oil quenched

Prior Heat Treatment : i) AHR condition, then
ii) homogenized at 1000°C for 1 hour followed by FC

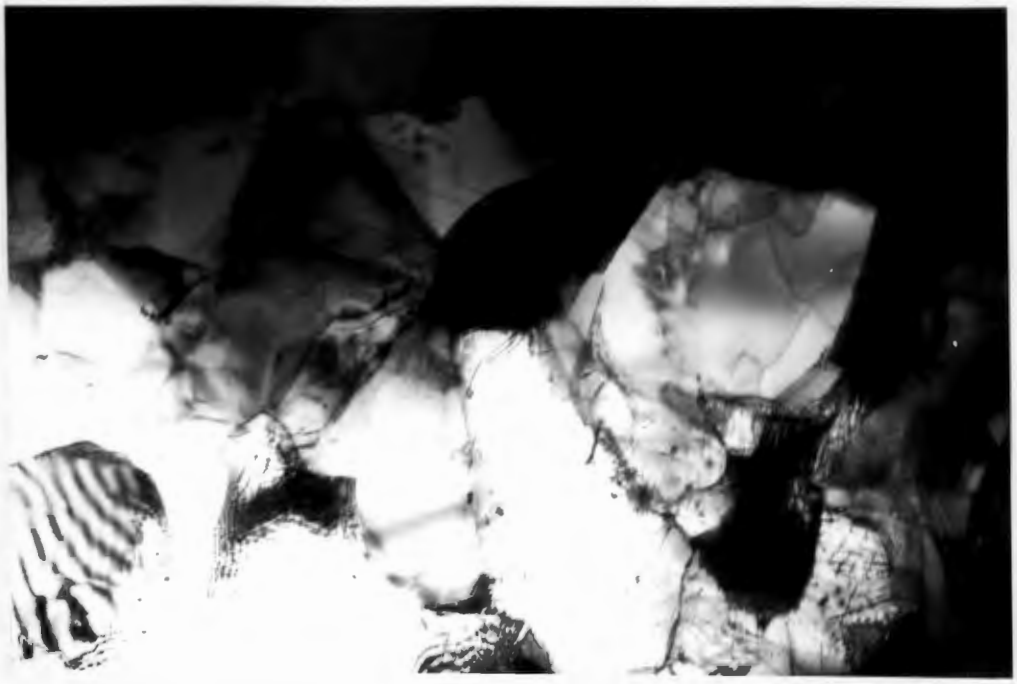

1 μm

FIG. 5.35

Alloy 6: (14,3%Cr ; 2,80%Ni)
showing predominantly ferritic structure

Heat Treatment: Held at temperature 707°C for 3 hours and then oil quenched

Prior Heat Treatment: i) AHR condition, then
ii) homogenizing treatment at 1000°C for (1 hour) followed by FC

5.2.5 Hardness Measurements

The hardness values obtained as a function of nickel content and annealing temperature are shown in Figs. 5.36 and 5.37, and also in Figs. 5.38 and 5.39.

Alloys with increasing nickel content display an increase in hardness (Fig. 5.36) and (Fig. 5.37). This increase in hardness is continuous through the ferrite and dual phase region, although no significant effect is derived in fully austenitic (martensitic) structures.

From Fig. 5.37 it can be seen that an increase in the annealing temperature will raise the hardness for a particular nickel content. However, it should be noted that a larger increase in strength is obtained for the alloys which enter the duplex ($\alpha+\gamma$) region and retain this dual phase structure [alloys 2 (0,98%Ni); 3 (1,41%Ni) and alloy 4 (1,8%Ni)] as compared with the alloys which are either fully ferritic, such as Alloy 1 (0,62%Ni) or almost fully martensitic [alloys 5 (2,40%Ni) - 9 (5,60%Ni)].

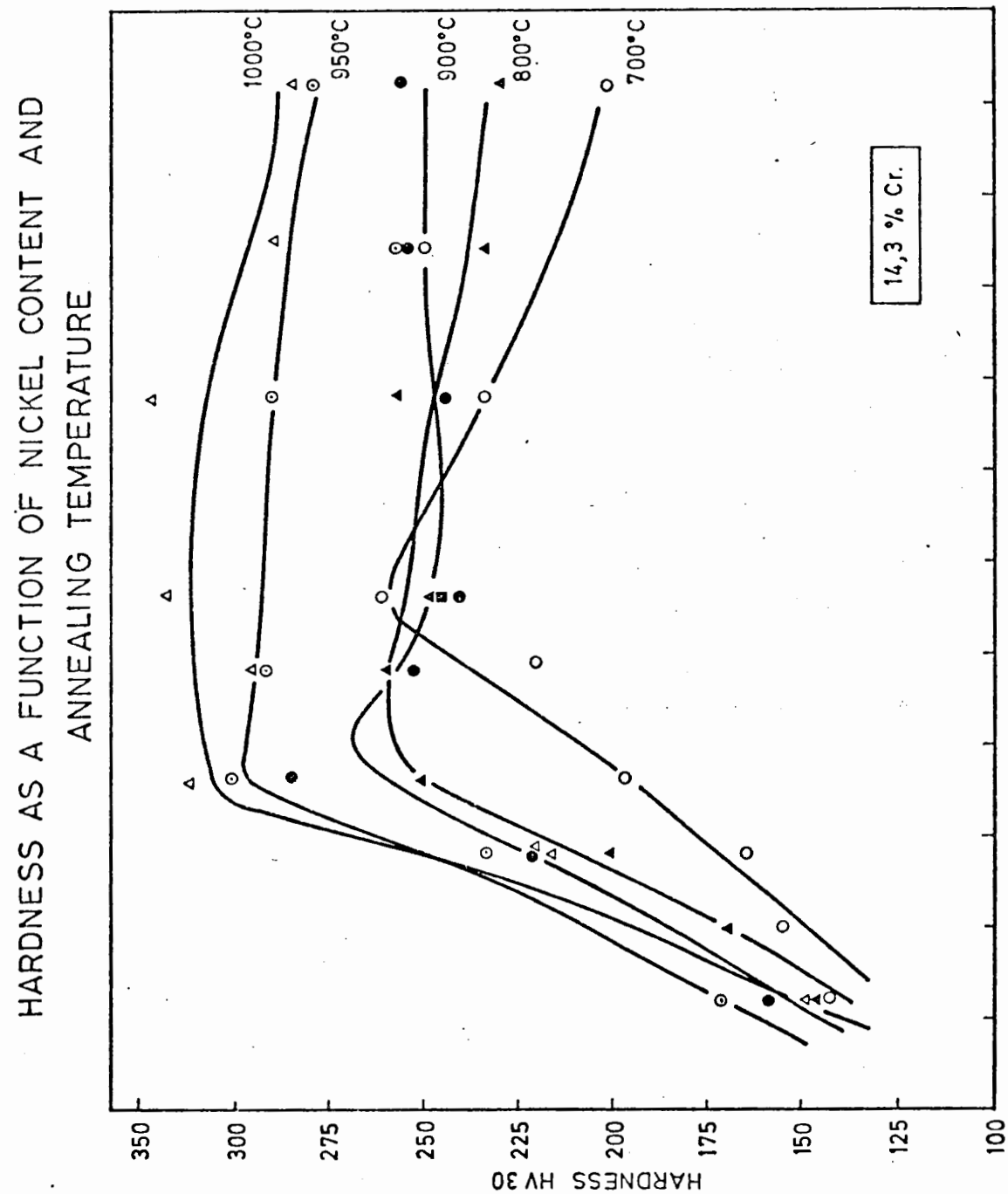

FIG 5.36 : Vickers Hardness measurements as a function of annealing temperature and nickel contents for the 14,3%Cr alloys.

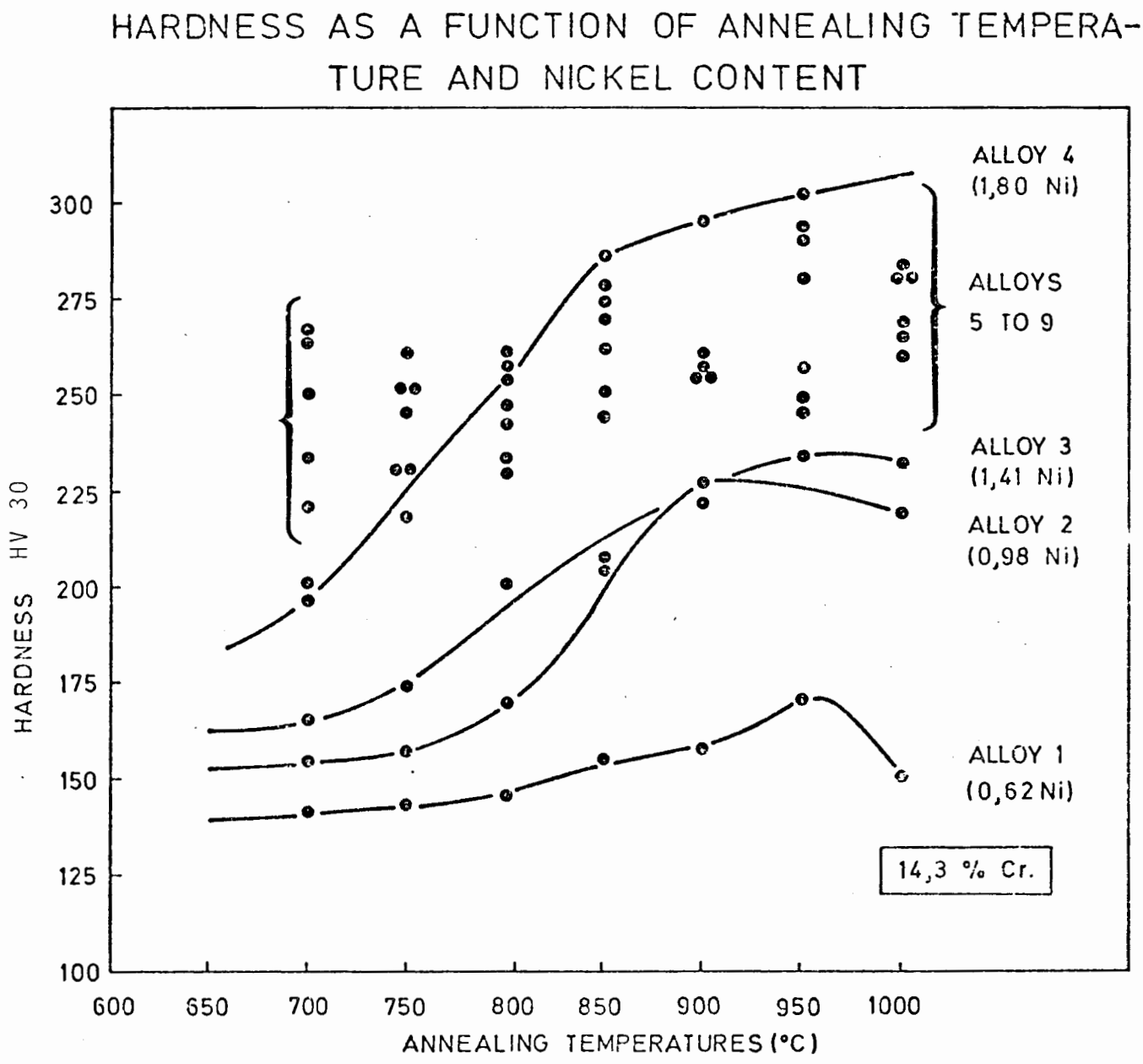

FIG. 5.37 Vickers hardness measurements as a function of annealing temperature and nickel contents for the 14,3%Cr alloys

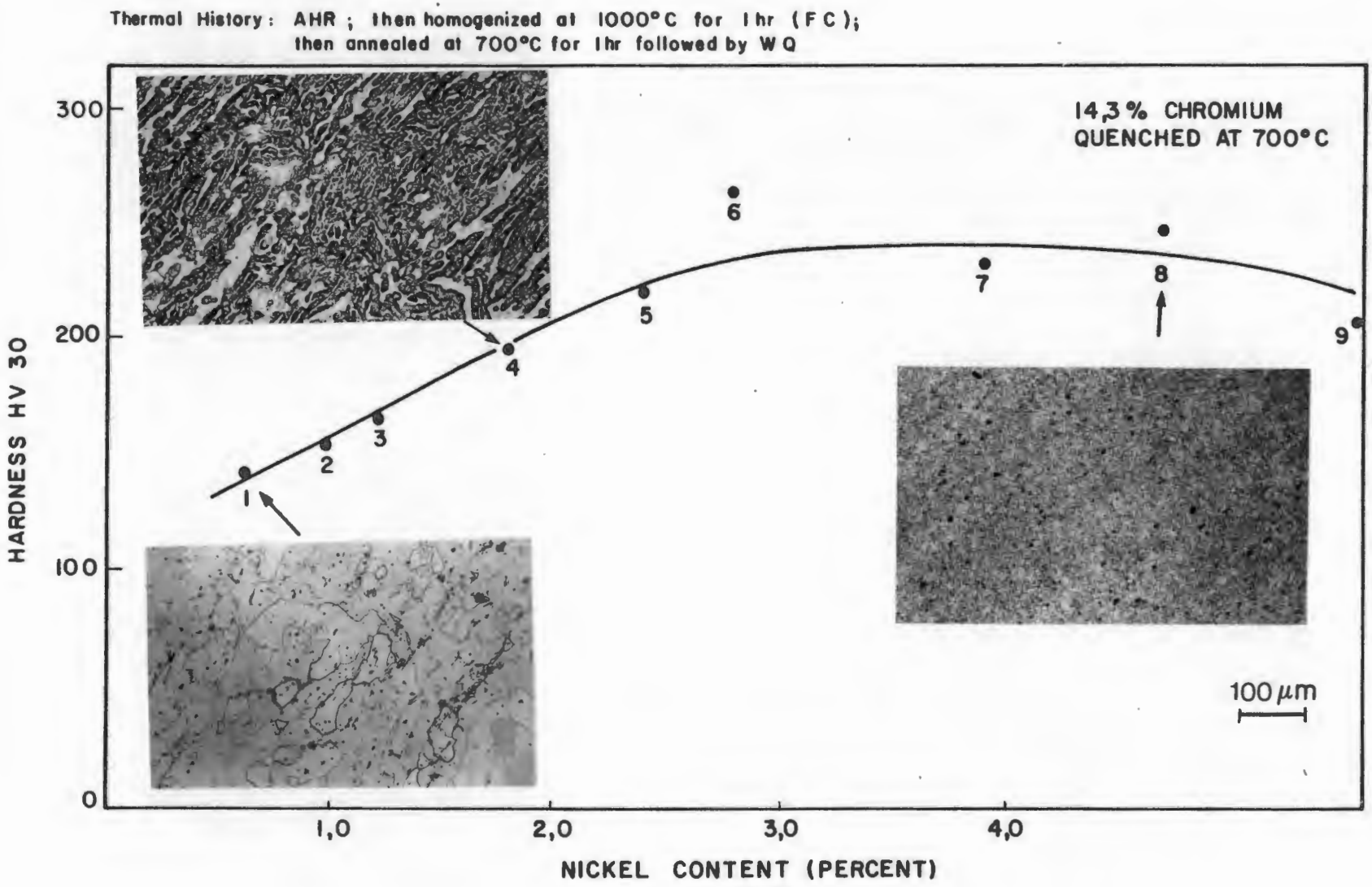

FIG 5.38 : Vickers Hardness as a function of nickel content (at 700°C) for the 14,3%Cr alloys. Included also is a typical micrograph for various alloys.

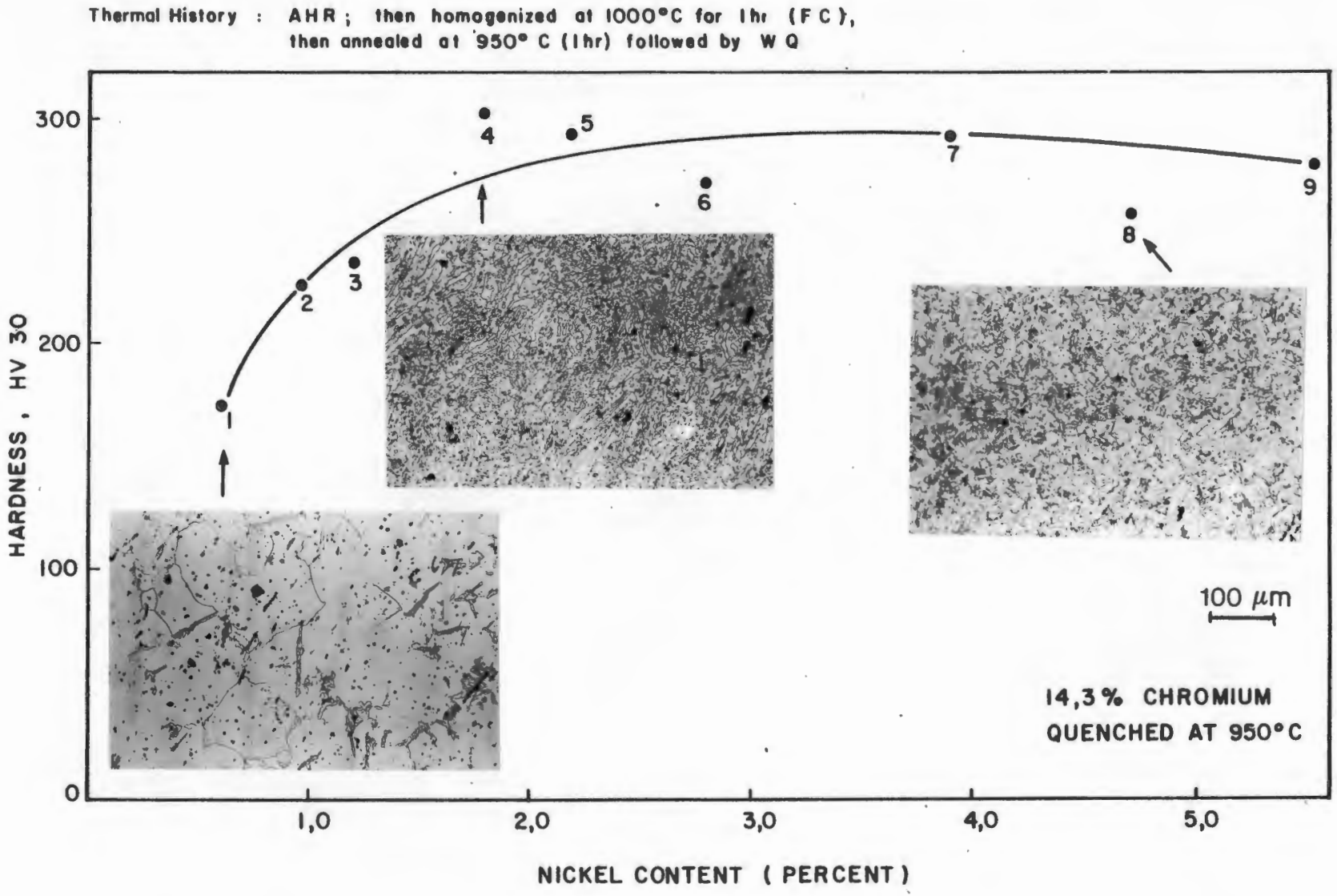

FIG 5.39 : Vickers Hardness as a function of nickel content (at 950°C) for the 14,3%Cr alloys. Included also is a typical micrograph for various alloys.

CHAPTER 6 : DISCUSSION

Various heat treatments and alloy element additions may be used in order to obtain a ferritic-martensitic microstructure. The advantage of a steel having such a microstructure has recently been recognised (Coldren & Eldis, 1980; and Rashid, 1981). An improvement in mechanical properties such as elongation to fracture or ductility is observed when the pearlite constituent of conventional microalloyed HSLA steels and plain carbon steels is replaced by martensite.

It has been shown (Hayden and Floreen, 1970) that a minimum or critical amount of martensite within a ferrite matrix is required for the improved mechanical properties observed. The martensite phase appears to inhibit crack initiation as well as crack propogation. A primary prerequisite for the martensite phase to toughen a cleavage prone matrix is that, in addition to being strong, it should also be tough. It is well known that the strength and toughness of the martensite is primarily influenced by the carbon content. Increasing the carbon content of the steel will increase the strength of the martensite phase; a 'lath' type martensite which is tough and is typical of low carbon alloys as opposed to a 'twinned' structure present in high carbon steels which is hard and brittle (Krauss and Marder, 1971). To avoid this twinned type martensite in plain carbon steels, a

maximum martensite carbon content of 0,03% is maintained (Koo & Thomas, 1977) while the overall carbon content of the alloy is kept below 0,1%. However, the total carbon and nitrogen levels in 3CR12 are each kept characteristically low at 0,03 (weight) percent ensuring improved toughness properties.

The design of these dual phase steels requires an understanding of the origin of this microstructure. In order to arrive at the optimum microstructure for a particular mechanical response, the various phases need to be identified and characterized. In addition, the influence of various alloying elements and thermal history on the resulting phase structure needs to be determined. Parameters such as volume fraction, grain size, and distribution of the various microconstituents is also required.

Dilatometry has been used to map the phase transformation diagram as a function of nickel content and temperature. A similar trend is observed in the phase diagrams obtained for the Fe-11,5%Cr and 14,3%Cr alloys as compared with previous work (Bain and Aborn, 1939). According to Myers (1977), "The Fe-Cr-Ni system is known only semi-quantitatively. However, precise information for a system composed of several pure elements and in a true state of equilibrium would seem to be of no increased usefulness with respect to identifying the structure of commercial

alloys. A comprehensive review of the Fe-Cr-Ni system was made by Bain and Aborn (1939) {and more recently by Rivlin and Raynor (1980)}. These studies have resulted in a series of semi-quantitative diagrams which show the effect of nickel and temperature on structure at various chromium contents ranging from 0 to 24%" (as noted in Fig 3.1). The shift of the 'nose' of the dual phase region for the 14,3%Cr alloys to higher nickel contents is to be noted. The edge of this nose is connected at approximately 0,3 percent nickel for the low chromium alloys and at approximately 0,7 percent nickel for the high chromium alloys. It is to be noted that increasing the chromium content requires an increased amount of nickel content in order to enter the dual phase region. Thus the successful design of the ferritic-martensitic dual phase alloy relies upon a critical balance of the austenitic promoting and ferritic promoting additions.

The two alloy series studied exhibit both a low temperature and a high temperature dual phase region. For the 11,5 percent chromium composition the ($\alpha+\gamma$) phase is present between approximately 620°C and 1000°C, while at high temperature ($\gamma+\delta$) is present between 1110°C and 1300°C (see Fig. 5.7). For the higher chromium content alloys, the ($\alpha+\gamma$) phase is present between 600°C and 900°C and the high temperature ($\gamma+\delta$) between 1080°C and 1380°C (Fig. 5.27).

Although some reproducable results may be obtained with the dilatometric technique used in this investigation, it was not possible to determine the effect of a wide range of controlled cooling rates due to the inadequacies of this type of dilatometer. Unfortunately, it was not therefore possible to construct continuous cooling curves which may assist the plant metallurgist in the choice of correct heat treatment procedure.

It is apparent from the phase diagram that the dual phase regime is rather narrow. The size of this loop is also considerably influenced by the exact composition of alloying elements. An important consideration in the large scale production of these steels is the enlargement of this region. It has been shown (Wright and Wood, 1977) that manganese (Fe-Cr-Mn system) expands this dual phase region to a larger degree than does nickel (see Appendix D). Precise control of heat treatment is thus less critical. However, the advantage of nickel is that it has been shown to increase the toughness of the martensite constituent.

Grain refinement occurs as a result of the various phase transformations and heat treatments used to produce the dual phase microstructure. Thermal history and starting microstructure of the steel has a powerful influence on the final microstructure obtained. The high hardenability of 3CR12 ensures

that a duplex ferritic-martensitic structure is obtained even over a wide range of cooling rates. For instance, the duplex ferritic-martensitic structure is observed after an annealing treatment (such as in a furnace cool), an air cool (intermediate cool) as well as after a relatively fast cool such as that experienced by a water quench.

In the as-rolled condition, 3CR12 consists of a banded structure of martensite and ferrite. Reheating this steel over the temperature range 200°C-600°C does not significantly alter the microstructure observed optically.

When the steel is heated to a temperature above the critical temperature, ie. the Ac_1 in the dual phase ($\alpha+\gamma$) region various phase transformations may occur. If the microstructure of the steel consists of ferrite, carbides are dispersed in the matrix as well as grain boundary carbides; the latter are usually sites for the nucleation of austenite (Lenel, 1980). Evidence for the grain boundaries acting as nucleation sites in these alloys may be seen from Fig. 5.28. This micrograph clearly depicts the second phase austenite (now martensite) nucleating at the grain boundaries of the primary phase ferrite matrix. Nucleation and growth modes of the austenite is dependent upon the transformation kinetics of the particular alloy. The transformation kinetics will

depend upon various factors such as the thermodynamic driving force and the rate of diffusion. Generally, the diffusion rate is increased and the driving force is decreased with an increase in temperature. As the temperature is decreased, the driving force increases and the diffusion rate decreases.

Diffusion of carbon and nitrogen and the partition of alloying elements to the various phases present will occur (Koo et al, 1980). For instance, carbon is more soluble in austenite than ferrite and is a powerful austenitizer. Although the carbon content of this steel is characteristically low at 0,03 percent, titanium is added to stabilise the steel against intergranular corrosion by preferentially forming cuboid titanium carbo-nitride precipitates. This process will lower the carbon content present in solution. The effect of the carbide precipitates on the dislocation structure and subsequent deformation and fracture is not clear. However, these precipitates have been observed in the ferrite phase, for instance see Fig. 5.29. The micrograph clearly depicts very finely dispersed carbide precipitates in the ferrite matrix. A cuboid titanium (carbo-nitride) precipitate, may also be observed in the ferrite matrix . Some authors (eg. Koo and Thomas, 1979) have reported that a "clean" or precipitate-free ferrite may lead to improved strength-ductility relationships. Further work is required in order to determine the precise effect of the distribution and morphology of the carbide precipitates in these alloys.

Nickel has also been observed to partition to the austenite phase during intercritical annealing (Koch and Eckstein, 1979; Leone & Kerr, 1980; Ball and Hoffman, 1979). Composition gradients may exist between the various phases and further work is required in order to determine the partitioning effect of the interstitial carbon and nitrogen as well as the substitutional nickel, chromium and manganese. This may elucidate the rate controlling mechanism operative in these steels.

Quenching the steel that has been intercritically annealed will produce a range of microstructures depending upon the cooling rate. The austenite transforms to martensite in an exceptionally fine grained ferrite matrix. Prior austenite grain size will determine the grain size of the martensite. It is not clear how the cooling rate affects the distribution of the martensite. In some low carbon dual phase steels, (Huppi et al, 1980, and Geib et al, 1980), transformed or 'epitaxial' ferrite (ie. ferrite that transforms from austenite on cooling) has been observed, in addition to the retained ferrite and martensite. Retained austenite and some bainite has also been observed, (Rigsbee and VanderArend, 1979). In this investigation the etching technique could not distinguish between the epitaxial and retained ferrite if present.

Supercritically heating the steel, ie. above Ac_3 in the austenitic region will produce a fully martensitic structure upon quenching. However, if the alloy composition lies within the 'nose' of the dual phase curve, the alloy will always be duplex ferrite-austenite (martensite) at all temperatures.

A sufficient holding time at temperature is required for 'equilibrium' conditions to be attained. Thus an investigation into the kinetics of the various phase transformations occurring in these alloys is required.

Further grain refinement of these duplex alloys is possible by thermal cycling through the dual phase region between the Ac_1 and Ac_3 temperatures (Wert, 1982). The mechanism of grain refinement in this case is nucleation of the product phase at grain boundaries in the parent phase. As grain size becomes finer during successive cycles, more nucleation sites are available for the next transformation. Eventually, saturation occurs at a very fine grain size and further cycling does not produce additional grain refinement. Dual phase steel with very fine grain size can be produced in the controlled rolling process. Controlled rolling can be done as a continuous process unlike thermal cycling; thus controlled rolling is more suitable for large scale production. Grain refinement and grain size control are essential for superplasticity. Ball and Hoffman (1979) have shown that high nickel 3CR12 exhibits

superplastic behaviour, and this effect is being further investigated. Design considerations from general studies dictate that decreasing the grain size (d) should increase strength (σy) according to the Hall-Petch relation($\sigma_y \propto d^{-\frac{1}{2}}$) (Pickering, 1978). The impact toughness and ductile to brittle transition temperature, DBTT, is also influenced by the grain size according to the relationship($\beta T = \ln\beta - \ln C - \ln d^{-\frac{1}{2}}$) (Pickering, 1978). The exact forms of this relationship for dual phase alloys could be investigated.

An increased nickel content decreases the Ac_1 and Ac_3 temperatures (see Figs. 5.7 and 5.27). Thus a higher nickel content will require a lower annealing temperature in order to obtain the beneficial dual phase structure. The effect of nickel additions on the microstructure may be seen from Figs. 5.32 (a-d). For Alloy 1 containing 0,62%Ni and annealed at 1000°C (1 hour) followed by a water quench, large polygonal ferrite grains are observed. This alloy is ferritic at all temperatures. By increasing the nickel content to 0,98% (Alloy 3) and after a similar heat treatment, the micrograph depicts a very fine-grained ferritic-martensitic dual phase microstructure. A similar microstructure is obtained for Alloy 5 (2,4%Ni). However, for Alloy 6 containing 2,8%Ni a predominantly martensitic structure is indicated. The effect of nickel additions on the microstructure of the 11,5%Cr alloys may also be seen from

Figs. 5.12(a) → 5.12(d). In alloy A (0,27%Ni) the second phase austenite (now martensite) may be seen to nucleate from the grain boundaries of the primary phase (in this case ferrite). Increasing the nickel to 0,49 percent appears to increase the volume fraction of the second phase. This process is accompanied by a grain refinement of the primary phase. It can be seen that increasing the nickel content further will markedly influence the morphology, ie. size, distribution and shape of the various constituents present. An extremely fine-grained duplex microstructure is evident for alloy C with 0,85 percent nickel; and with 1,19 percent nickel, the second phase now appears to consist of a fibrous distribution of martensite in a ferrite matrix (Fig. 5.12(d)).

Similar results have been reported by Koo and Thomas, (1979), who noted that the morphology of the second phase martensite (in dual phase plain carbon steels) may be markedly influenced by the additions of a few percent silicon.

Transmission electron microscopy has confirmed the lath type structure expected of a low carbon martensite (see Fig. 5.13). These laths are arranged in parallel arrays within a former austenite grain and have a high dislocation density. It is anticipated that this lath martensite is both strong and tough and essential to the good deformation

characteristics of these alloys. The ferrite grains have a moderate dislocation density compared to the heavily dislocated martensite. It is frequently observed (Fig. 5.14) that the ferrite grain interiors have a low dislocation density relative to the martensite islands or regions. Some authors refer to these martensite islands or regions as "particles" (Cribb and Rigsbee, 1979; and Koo and Thomas, 1979{b}). The apparent cause for the high dislocation densities around the martensite islands is the volume expansion and shear accompanying the austenite to martensite transformation. This inhomogeneous distribution of dislocation structure will have an important consequence on the yielding and hence deformation behaviour typical of this steel.

It is anticipated that the martensite islands will act as sources of dislocations which are mobile in the ferrite. The high density of dislocations is unlikely to be pinned by the small concentration of available carbon. The free dislocations produced will move at stresses much lower than those required to move pinned dislocations, such as those commonly present in the ferrite-pearlite carbon steels. Thus, the material has a multitude of sources of free dislocations for the initiation of plastic flow. This explains the absence of yield point or Lüders band (continuous yielding behaviour) and the high work hardening rate observed (particularly at low strains) in duplex ferritic-martensitic alloys.

The good coherency of the ferritic-martensitic interface is also an important criterion for the improved ductility and formability. (Koo and Thomas, 1979{b}). Because of the low carbon content of this steel, distortion of the body centred tetragonal (or cubic) lattice is minimal (refer to Fig B.1, Appendix B). This should result in a good atomic fit between the martensitic and ferritic phase. Since the micro-mechanical deformation of these dual phase steels depends upon the coherency between the martensite and ferrite (a high degree of coherency preventing the initiation of ductile tearing at the grain boundaries), detailed studies of the relationship between martensite/ferrite morphology and deformation should be undertaken.

Of particular significance is the location of the temperature at which martensite starts (Ms) to form upon cooling an austenitic structure. For both alloy series increasing nickel depresses the Ms temperature (see Figs. 5.7 and 5.27). Nickel is a good austenitizer and enlarges the range over which austenite is stable, and lowers the transformation temperature of austenite to martensite.

This effect is clearly shown in Fig. 5.1 where the dilatometric trace of a low nickel alloy is compared with a high nickel alloy. These dilatometric traces may be compared with those obtained by Bee and Honeycombe, 1978 (see Appendix C). Dilatometry was

used in this investigation in order to determine the transformation characteristics of a high purity Fe-9,6%Cr alloy. It is clear from these diagrams that increasing the chromium content also increases the hysteresis in the $\alpha \rightarrow \gamma \rightarrow \alpha$ transformation. It is suggested (Bee and Honeycombe, 1978) that the reaction is interface controlled, and supports the existence of a "solute-drag" effect by carbon even at very low concentrations (0,003 -0,007 percent).

The effect of two different cooling rates (furnace cool, FC and air cool, AC) on the Ms is included in Tables A.1-A.4 (see Appendix A). Air cooling these alloys as opposed to a furnace cool may further depress the Ms (see Figs. A.1 → A.6). It is evident from these figures that air cooling may depress the Ms by as much as 200°C. In Tables A.2 and A.4 of Appendix A, a comparison of Ms furnace cool (FC) is made with Ms air cool (AC) for the 11,5%Cr and the 14,3%Cr alloys respectively. The Ms determined experimentally is found to be seriously cooling rate dependent with changes of for example, (see Table A.2) 270°C for alloy C (11,5%Cr) and 210°C for alloy I (11,5%Cr).

E.R. Petty in "Martensite: Fundamentals and Technology", 1970, has the following to say about the characteristics of martensite transformations. "The reaction begins after considerable undercooling at a temperature known as Ms which is stated to be constant

for an alloy irrespective of cooling rate. Some recent results show that this is not the whole truth and it is also known that Ms is affected by prior heat treatment conditions." Furthermore, in a constitutional study of a 9Cr-1Mo alloy, Pickering and Vassiliou, 1980, observed slight variations in the Ms temperature which were correlated with the effect of undissolved ferrite and carbide on the composition of the austenite.

It is suggested below that Ti(C,N) formation may explain the observed effects of Ms dependence upon cooling rate for 3CR12.

If the information which is presented in Table 3 (depression of Ms temperature) in Appendix F is considered, then it appears that the effect of Ti(C,N) may be a possible explanation for the observed differences in Ms (FC) and Ms (AC). For instance, according to Hull, 1973, the effect of one percent carbon is to depress the Ms by as much as 2388°C.

Similarly each percent of nitrogen and titanium added will further depress the Ms by 3222°C and 180°C respectively. Thus, for a carbon and nitrogen content of 0,03 percent, the Ms may be depressed by as much as 71,6°C and 96,6°C respectively. For a titanium content of 0,32 percent, the Ms may be depressed by 57,6°C. Therefore, the combined effect of Ti (C,N) may depress the Ms by as much as 225°C.

At 1000°C, most of the carbon (and nitrogen) will be present in solution in the austenite phase, since it has been shown (Pickering and Vassiliou, 1980) that most, but not all, of the carbides will dissolve in this temperature range (ie. 1000°C-1200°C). Cooling the steel back to room temperature will transform the austenite to martensite at a particular temperature, ie. the Ms. It is well established that all alloying elements (except cobalt and aluminium) depress the Ms, carbon and nitrogen having the most powerful influence, followed by manganese and nickel (Pickering, 1978). It is also well known that the hardenability of the austenitic pool (which is determined by the presence of alloying elements in solution) will influence the cooling rate necessary to transform the austenite to martensite and not some other constituent, such as bainite or pearlite. A lower hardenability requires a faster quench rate in order to ensure martensite formation, whereas a highly alloyed steel such as 3CR12 with a higher hardenability does not require as fast a quench.

During the cooling cycle, precipitation of carbides may occur. This process will deplete the amount of carbon present in solution thereby lowering the hardenability of the alloy. This, in turn, will increase the cooling rate required to form martensite. Furthermore, with a lower overall alloy content in solution, (in the austenite), the temperature at which the martensite phase transformation starts will

increase. During a furnace cool, more time is allowed for the diffusion of carbon and the subsequent formation of precipitates. However, during an air cool, there is less time for the diffusion of carbon and consequent formation of precipitates. Therefore, by air cooling more carbon remains in solution; and increasing the total alloy content present in solution usually depresses the Ms.

However, it should also be noted that for an alloy within the 'nose' of the dual phase region (for example Alloy C) a two-phase structure is anticipated at 1000°C. In this case, partitioning of the alloying elements may occur in the ferrite phase as well (Kock and Eckstein, 1978 and Leonne & Kerr, 1982) and thus alter the compositional balance and phase structure of the various phases (in particular austenite). This in turn will affect the Ms temperature.

It has been shown (Tanaka, 1979; Huppi, 1980) in some plain carbon dual phase steels that a faster quench rate will also lower the Ms, significantly change the microstructure and increase the strength of the alloy.

However, in this work the consequence of a lower Ms, especially on the resultant microstructure and strength of the alloys, has not yet been determined. A correlation between the cooling rate, the Ms, the microstructure and the strength of the alloy may provide a useful guide for the optimum commercial

production of these alloys. It should be noted that an important design consideration for these alloys requires that the Ms is not depressed to below room temperature.

The temperature at which martensite formation is complete, ie. the Mf, is also decreased as the nickel content increases. According to the tables in Appendix A (A.1 and A.2) it can be seen that the Ms-Mf temperature range is of the order of approximately 110°C for the 11,5%Cr alloys and of the order of 85°C for the 14,3%Cr alloys. (Tables A.3 and A.4 in Appendix A).

Furthermore, a high nickel content may have the consequence of a higher amount of retained austenite. The amount of retained austenite could be important in applications where the wear and abrasion resistance of the alloy is to be exploited. It is known that under the severe conditions of stress and strain rate typical of abrasion, the retained austenite can undergo a stress-induced transformation to martensite, absorbing energy in the process and hence giving the alloy good wear resistance. Thus a high nickel content may be beneficial in such circumstances. This phase transformation property coupled with the corrosion resistance benefits of this alloy is unique and could be of considerable importance in hostile abrasion and corrosion conditions such as the South African gold mining industry.

The tempering results (Figs. 5.19 and 5.20) are consistent with the observation that the martensite has a low carbon content (due to the lath type structure). Usually a continuous decrease in hardness with tempering temperature is expected. For the experimental alloys there is no decrease over the temperature range 300°C-500°C, and a 25% decrease in hardness between 500°C-700°C. (Fig. 5.20). The micrographs (Fig. 5.19) depict no significant changes for tempering temperatures below 500°C. However, at 600°C and especially at 700°C the micrographs depict a very finely dispersed carbide precipitate throughout the matrix. It is assumed that the very low carbon content (0,03%) prevents significant decomposition of the martensite in the lower temperature range whereas above 600°C the diffusion of carbon and the consequent formation of precipitates is thermally assisted.

Although Pickering and Vassiliou (1980) observed a similar trend in the tempering characteristics for a 9Cr-1Mo (unstabilised) alloy, a slight difference is to be noted. A slight secondary hardening effect was observed at 500°C mainly as a result of Cr_2N precipitation. This effect was not observed for the 11,5%Cr alloys investigated in this work. However, E.R. Petty, 1970, in 'Martensite: Fundamentals and Technology', has the following to say on the tempering of alloy steels. "Above about 550°C alloy carbides are formed at the expense of cementite and the process is accompanied either by slight softening or by an increase in hardness."

The hardness data gives some indication of the expected strength of the alloys. For the 11,5%Cr alloys (Fig. 5.16) we note that the hardness increases as the nickel content and annealing temperature is raised. To determine how the hardness is affected by the different phases, the phases present at a particular annealing temperature are indicated in Fig. 5.17 (700°C) and Fig. 5.18 (900°C). It is evident from these figures that nickel additions result in increasing strength in both the single phase fully ferritic and dual-phase ferrite plus austenite (martensite) region.

The strengthening effect observed is probably due to solid solution hardening of nickel in the ferrite. The presence of a second phase (in this case low carbon martensite), and the consequent fine grain size will further increase the strength.

Once the fully martensitic phase is present, increasing nickel has no signficant effect on the strength. It therefore appears that the effect of nickel on the strength of the martensite phase itself is minimal. This should be contrasted to the large effect that carbon (and nitrogen) will have on the martensite strength.

For a particular annealing temperature within the dual phase region increased nickel content results in higher strength. The volume fraction of austenite

(hence martensite) will be determined by the 'lever rule' for 'equilibrium' systems. Thus, for a particular annealing temperature, within the ($\alpha+\gamma$) region, increasing the nickel content will increase the proportion of the austenite phase thereby increasing the strength of the alloy (see phase diagrams). Thus nickel promotes the formation of martensite in these alloys thereby enhancing the mechanical properties.

A larger volume fraction of austenite is also obtained when the intercritical annealing temperature is raised (up to a particular temperature, ie. the temperature at which the edge of the nose of the phase diagram is located - which is at approximately 1000°C).

If the intercritical annealing temperature is increased even further, ie. above approximately 1000°C, then the volume fraction of austenite (martensite) will progressively decrease until the upper limit of the phase boundary is reached and a fully ferritic (delta ferrite) structure is indicated. Grain growth or grain coarsening which in general embrittles the alloy may then occur. Since the control of this grain growth is an important design consideration, a necessary requirement would seem to be that the alloy composition lies within the duplex ($\alpha+\gamma$) or ($\gamma+\delta$) region, and that fabrication and annealing temperatures are maintained below about 1100°C.

A similar effect is observed for the 14,3%Cr alloys. With an increase in nickel content a continuous increase in hardness is observed through the fully ferritic and dual phase region but no strengthening effect is observed within the fully martensitic region (see Figs. 5.36 - 5.39).

In fact, a slight drop in hardness is evident for the higher nickel alloys for example alloy 9 (5,6%Ni) which may possibly be due to a small amount of retained austenite.

For strengthening applications the following can therefore be recommended.

(a) For the 11,5%Cr alloys, a maximum nickel content of 1,5 percent.

(b) For the 14,3%Cr alloys, a maximum nickel content of 2,0 percent.

Various strengthening mechanisms are operative in these steels. These may include:

1. Martensite strengthening due to the volume fraction of this phase.

2. Solid solution strengthening of the ferrite due to alloy additions.

3. Grain size strengthening.

The precise chemical composition and heat treatment of these alloys needs to be critically controlled to achieve the optimum properties.

The phase transformation diagrams assist in this optimisation process by identifying the phase balance at different temperatures and showing the effect of alloy additions. Initial strength data indicate that these alloys show potential as moderate strength, and high formability materials, and have economic competitiveness because of the anticipated corrosion resistance.

CHAPTER 7 : SUMMARY

1. Phase transformation diagrams have been mapped as a function of nickel content and temperature, for a series of alloys containing 11,5 and 14,3 percent chromium. Dual phase regimes comprising austenite (martensite) and ferrite have been established.

2. The duplex ferritic-martensitic microstructure has been identified and confirmed by both optical and transmission electron microscopy. The low carbon 'lath' type martensite, within a very fine-grained ferrite matrix, is expected to be both strong and tough and is anticipated to be responsible for the improved toughness and formability properties characteristic of these steels. This lath type martensite is highly dislocated and may act as a source of mobile dislocations within the ferrite matrix.

3. The work has demonstrated the influence of thermal history and alloying element additions on the resultant microstructure and hardness measurements.

4. The tempering characteristics of the 11,5 percent chromium alloys were investigated over the temperature range of 100°C - 700°C. No

significant decrease in hardness was observed during tempering over the temperature range 100 - 500°C. However, a decrease in hardness was observed in the 500 - 700°C temperature range. The latter temperature range is suggested where tempering treatments are required.

5. Since it has been shown that both silicon (in plain carbon dual phase steels) and manganese (microduplex stainless steels) increase the size of the dual phase ($\alpha + \gamma$) regime, the effect of increasing silicon and manganese levels could be investigated for this steel. It is anticipated that the carbide forming titanium may play a significant role in determining the microstructural characteristics of the alloy. The influence of this alloying element on the ultimate phase balance could be further investigated.

6. A Time, Temperature, Transformation and a Continuous Cooling Transformation diagram is required in order to facilitate the 'design' of the large scale production of these alloys. These diagrams may provide useful information particularly for the as-rolled dual phase (ARDP) steel. Since the key to successful production of ARDP steel is reproducability in the control of the steel's transformation characteristics, a laboratory study in conjunction with a commercial mill trial is required in order to develop a

composition with transformation characteristics relatively insensitive to variations in thermomechanical treatment, (especially to the normal variations in hot-mill finish-rolling temperature, runout-table cooling rate and coiling temperature).

REFERENCES

ARAKI, K., TAKADA, Y., and NAKAOKA, K., "Work Hardening of Continuously Annealed Dual-Phase Steels", from Achives of the Iron and Steel Institute of Japan, Transactions [S], Vol. 17, 1977 pp 710 - 717.

BAIN, E.C., and ABORN, R.H., "The Iron-Nickel-Chromium Systems", Metals Handbook, American Society for Metals, Cleveland, Ohio, 1939, pp 418-422.

BALL, A., and HOFFMAN, J.P., "Microstructure and Properties of a Steel Containing 12%Cr", Metals Technology, Sept. 1981, pp 329-338.

BALL, A., "Properties and Microstructure of a Ferritic Stainless Steel" Report submitted to Middelburg Steel and Alloys (Pty) Ltd., 1979.

BEE, J.V., and HONEYCOMBE, R.W.K., "The Isothermal Decomposition of Austenite in a High Purity Iron-Chromium Binary Alloy", Metallurgical Transactions A, Vol. 9A, April 1978, pp 587-393.

COLDREN, A.P., and ELDIS, G.T., "Physical Metallurgy of the Dual Phase Steels", Molybdenum Mosaic, The Journal of Molybdenum Technology, Vol. 4, 1980, No. 3, pp 3-5.

COLDREN, A.P., and ELDIS, G.T., "Using CCT diagrams to optimise the compositon of an As-Rolled Dual-Phase Steel", Journal of Metals, Vol. 32, No. 3, March 1980, pp 41 - 48.

COLDREN, A.P., TITHER, G., CORNFORD, A., and HIAM, J.R., "Development and Mill Trial of As-Rolled Dual-Phase Steel", 'Formable HSLA and Dual-Phase Steels', A.T. Davenport, ed,; AIME, New York, N.Y., 1979, pp 205 - 230.

COLOMBIER, L., and HOCHMANN, J., (editors) "Stainless and Heat Resisting Steels", Edward Arnold, (Publishers), Ltd. London, 1967.

COTTRELL, A., "An Introduction to Metallurgy" 2nd edition, Edward Arnold (Publishers) Ltd, London, 1975.

CRIBB, W.R., and RIGSBEE, J.M., "Work Hardening Behaviour and its Relationship to the Microstructure and Mechanical Properties of Dual-Phase Steels", taken from 'Structure and Properties of Dual Phase Steels', Kot, R.A., and Morris, J.W., (editors), The Metallurgical Society of AIME, New York, N.Y., 1979 pp 91 -117.

DAVIES, R.G., "Influence of Martensite Composition and Content on the Properties of Dual Phase Steels", Metallurgical Transactions, Vol. 9A, May 1978, pp 671-679.

DAVIES, R.G., "Influence of Silicon and Phosphorous on the Mechanical Properties of Both Ferrite and Dual Phase Steels", Metallurgical Transactions, Vol. 10A, January 1979{a}, pp 113-118.

DAVIES, R.G., "On the Ductility of Dual Phase Steels", in 'Formable HSLA and Dual-Phase Steels', Davenport, A.T., ed., AIME, New York, N.Y., 1979{b}, pp 25 - 39.

ELDIS, G.T., "The Influence of Microstructure and Testing Procedure on the Measured Mechanical Properties of Heat Treated Dual-Phase Steels", taken from 'Structure and Properties of Dual Phase Steels', Kot, R.A., and Morris, J.W., (editors), The Metallurgical Society of AIME, New York, N.Y. 1979 pp 202 - 219.

FURUKAWA, T., MORIKAWA, H., TAKECHI, H., KOYAMA, K., "Process Factors for Highly Ductile Dual-Phase Sheet Steels," taken from 'Structure and Propeties of Dual-Phase Steels', Kot, R.A., and Morris, J.W., (editors), The Metallurgical Society of AIME, New York, N.Y., 1979. pp 281-303.

GEIB, M.D., MATLOCK, D.K., and KRAUSS, G., "The Effect of Intercritical Annealing Temperature on the Structure of Niobium Microalloyed Dual-Phase Steel", Metallurgical Transactions A, Vol. 11A, October 1980, pp 1683-1689.

GIBSON, R., "Structure and Constitution of Wrought Microduplex Stainless Steels", Handbook of Stainless Steels, Peckner, D., and Bernstein, I.M., (editors), McGraw-Hill Inc. 1977, Chapter 7, pp 12.

GREDAY, T., MATHY, H., MESSIEN, P., "About Different Ways to obtain Multiphase Steels", taken from 'Structure and Propeties of Dual-Phase Steels', Kot, R.A., and Morris, J.W., (editors), The Metallurgical Society of AIME, New York, N.Y., 1979.pp 260-280.

HAYDEN, H.W., and FLOREEN, S., "The Influence of Martensite and Ferrite on the Properties of Two-Phase Stainless Steels Having Microduplex Structures", Metallurgical Transactions, Vol. 1, July 1970, pp 1955-1959.

HONEYCOMBE, R.W.K., "Steels: Microstructure and Properties", Edward Arnold (Publishers) Ltd., London, 1981.

HULL, F.C., "Delta Ferrite and Martensite Formation in Stainless Steels," WELD, J., Res. Suppl., May, 1973, cited in WEISER, P.F., 'Structure and Constitution of Cast Iron- Chromium Alloys', Handbook of Stainless Steels, PECKNER, D., and BERNSTEIN, I.M., (editors) McGraw-Hill Inc. 1977, Chapter 9, pp 10-13.

HUME-ROTHERY, W., CHRISTIAN, J.W., and PEARSON, W.B., "Metallurgical Equilibrium Diagrams", The Institute of Physics, London, 1952.

HUPPI, G.S., MATLOCK, D.K., and KRAUSS, G., "An Evaluation of the Importance of Epitaxial Ferrite in Dual-Phase Steel Microstructures", Scripta Metallurgica, Vol. 14, 1980, pp 1239-1243.

KALTENHAUSER, R.H., "Improving the Engineering Properties of Ferritic Stainless Steels", Metals Engineering Quarterly, May 1971, pp 41-47.

KOCH, F., and ECKSTEIN, M.J., "Studies of the Redistribution of Chrome and Nickel during the Ferrite-Austenite Transformation in Chrome-nickel Steels of the 26.6 Type", Steel Furnace Monthly, Vol. 13, no 11, Nov. 1978 pp 441 - 445.

KOO, J.Y., and THOMAS, G., "Design of Duplex Fe/X/0,1C Steels for Improved Mechanical Properties", Metallurgical Transactions A, Vol. 8A, March 1977, pp 525-528.

KOO, J.Y., and THOMAS, G., "Metallurgical Factors Controlling Impact Properties of Two Phase Steels", Scripta Metallurgica, Vol. 13, 1979 (a), pp 1141-1145.

KOO, J.Y., and THOMAS, G., "Design of duplex Low Carbon Steels for Improved Strength: Weight Applications" taken from 'Formable HSLA and Dual-Phase Steels', Davenport, A.T., (editor), The Metallurgical Society of AIME, New York, N.Y., 1979 (b).

KOO, J.Y., RAGHAVAN, M., and THOMAS, G., "Compositional Analysis of Dual Phase Steels by Transmission Electron Microscopy", Metallurgical Transactions A, Vol. 11A, February 1980, pp 351-354.

KORZEKWA, D.A., LAWSON, R.D., MATLOCK, D.K., and KRAUSS, G. "A Consideration of Models Describing the Strength and Ductility of Dual-Phase Steels", Scripta Metallurgica, Vol. 14, pp 1023 - 1028, 1980, Printed in the U.S.A., Pergamon Press Limited.

KRAUSS, G., and MARDER, A.R., "The Morphology of Martensite in Iron Alloys", Metallurgical Transactions, Vol. 2, September 1971, pp 2344-2357.

LANZILLOTTO, C.A.N., and PICKERING, F.B., "Structure-Property relationships in Dual-Phase Steels", Metal Science, Vol. 16, August, 1982, pp 371-382.

LENEL, U.R., "The Reaustenitization of some Alloy Steels", PH.D. Thesis, Cambridge, 1980.

LEONE, G.L., and KERR, H.W., "The Ferrite to Austenite Transformation in Stainless Steels", Welding Journal, 61(1), Jan. 1982 pp 13-s - 21-s.

MARDER, A.R., "The Effect of Heat Treatment on the Properties and Structure of Molybdenum and Vanadium Dual-Phase Steels", Metallurgical Transactions, Vol. 12A, Sept. 1981, pp 1569-1579.

MARDER, A.R., and BRAMFITT, B.L., "Processing of a Molybdenum-Bearing Dual-Phase Steel", taken from "Structure and Properties of Dual-Phase Steels", Kot, R.A., and Morris, J.W., (editors). The Metallurgical Society of AIME, New York, N.Y., 1979.pp 242-259

MATLOCK, D.K., KRAUSS, G., RAMOS, L.F., and HUPPI, G.S., "A Correlation of Processing Variables with Deformation Behaviour of Dual-Phase Steels," taken from 'Structure and Properties of Dual Phase Steels', Kot, R.A., and Morris, J.W., (editors) The Metallurgical Society of AIME, New York, N.Y., 1979. pp 62-89

MELVILL, M.L., MAHONEY, C.S., HOFFMAN, J.P., and DEWAR, K., "The Development of a Chromium Containing Corrosion Resisting Steel", Paper presented at the Third South African Corrosion Conference, March 1980.

MYERS, L.P., "Effect of Chromium on the Structure and Properties of Stainless Steels", Handbook of Stainless Steels, PECKNER, D., and BERNSTEIN, I.M., (editors), McGraw-Hill Inc., 1977, Chapter 11 p.3

Öström, P., "Deformation Models for Two-Phase Materials", Metallurgical Transactions A, Vol. 12A, February, 1981, pp 355 - 357.

PETTY, E.R., (editor) of "Martensite: Fundamentals and Technology" Longman (Publishers), London, 1970.

PICKERING, F.B., "Physical Metallurgy and the Design of Steels", Applied Science Publishers, Ltd., London, 1978.

PICKERING, F.B., Private Communication, 1980.

PICKERING, F.B., and VASSILOU, A.D., "Effect of Austenitizing Temperature on Constitution, Transformation and Tempering of 9Cr-1Mo Steel", Metals Technology, October 1980, pp 409-413.

RASHID, M.S., "Relationship between Steel Microstructure and Formability" taken from "Formable HSLA and Dual-Phase Steels', Davenport, A.T., (editor) The Metallurgical Society of AIME, New York, N.Y., 1979.

RASHID, M.S., "Dual Phase Steel", Ann. Rev. Mater. Sci., Vol.11, 1981, pp 245-266.

REED-HILL, R.E., "Physical Metallurgy Principles", 2nd edition, D. Van Nostrand Company, New York, N.Y., 1973.

RICKS, R.A., BEE, J.V., and HOWELL, P.R., "The Decomposition of Austenite in a High Purity Iron-Chromium- Nickel Alloy", Metallurgical Transactions A, Vol. 12A, September 1981, pp 1587 - 1594.

RIGSBEE, J.M., and VANDERAREND, P.J., "Laboratory Studies of Microstructures and Structure-Property Relationships in Dual-Phase HSLA Steels", in 'Formable HSLA and Dual-Phase Steels, A.T. Davenport, (editor), AIME, New York, N.Y., 1979, pp 58 - 88.

RIVLIN, V.G., and RAYNOR, G.V., "Critical Evaluation of Constitution of Chromium - Iron - Nickel Systems", International Metals Reviews, 1980, No 1, pp 21 - 38.

ROBERTS, C.S., "The Effect of Carbon on the Volume Fractions and Lattice Parameters of Retained Austenite and Martensite", Journal of Metals, February, 1953, pp 203-204.

SNAPE, E., "Effect of nickel on the Structure and Properties of Wrought and Cast Stainless Steels", Handbook of Stainless Steels Peckner, D., and Bernstein, I.M., (editors), McGraw-Hill Inc., 1977, Chapter 12, pp 17-19.

TANAKA, T., NISHIDA, M., HASHIGUCHI, K., and KATO, T., "Formation and Properties of Ferrite Plus Martensite Dual Phase Structures", taken from 'Structure and Properties of Dual-Phase Steels', Kot, R.A., and Morris, J.W., (editors), The Metallurgical Society of AIME, New York, N.Y., 1979. pp 221-241

THOMAS, C.R., "SX 3CR12 A Material for Abrasion/Corrosion Control", The South African Institute of Metallurgists, Colloquim 'Wear and Abrasion in Industry', April, 1981.

THOMAS, G., and KOO, J.Y., "Developments in Strong, Ductile Duplex Ferritic-Martensitic Steels", taken from 'Structure and Properties of Dual-Phase Steels', Kot, R.A., and Morris, J.W., (editors), The Metallurgical Society of AIME, New York, N.Y., 1979. pp 183-201

WEISER, P.F., "Structure and Constition of Cast Iron-Chromium Alloys", Handbook of Stainless Steels, Peckner, D., and Bernstein, I.M., (editors) McGraw-Hill Inc., 1977, Chapter 9, pp 10 -11.

WERT, J.A., "Grain Refinement and Grain Size Control", taken from 'Superplastic Forming of Structural Alloys', Paton, N.E., and Hamilton, C.H., (editors). Conference Proceedings, The Metallurgical Society of AIME, 1982. pp 69-81

WRIGHT, R.N., and WOOD, J.R., "Fe-Cr-Mn Microduplex Ferritic-Martensitic Stainless Steels", Metallurgical Transactions A, Vol. 8A, December, 1977, pp 2007-2011.

APPENDIX A

11,5% CHROMIUM ALLOYS							
Alloy	% Ni	Ms(FC)	M_f(FC)	M_s(FC) - M_f(FC)	M_s (AC)	M_f(AC)	M_s(AC) - M_f(AC)
A	0.27						
B	0,49	760	680	80			
C	0.85	560	455	105	290	200	90
D	1,19	480	360	120	280		
E	1,34	450	340	110	275	200	75
F	1,77	430	325	105	200		
G	1,84	425	320	105	160	100	60
H	2,71	360	255	105	150	110	40
I	3,50	340	230	110	130	110	20

*Note: The above values for M_s and M_f are taken from the low temperature ($T<1000^oC$) experiment. Above temperatures in °C. This also applies to Tables A.3 - A.4.

Table A.1 : Ms(FC); M_f(FC) and M_s-M_f(FC);
Also Ms(AC); M_f(AC) and M_s-M_f(AC) for the 11,5%Cr alloys.

11,5% CHROMIUM ALLOYS							
Alloy	% Ni	Ms(FC)	M_s(AC)	M_s(FC) - M_s(AC)	M_f (FC)	M_f(AC)	M_f(FC) - M_f(AC)
A	0,27	*	*		*	*	
B	0.49	760	*		680	*	
C	0,85	560	290	270	455	200	255
D	1,19	480	280	200	360	*	
E	1.34	450	275	175	340	200	140
F	1,77	430	200	230	325	*	
G	1,84	425	160	265	320	100	120
H	2,70	360	150	210	255	110	145
I	3,50	340	130	210	230	110	120
* No transformation temperature observed on dilatometric trace							

TABLE A.2: Comparison M_s (FC) with M_s (AC.)
Also comparison of M_f (FC) with M_f (AC)
- 11,5%Cr alloys.

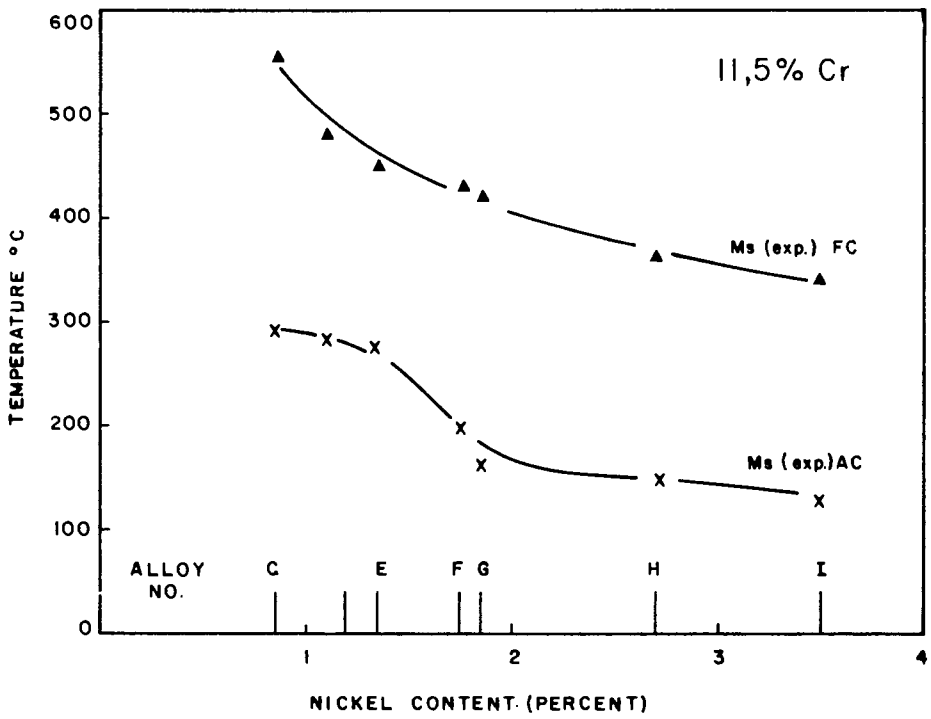

FIG. A.1 Comparison of Ms (FC) and Ms (AC) (11,5%Cr alloys)

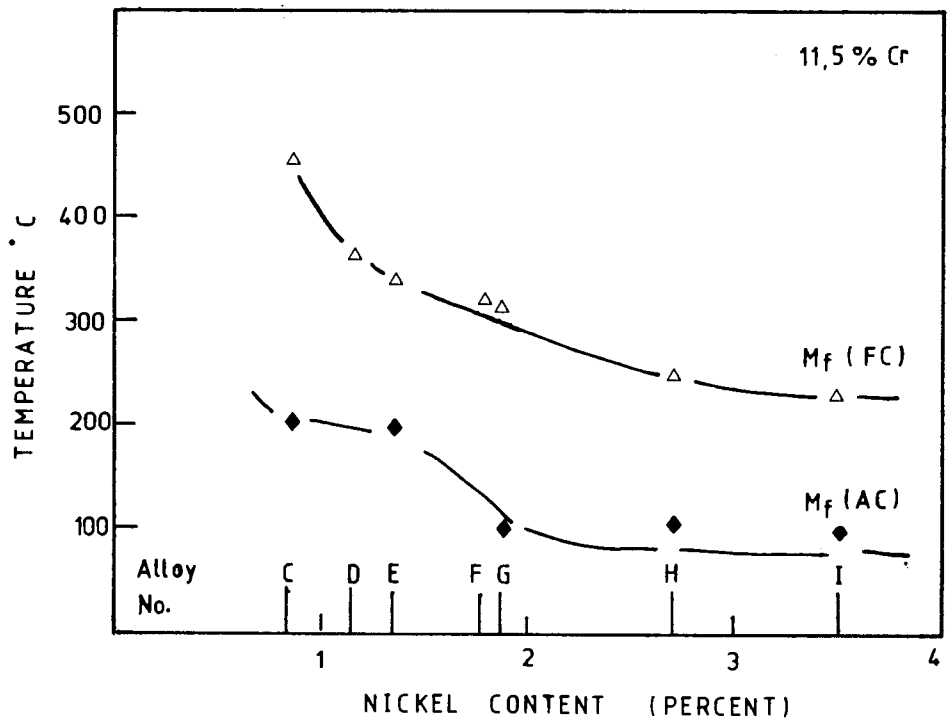

FIG. A.2 Comparison of M_f (FC) and M_f (AC) (11,5%Cr alloys)

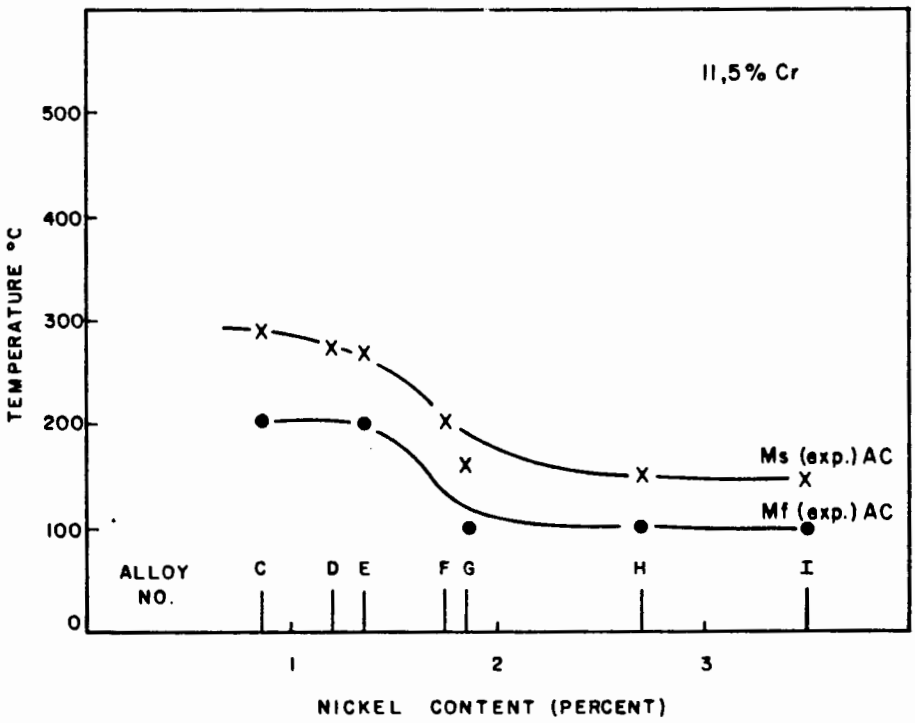

FIG. A.3 M_S (AC) and M_f (AC) for the 11,5%Cr alloys.

14,3% CHROMIUM ALLOYS							
Alloy	% Ni	Ms(FC)	M_f(FC)	M_s(FC) - M_f(FC)	M_s (AC)	M_f(AC)	M_s(AC) - M_f(AC)
1	0,62						
2	0.98	420	330	90			
3	1,41	410	325	85	275	180	95
4	1,80	360	280	80			
5	2,40	340	260	80	160	75	85
6	2,80	320	225	95	155	80	75
7	3,90	300	195	105	150	75	75
8	4,70	230	150	80	110	30	80
9	5,60	200	125	75	100	10	90

*Note: M_s and M_f transformation temperatures are taken from the low temperature ($T<1000^oC$) experiment. Above temperatures in °C.

Table A.3 : Ms(FC); M_f(FC) and M_s-M_f(FC);
Also Ms(AC); M_f(AC) and M_s-M_f(AC) for the 14,3%Cr alloys.

14,3% CHROMIUM ALLOYS							
Alloy	% Ni	Ms(FC)	M_s(AC)	M_s(FC) − M_s(AC)	M_f (FC)	M_f(AC)	M_f(FC) − M_f(AC)
1	0,62	*	*	-	*	*	-
2	0,98	420	*	-	330	*	-
3	1,41	410	275	135	325	180	145
4	1,80	360	*	-	280	*	-
5	2,40	340	160	180	260	75	185
6	2,80	320	155	165	225	80	145
7	3.90	300	150	150	195	75	120
8	4,70	230	110	120	150	30	120
9	5,60	200	100	100	125	10	115
* No transformation temperature observed on dilatrometric trace							

TABLE A.4: Comparison of M_s (FC) with M_s (AC)
Included also comparison of M_f (FC) with M_f (AC)
- 14,3%Cr Alloys.

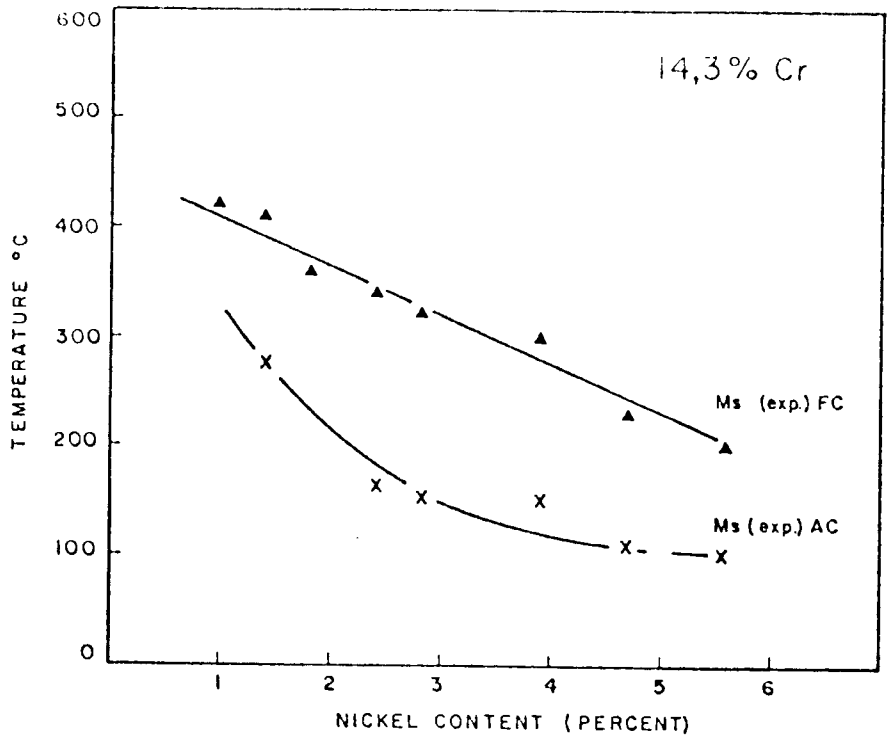

FIG. A.4 Comparison of M_s (FC) and M_s (AC) (14,3%Cr alloys)

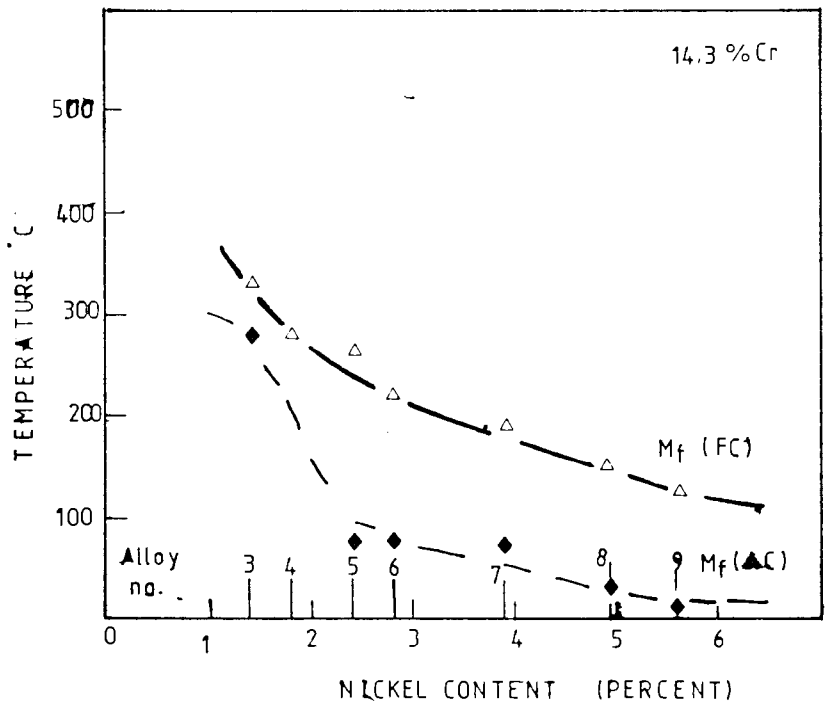

FIG. A.5 Comparison of M_f (FC) and M_f (AC) (14,3%Cr alloys)

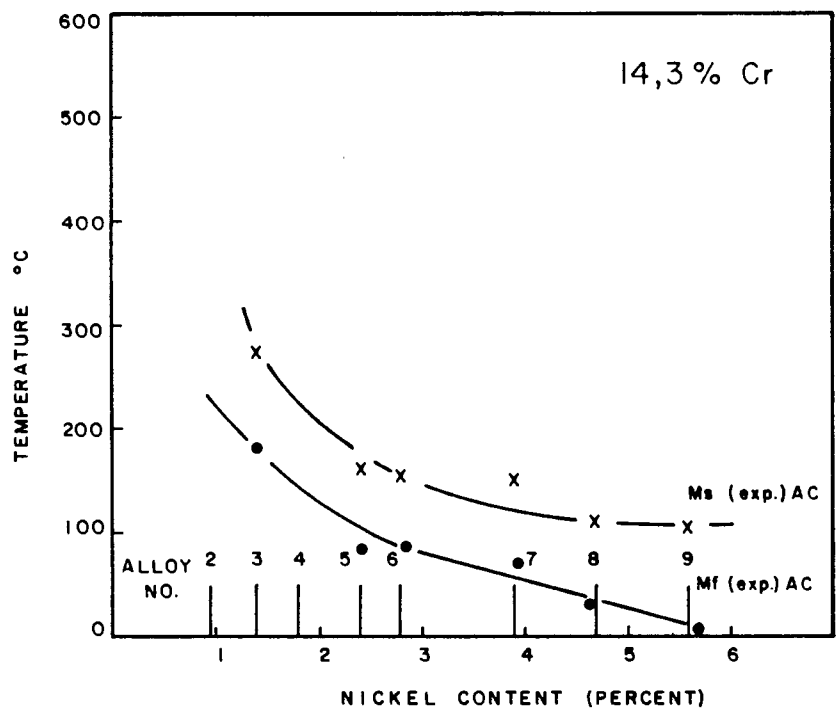

FIG. A.6 M_s (AC) and M_f (AC) for the 14,3%Cr alloys.

APPENDIX B

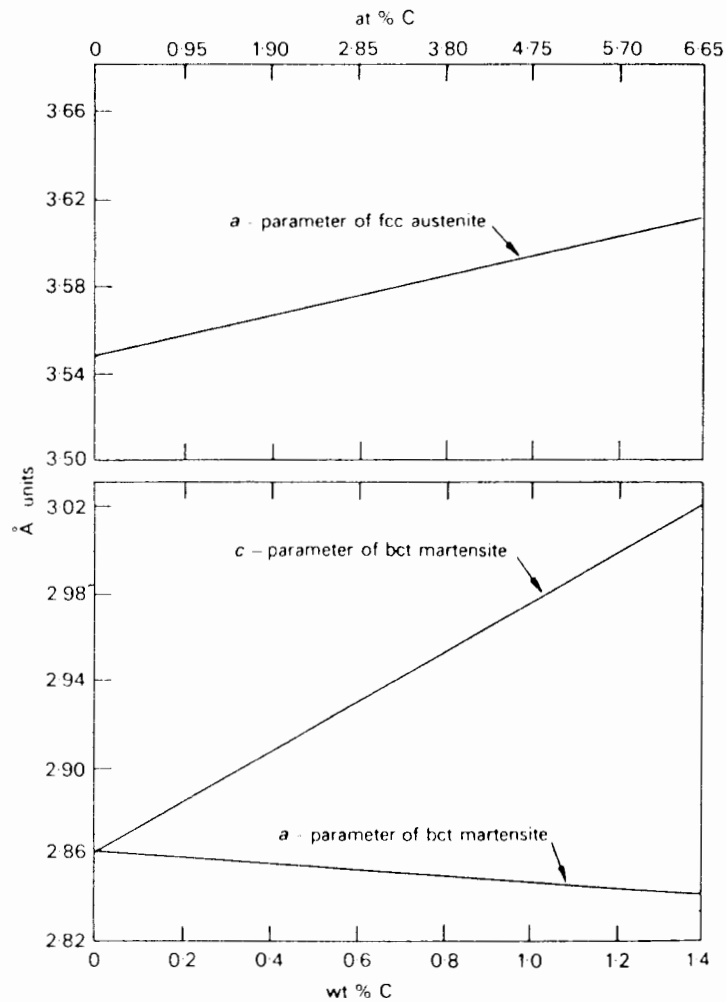

FIG. B.1 Effect of carbon on the lattice parameters of austenite and martensite. (Taken from Honeycombe, 1981).

APPENDIX C

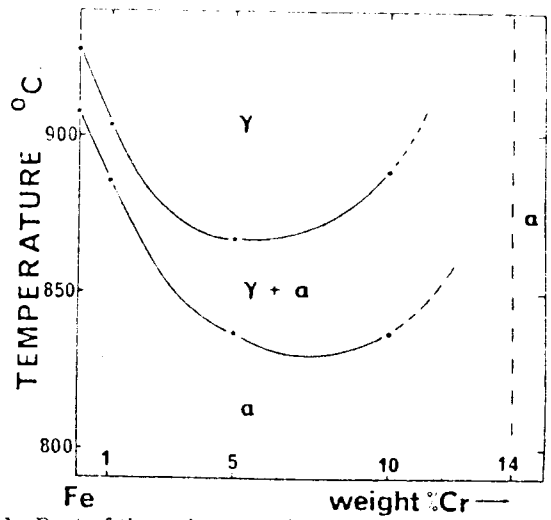

Fig. 1—Part of the γ-loop for the Fe-Cr system, as determined by dilatometry using a heating rate of 1°C min^{-1}.

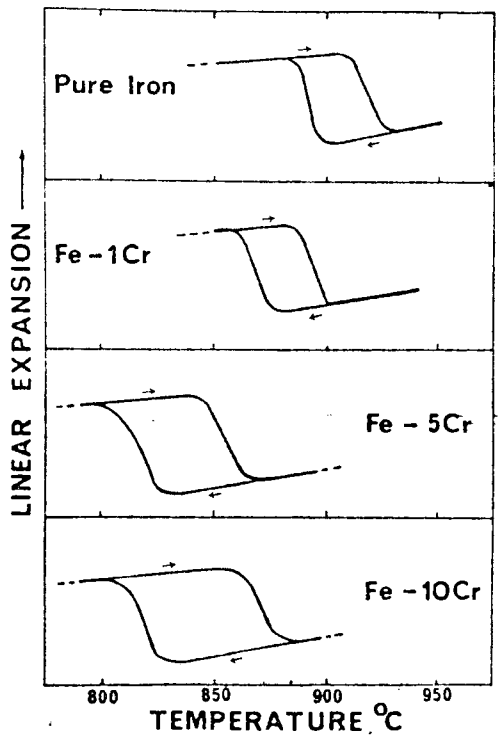

Fig. 2—Dilatation-temperature curves for the third cycle through the A_3 transformation.

Taken from Bee & Honeycombe, 1978

APPENDIX D

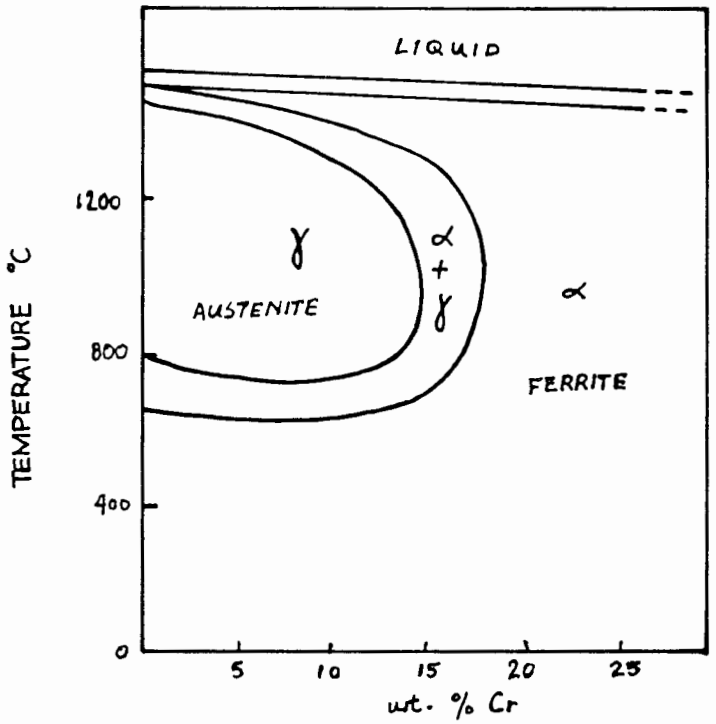

Fig.D1 The Fe(3 pct Ni)-Cr pseudobinary phase diagram

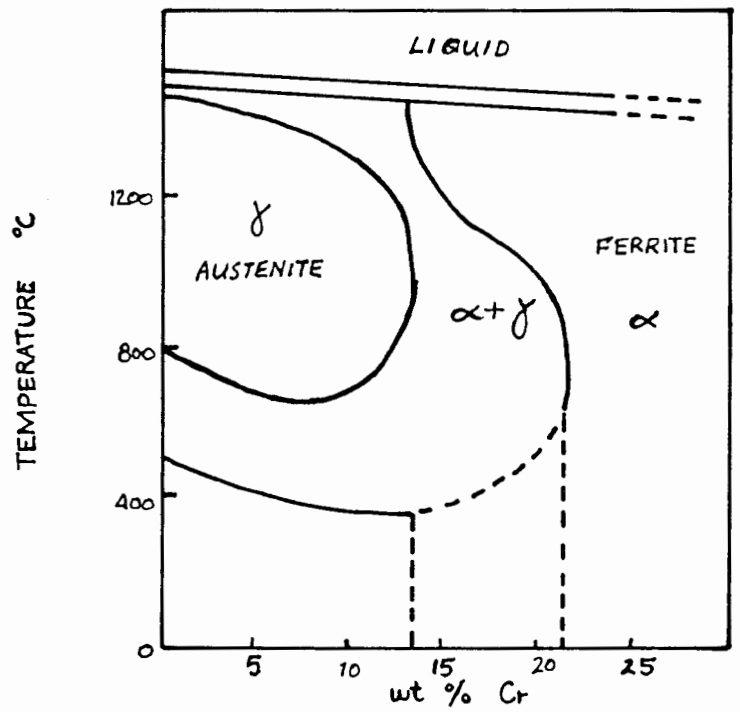

Fig. D2 The Fe(3 pct Mn)-Cr pseudobinary phase diagram

Taken from Wright & Wood, 1977

APPENDIX E

11,5% Cr		TRANSFORMATION TEMPERATURES (°C)					
Alloy	% Ni	T<1000°C (Heating)		T>1000°C (Heating)		$\lceil T_1 (T>1000°C) \rceil$ $\lfloor -T_1 (T<1000°C) \rfloor$	$\lceil T_2 (T>1000°C) \rceil$ $\lfloor -T_2 (T<1000°C) \rfloor$
		$T_1(A_{c1})$	$T_2(A_{c3})$	$T_1(A_{c1})$	$T_2(A_{c3})$		
A	0,27	900	*	940	1000	40	-
B	0,49	870	950	840	975	30	25
C	0,85	819	907	820	980	10	73
D	1,19	775	860	780	920	5	40
E	1,34	755	840	760	920	5	80
F	1,77	750	820	730	850	20	30
G	1,84	725	830	660	830	65	0
H	2,71	655	770	665	850	0	80
I	3,50	630	760	630	800	0	40
* No transformation temperature observed on dilatometric trace							

TABLE E.1 : Comparison of transformation temperatures obtained from the low temperature experiment (T<1000°C) with the values obtained from the high temperature experiment (T>1000°C) (heating cycle only) - 11,5% Cr alloys.

11,5% Cr		TRANSFORMATION TEMPERATURES (°C)					
Alloy	% Ni	T<1000°C (Cooling)		T>1000°C (Cooling)		$\lceil T_7$ (T>1000°C)$\rceil$ $\lfloor -T_5$ (T<1000°C)$\rfloor$	$\lceil T_8$ (T>1000°C)$\rceil$ $\lfloor -T_6$ (T<1000°C)$\rfloor$
		T_5(Ms)	T_6(M_f)	T_7(Ms)	T_8(M_f)		
A	0,27	*	*	*	*	-	-
B	0,49	760	680	*	*	-	-
C	0,85	560	455	550	450	10	5
D	1,19	480	360	540	420	60	60
E	1,34	450	340	520	400	70	60
F	1,77	430	325	455	360	25	35
G	1,84	425	320	*	*	-	-
H	2,71	360	255	420	270	60	15
I	3,50	340	230	225	225	10	5
* No transformation temperature observed on dilatometric trace							

TABLE E.2 : Comparison of transformation temperatures obtained from the low temperature experiment (T<1000°C) with the values obtained from the high temperature experiment (T>1000°C) (cooling cycle only) - 11,5% Cr alloys.

14,3% Cr		TRANSFORMATION TEMPERATURES (°C)					
Alloy	% Ni	T<1000°C (Heating)		T>1000°C (Heating)		$\lceil T_1 (T>1000°C) \rceil$ $\lfloor -T_1 (T<1000°C) \rfloor$	$\lceil T_2 (T>1000°C) \rceil$ $\lfloor -T_2 (T<1000°C) \rfloor$
		$T_1(A_{c1})$	$T_2(A_{c3})$	$T_1(A_{c1})$	$T_2(A_{c3})$		
1	0,62	*	**	*	*	-	-
2	0,98	780	*	800	890	20	-
3	1,41	740	*	*	900	-	-
4	1,80	735	835	*	850	-	15
5	2,40	680	800	690	875	10	75
6	2,80	655	775	680	780	25	5
7	3,90	635	750	630	745	5	5
8	4,70	630	740	620	730	10	10
9	5,60	620	735	620	735	0	0
* No transformation temperature observed in dilatometric trace							

TABLE E.3 : Comparison of transformation temperatures obtained from the low temperature experiment (T<1000°C) with the values obtained from the high temperature experiment (T>1000°C) (heating cycle only) - 14,3% Cr alloys.

14,3% Cr		TRANSFORMATION TEMPERATURES (°C)					
Alloy	% Ni	T<1000°C (Cooling)		T>1000°C (Cooling)		$\lceil T_7$ (T>1000°C)$\rceil$ $\lfloor -T_5$ (T<1000°C)$\rfloor$	$\lceil T_8$ (T>1000°C)$\rceil$ $\lfloor -T_6$ (T<1000°C)$\rfloor$
		T_5(Ms)	T_6(M_f)	T_7(Ms)	T_8(M_f)		
1	0,62	*	*	*	*	-	-
2	0,98	420	330	420	370	0	40
3	1,41	410	325	460	*	50	-
4	1,80	360	280	400	310	40	30
5	2,40	340	260	420	320	80	60
6	2,80	320	225	360	250	40	25
7	3,90	300	195	275	150	25	45
8	4,70	230	150	250	100	20	50
9	5,60	200	125	200	50	75	

* No transformation temperature observed in dilatometric trace

TABLE E.4 : Comparison of transformation temperatures obtained from the low temperature experiment (T<1000°C) with the values obtained from the high temperature experiment (T>1000°C) (cooling cycle only) - 14,3% Cr alloys.

APPENDIX F

TABLE 3 Depression of M_s Temperature* by 1% Alloying Element (°C)

Element	Ref. 13	Ref. 15
Carbon	474	2388
Manganese	33	54
Molybdenum	21	55
Chromium	17	47
Nickel	17	59
Silicon	11	37
Tungsten	11	43
Vanadium		127
Titanium		180
Columbium		50
Tantalum		75
Nitrogen		3222
Cobalt		13
Copper		85
Aluminum		306

* Approximately 300°C (570°F) for base 12% Cr steel.[13]

Appendix F: Depression of M_S temperature by 1% Alloying Element. (Taken from WEISER, 1977)

Ref.15 cited above in table: Hull, F.C., "Delta Ferrite and Martensite Formation in Stainless Steels", 1973.

Ref.13 cited in table above: Briggs, J.Z., and Parker, T.D., "The Super 12% Cr Steels", Climax Molybdenum Co., N.Y. 1965.

28 JUN 1984